Influence of Sn addition on the ageing behavior of Al-Mg-Si alloys

vorgelegt von

Master of Science in Engineering

Xingpu Zhang

ORCID: 0000-0002-9861-0995

von der Fakultät III – Prozesswissenschaften

der Technischen Universität Berlin

zur Erlangung des akademischen Grades

Doktor der Ingenieurwissenschaften

-Dr. -Ing.-

genehmigte Dissertation

Promotionsausschuss:

Vorsitzender: Prof. Dr. Aleksander Gurlo

Gutachter: Prof. Dr. John Banhart

Gutachter: Prof. Dr. Reinhard Krause-Rehberg

Tag der wissenschaftlichen Aussprache: 5. November 2019

Berlin 2019

Abstract

In this work, the ageing behavior of age hardenable Al-Mg-Si(Sn) alloys has been systematically studied by positron annihilation lifetime spectroscopy (PALS), hardness measurements, differential scanning dilatometry (DSC), electrical resistivity measurements and transmission electron microscopy (TEM).

At 'room temperature', i.e. around 20 °C, vacancies, which can assist the diffusion of solute atoms, are bound by Sn atoms due to strong Sn-vacancy interactions. As a result, clustering is strongly retarded, thus mitigating the deleterious effect of natural ageing (NA) on subsequent artificial ageing (AA). The largest effect of Sn was gained in an alloy with low solute concentration solutionised at an increased temperature. The possibility of adding other elements with strong binding with vacancies such as In in inhibiting NA was also verified.

With the increase of temperature, binding between Sn and vacancies weakens but still delays the formation of pre-ageing (PA) clusters at 100 °C and 140 °C. Distinctive stages of positron lifetime evolution similar to the ones at room temperature are observed. At the standard ageing temperature of 180 °C, Sn addition shows the opposite effect on the ageing kinetics of lean and concentrated alloys. When temperature is further increased to 210 °C and 250 °C, accelerated kinetics with an enhanced hardening response were obtained after adding Sn.

A combination of Sn addition and PA at 100 °C or 180 °C was also studied. The results showed that PA can enhance the retarding effect of Sn on NA and improve the hardening response after 1 week of natural secondary ageing (NSA). For a better PA performance in Sn-added alloys, a higher PA temperature is required and the undesired high hardness after PA and NSA can be lowered by Sn addition. Moreover, natural pre-ageing (NPA) prior to PA can promote the effect of PA at 100 °C in Sn-added alloys.

The combination of five characterization techniques allows for an interpretation of the ageing behaviors in Sn-containing alloys from different viewpoints and shows that different vacancy behaviors in the presence of Sn during ageing at various temperatures control the different ageing processes.

Kurzfassung

In dieser Arbeit wurde das Alterungsverhalten von aushärtbaren Al-Mg-Si(Sn)-Legierungen systematisch mittels Positronen-Lebensdauerspektroskopie (PALS), Härtemessungen, Thermoanalyse (DSC), Messungen des elektrischen Widerstands und Transmissionselektronenmikroskopie (TEM) untersucht.

Bei ‚Raumtemperatur' (also ca. 20 °C) werden Leerstellen, die die Diffusion von gelösten Atomen unterstützen, aufgrund der starken Sn-Leerstellen Wechselwirkung an Sn-Atomen gebunden. Infolgedessen wird die Clusterbildung stark verzögert, wodurch die schädlichen Auswirkungen der Kaltauslagerung auf die nachfolgende Warmauslagerung gemindert werden. Der größte Effekt von Sn wurde in einer Legierung mit niedriger Konzentration von Legierungselementen bei erhöhter Temperatur erzielt. Die Zugabe von Indium zur Unterdrückung der Kaltaushärtung wurde ebenfalls überprüft.

Mit zunehmender Temperatur schwächt sich die Bindung zwischen Sn und Leerstellen ab, verzögert aber dennoch die Bildung von Clustern bei 100 °C und 140 °C. Die Positronen-Lebensdauer verhält sich dabei ähnlich wie bei Raumtemperatur. Bei der Standard-Alterungstemperatur von 180 °C zeigt die Sn-Zugabe einen entgegengesetzten Einfluss auf die Alterungskinetik von verdünnten und konzentrierten Legierungen. Wenn die Temperatur weiter auf 210 ºC und 250 ºC erhöht wird, wird durch Zugabe von Sn eine beschleunigte Kinetik mit einer verbesserten Härtungsreaktion erhalten.

Eine Kombination aus Sn-Zugabe und Vorauslagerung bei 100 °C oder 180 °C wurde ebenfalls untersucht. Vorauslagerung verstärkt die verzögernde Wirkung von Sn auf NA und verbessert die Härtungskinetik auch nach 1 Woche Raumtemperaturauslagerung. Für eine bessere Wirkung der Vorauslagerung in Sn-haltigen Legierungen ist eine höhere Temperatur erforderlich. Die unerwünschte hohe Härte nach Vorauslagerung und anschließender Raumtemperatur-Auslagerung kann durch Sn-Zusatz verringert werden. Darüber hinaus kann eine zusätzliche Raumtemperatur-Auslagerung vor der Vorauslagerung bei 100 ° C deren Wirkung in Legierungen mit Sn-Zusatz fördern.

Die Kombination von fünf Messtechniken ermöglicht die Interpretation des Alterungsverhaltens in den Sn-haltigen Legierungen aus verschiedenen Blickwinkeln und zeigt, dass das Verhalten der Leerstellen in Gegenwart von Sn während der Alterung bei verschiedenen Temperaturen die einzelnen Alterungsprozesse steuert.

Abbreviations

AA	artificial ageing
AQ	as-quenched
CFD	constant fraction discriminator
DSC	differential scanning calorimetry
FWTH	full width at half maximum
GP	Guinier-Preston
HRTEM	High-resolution transmission electron microscopy
LM	liquid metal
LT	low temperature
MCA	multi-channel analyzer
NA	natural ageing
NPA	natural pre-ageing
NSA	natural secondary ageing
PA	pre-ageing
PALS	positron annihilation lifetime spectroscopy
PLT	positron lifetime
SCA	single-channel analyzer
SHT	solution heat treatment
SSSS	supersaturated solid solution
TAC	time-to-amplitude converter
TEM	Transmission electron microscopy

Table of Contents

1. Introduction

1.1 Aluminium alloys

Aluminium (symbol: Al, atomic number: 13, melting point: 660 °C, density: 2.70 g/cm^3, appearance: silvery-white) is the most common metallic element in the Earth's crust. Due to its high chemical activity, aluminium in the free state does not exist in the nature. In 1827, German chemist Friedrich Wöhler isolated pure aluminium successfully by reduction using potassium. Limited by the low productivity, however, aluminium was still treated as precious metal. The pyramid cap of the Washington Monument and the statue of Anteros in Piccadilly Circus, London, are representative early applications of aluminium. With the invention of Hall–Héroult process in 1886, the industrial large-scale production of aluminium caused a cost drop and widened its practical application.

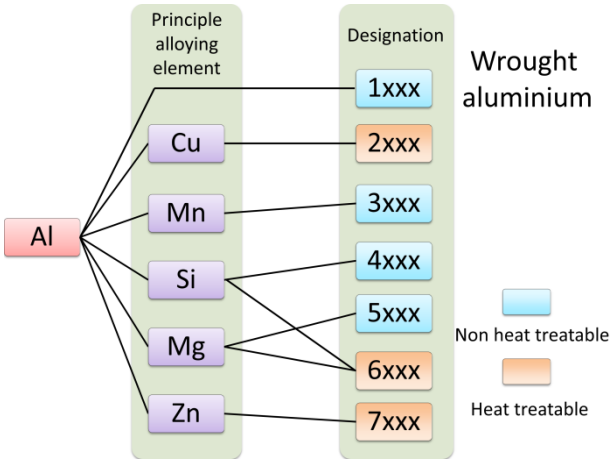

Fig. 1. Classification of wrought aluminium alloys

Instead of soft pure Al, different series of Al alloys with a wide range of improved properties, which can be adjusted by changing the alloying elements (Cu, Mn, Mg, Si, Zn, etc.), were developed to meet the requirements in different application areas. For example, the low density (only one third of steel), excellent corrosion resistance and age hardenability of Al alloys with Mg and Si enable their wide application in automobiles, aircrafts, railroad cars, etc. Wrought and casting alloys are the two main classifications of Al alloys and are further grouped according to the alloy compositions. Codes of four-digit number are used to assign the alloys. The designation and corresponding main alloying elements of wrought alloys are given in Fig. 1. With the increasingly stringent emission standard, a further huge growth in the use of 6xxx (Al-Mg-Si) alloys in vehicles can be expected. This work will focus on such alloys, which can be strengthened by heat treatment – age hardening.

1.2 Age hardening of Al-Mg-Si alloys

Age hardening, also known as precipitation hardening, is a commonly used technique to enhance the mechanical properties of a variety of alloys, including aluminium, magnesium, nickel, titanium alloys and certain steels. During ageing at defined temperatures, second-phase particles are formed and impede the movement of dislocations – by which plastic deformation occurs. Thus, the alloys are reinforced. For Al-Mg-Si alloys, ageing hardening is usually carried in three steps: 1) Solution heat treatment (SHT), normally at temperatures higher than 500 °C. During SHT, most solute atoms are dissolved and homogeneously distributed in the Al matrix. 2) Rapid cooling (quenching). Due to the drop in solid solubility of solutes at lower temperature, a supersaturated solid solution (SSSS) is obtained after quenching. 3) Ageing. Alloys are reheated and kept at an intermediate temperature for certain times and the formation of finely dispersed second phases (precipitates) driven by the solute supersaturation hardens the alloys.

1.2.1 Role of vacancies

The formation of clusters and precipitates during ageing of Al-Mg-Si alloys is realized by solute diffusion (substitutional type) mediated by vacancies. As a type of point defect, vacancy forms when one atom in the crystal is missing. The equilibrium vacancy concentration shows temperature dependence and can be expressed by [1]:

$$C_V = \exp(-\frac{G_V^f}{k_B T})$$

where C_V is vacancy concentration, G_V^f is the Gibbs free energy of vacancy formation, k_B is the Boltzmann constant and T is the absolute temperature. During SHT at 540 °C, a site fraction of equilibrium vacancies in Al was calculated to be 1.4 x 10^{-4} [2]. After or even during quenching, certain amounts of vacancies go to sinks and a site fraction of 5 x 10^{-5} has been reported for an alloy 6061 with a quenched rate of 10000 K/s [3]. Upon the following ageing, vacancies keep changing sites with solute atoms, assist their diffusion and promote the formation of secondary phases.

1.2.2 Clustering and precipitation processes in Al-Mg-Si alloys

In addition to vacancies, solute clusters in Al-Mg-Si alloys directly after SHT and quenching have also been detected by positron annihilation lifetime spectrometer (PALS) measurements carried out at low temperatures (-60 °C – -180 °C), revealing the formation of vacancy-free solute clusters during quenching [4,5].

1.2.2.1 Natural ageing

Different methods, both direct and indirect, have been used to characterize the natural ageing (NA) process at RT, revealing the NA mechanism from different angles.

PALS measurements have shown five stages of evolution during NA (Fig. 2) and the complex interaction between vacancies and solute atoms/clusters was identified [2,6,7]. Stage 0: Experimentally invisible sharp decrease in PLT, proposed to be a process involving the formation of vacancy-solute complexes. Stage I: Constant or slightly increasing PLT, observed preferably only in the early ageing stage of alloys high in Mg. The reason for this has yet not been clarified. Stage II: Following Stage I in alloys with high Mg content or being the first observable stage in alloys with intermediate Mg content, PLT drops continuously. It is thought to be related to the loss of vacancies and the formation of solute clusters with a lifetime of ~0.210 ns [2,7]. Due to the high jump frequency of Si atoms (18200 s^{-1}) compared Mg atoms (190 s^{-1}) at RT [8], Si-rich clusters appear to prevail. Stage III: Re-increasing PLT. By varying the Mg content (Fig. 2), the aggregation of Mg atoms into the already formed clusters is suggested to be the reason [7]. Stage IV: Re-decrease in PLT, which has been explained by ordering in clusters observed under high-resolution transmission electron microscopy (HRTEM) [9].

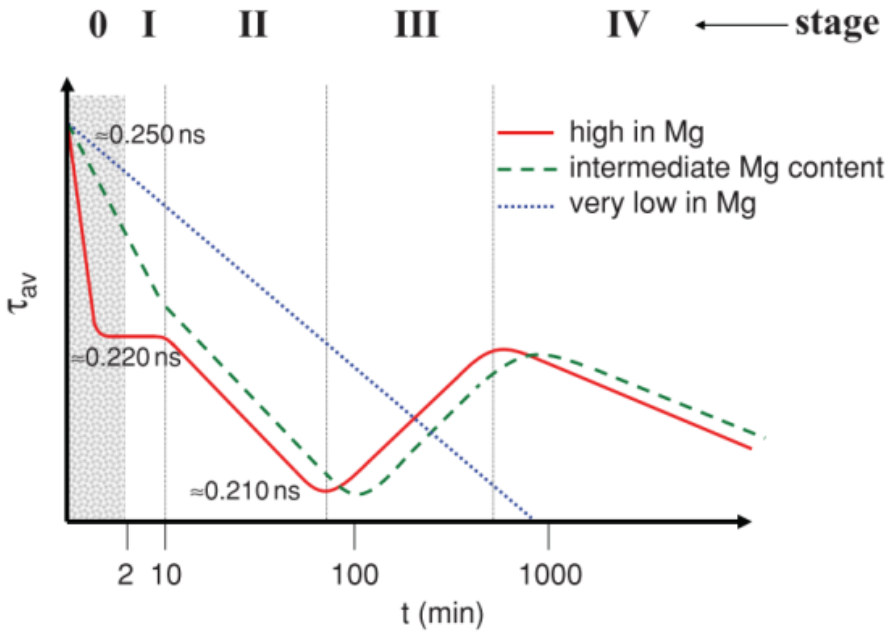

Fig. 2. Schematic evolution of PALS of five stages during NA in Al-Mg-Si alloys [7].

The formation of clusters during NA can impede the motion of dislocations and thus leads to the increase in hardness [4,6,10]. A continuous decrease in the hardening rate during NA has been reported [2], which reflects the decreasing clustering rate caused by the continuously lowered vacancy concentration and solute supersaturation.

Electrical resistivity is known to be decreased by solute depletion and annihilation of vacancies [11] but increased by the formation of NA clusters with enhanced power in scattering electron [12,13]. A transition from fast increase to slow one has been reported in the literature [6,12]. Seyedrezai et al. [14] observed three different stages of resistivity evolution during NA and claimed the relationship between cluster growth and vacancy by combining with PALS measurements. Besides, a model describing the clustering process based on the interaction between solutes and vacancies, which has been verified by several resistivity results, was proposed [15].

The formation of NA clusters can also be detected in linearly heated alloys by differential scanning calorimetry (DSC). Clustering reaction C1 (peaking at 40-50 °C), which is shown to finish in 1 hour of NA [16,17], is thought to be associated to the clusters formed during Stage II of PALS [7]. The reason for the relatively higher temperature located (~80 °C) clustering reaction C2 is still under controversy. Chang and Banhart et.al [7,16] suggested that the formation of C2 takes place after 1 hour NA at RT and finishes after 2 weeks. Due to the longer positron lifetime in C2 than in C1, the formation of C2 leads to the increasing PLT during Stage III, while the coarsening or ordering of C2 causes the drop in Stage IV. However, it also has been argued that C2 is identical to the clusters formed at ~100 °C and can suppress the formation of C1 [17,18].

Atom probe tomography (APT) has provided more direct information of NA clusters, e.g. number density, composition, size, etc. Restricted by the long sample preparation time, the measurements have been normally carried out at least after hours of NA [3,6,17,19–25]. Zandbergen et al. [21] reported that the number density of clusters increases up to 1 week of NA and then keeps stable. The Mg/Si ratio of NA clusters is reported to have a wide distribution [17], while Torsæter et al. [26] demonstrated that NA clusters have Mg/Si ratios similar to those of the investigated alloys. There are also some works that revealed NA clusters are Si-rich originally and by a subsequent Mg-enrichment process the Mg/Si ratio of the clusters approaches a value slightly lower than 1.0 with prolonged NA time [3,23,27]. Recently, Dumitraschkewitz et al. [28] made the as-quenched state accessible with a cryo-transfer enabled APT and found that only Si atoms are involved in the early-stage clustering of an as-quenched Al-Mg-Si-(Cu) alloy.

The wide attention on NA originates from the adverse effect of NA on the following artificial ageing (AA) at 180 °C, the so-called “negative effect”. Both the hardening rate and hardenability are diminished [6,29]. The peak of β’’ (the main strengthening phase formed during AA, as will be discussed below) on DSC traces is postponed to higher temperature following the dissolution trough of NA clusters formed during prior NA [30,31]. Transmission electron microscopy (TEM) measurements showed that NA causes coarse β’’ precipitates with low number density in the artificially peak-aged state [29,32]. APT studies revealed the strongly delayed formation and growth of β’’ after paint baking (PB, 30 min at ~180 °C) [21,33]. This adverse effect of NA is

argued to be caused by the lowered vacancy concentration and solute depletion [21] and also by the formation of Si-rich NA clusters, which can neither dissolve nor transform into β'' when AA is applied [23]. A "vacancy prison" model – NA clusters trap vacancies at RT and even at standard AA temperatures (e.g. 170 °C) proposed by Pogatscher et al. [10] explains the adversely influenced AA with the reduced mobile vacancy concentration after NA. Nevertheless, in the case of alloys with lean Mg and Si content, a positive effect of NA has been reported [20,34]. Chang et al. [20] claimed that the clusters formed during NA can act as nucleation sites for precipitation, while Lai et al. [34] reported that due to the presence of NA clusters β' precipitates are formed instead of β''. However, the lower strength of such alloys limits their commercial application and therefore only few scientific investigations have been carried out.

1.2.2.2 Pre-ageing and interrupted quenching

As an effective method to eliminate the "negative effect" of NA, the mechanisms of pre-ageing (PA) have also been explored by many researchers. It is found that the PB response of alloys after given times of NA (T4) can be effectively improved by PA at temperature above ~67 °C after SHT and quenching [35]. The formation of PA clusters during PA, which are ready to transform into β'' upon subsequent AA, and the reduced concentration of vacancies available to assist the following NA were proposed to be the reason [21,25,30,33,36–39]. By now, no consensus has been reached regarding the notation of the formed phase – GP zone [25,38], pre-β' [32,40], PA cluster [21] and cluster (2) [17] have been used in literature. Buha et al. [41] reported a PLT of 208 ps for GP zones formed in the early stage of ageing at 177 °C. Serizawa et al. [17] have identified PA cluster formed at 100 °C with the DSC exothermic reaction peaking at approximately 77 °C. It has been shown that PA treatments can remove the endothermic troughs related to the dissolution of NA clusters formed during RT storage and shift the peak of β'' to lower temperatures [36,42,43]. Different from NA clusters that are unobservable under TEM, GP zones/pre-β'' phases give obvious contrast [25,32]. GP zones formed at 70 °C [25] and at 65 °C [44] are identified to be spherical and fully coherent with the Al matrix, while Marioara et al. [32,40] showed that the pre-β'' phase formed at 100 °C and 150 °C has a needle shape oriented along the <100> direction. APT measurements revealed that clusters formed during PA are larger than NA clusters [21,25,27,33]. According to Murayama et al. [25], a critical size of clusters is necessary to act as nucleation site for β'', which could explain the NA clusters (below the critical size) act negativly but PA clusters (above the critical size) positively on the formation of β''. In addition, the distribution of Mg/Si ratios of PA clusters is found to be more uniform than that of NA clusters [21,27] and the average Mg/Si ratio is higher than that of NA clusters and close to that of β'' [17,21,26].

Interrupted quenching (IQ) – quenching from the solutionising temperature is interrupted at an intermediate temperature for given times – has also been found to be a feasible method in promoting AA after NA, the mechanism of which has been proposed to be similar to that of PA [42,45,46]. To obtain the positive effect of IQ, an appropriate temperature range is essential [42,46].

1.2.2.3 Artificial ageing at standard temperature

To meet the requirement in strength for industrial applications, artificial ageing (AA) is normally carried out at around 180 °C. Madanat [47] found a sharp drop in PLT during the first seconds of ageing in liquid metal (Bi57Sn43) at 180 °C, which was explained by the loss of vacancies in the early stage of AA. Calculations for an alloy 6016 also revealed the annihilation of excess vacancy in the first few minutes at 185 °C [48]. Fine GP zones with no clear structure are identified in alloy 6061 underaged at 175 °C for 10 min [49] and at 180 °C for 20 min [44]. In peak-aged Al-Mg-Si alloys, fully coherent needle-like β'' (Mg_5Si_6 [50]) is found by TEM to be the main strengthening phase [51,52]. β'' precipitates have a monoclinic structure (a = 1.516 nm, b = 4.050 nm, c = 0.674 nm and β = 105.3° [50]) and are oriented parallel to the <100> direction [32,53]. A characteristic PLT of 200–210 ps for β'' has been reported [41,47,54,55] and the exothermic peaks at ~250 °C of the DSC curves are thought to be associated to the formation of β'' [49,51,56]. APT measurements revealed that elongated β'' has a Mg/Si ratio ~1.0 [21,24,25,49] and is more enriched in solute than NA clusters [10]. With prolonged ageing time, overageing takes place and hardness starts to decrease. Rod-shaped β' precipitates, which do not contribute much to strength, are formed [49]. A hexagonal structure of β' with unit cell parameters a = 0.715 nm, c = 1.215 nm and γ = 120° has been reported by Vissers et al. [57]. The semi-coherency of β' [58] leads to a higher PLT than β'' [47,54,55]. Moreover, long period artificial ageing usually leads to a decrease in electrical resistivity due to solute depletion and formation of larger precipitates [29,59,60].

1.2.2.4 Artificial ageing at high temperatures

AA temperatures higher than 200 °C were found to accelerate hardening kinetics but decrease maximum hardness [10]. This was explained by both the decreased solute super-saturation as a driving force and more greatly reduced vacancies. Liu et al. [61] proposed that β' precipitates are the main strengthening phase of Mg-excess Al-Mg-Si alloys (no prior NA) at 250 °C. An earlier transformation from β'' to β' in an AW6060 alloy aged at 210 °C than at 180 °C after quenching has been observed by PLT and dilatometry measurements [54]. TEM investigations carried out by Marioara [62] showed that at 250 °C and 260 °C the Mg/Si ratio of the alloys determines the type of the precipitates formed (β'', β'', U1 or U2).

The reduced achievable peak hardness at high temperatures is found to be compensated by prior NA [10,61]. Various explanations have been given: 1). vacancies trapped by NA clusters, which dissolve at high temperature, are released and enhance precipitation [10]; 2). NA clusters tune the precipitation pathways and promote the formation β'' at 250° [61].

1.2.3 Influence of Sn addition

Because NA occurs with the diffusion of solutes assisted by vacancies, the negative effect of NA thus can be diminished by reducing the available vacancy concentration. Adding Sn just shows the potential in preventing NA due to the much stronger Sn-vacancy interaction (0.281 eV) than Mg-vacancy (0.026 eV) and Si-vacancy (0.033 eV) [63]. The delaying effect of Sn addition on NA was firstly reported for Al-Cu alloys [64,65]. Nagai et al. [66] proposed that Sn addition in Al-Cu alloys traps quenched-in vacancies and delays the formation of GP zones based on positron annihilation measurements. Moreover, Sn clusters [65,67,68] or Sn atoms [69] were found to act as nucleation sites for θ' at high ageing temperatures (160 °C – 200 °C), resulting in the substantially improved strengthening of Al-Cu alloys.

Similar delaying effect of Sn addition on NA for Al-Mg-Si alloys was firstly reported by Muromachi and Mae [71] and they found that the negative effect of NA on AA below 200 °C can be mitigated by Sn addition. In 2014, Pogatscher et al. [70] demonstrated a "diffusion on demand" model, proposing that vacancies, which assist the solute diffusion, are trapped during NA but released during AA at higher temperature with the weakened Sn-vacancy binding. As a result, a retarded NA and a consequent well-kept AA kinetics and response were obtained (Fig. 3). Further study [72] has shown that a high dissolvable amount of Sn is required to achieve its maximum potential in suppressing NA. Therefore, the solutionising treatment temperature and the concentration of Mg and Si solutes, which influence the solubility of Sn, should be controlled. An ultra-fast hardening kinetics has been observed for Sn-added Al-Mg-Si alloys aged at 250 °C [73,74]. Werinos et al. [73] attributed this to more retained vacancies by Sn while Liu et al. [74] suggested that a transformation from β' precipitates to composite β'/β'' precipitates is stimulated by Sn-vacancy complexes.

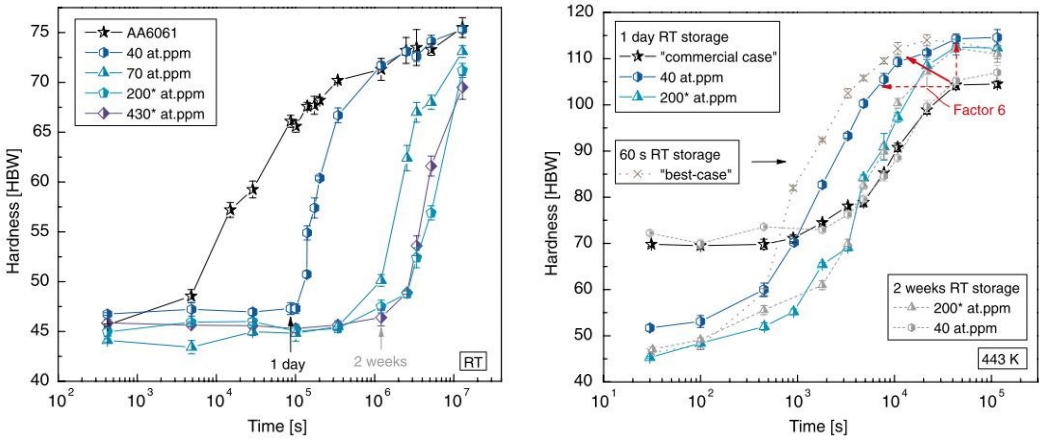

Fig. 3. The influence of Sn addition on NA and AA, reported by Pogatscher et al. [70].

2. Positron annihilation lifetime spectroscopy

Non-destructive positron lifetime spectroscopy (PALS) has been widely used in the study of defects in materials. The high detection sensitivity of PALS up to atomic scale (i.e. vacancies with a site fraction of ~10^{-7} in metals can already be detected) makes it a powerful method to derive information about vacancy-type defects and atom clusters/precipitates in Al-Mg-Si alloys. An introduction on PALS is given below.

2.1 Basics of positron lifetime spectroscopy

As the antiparticle of the electron, the positively charged positron (+1 e) has a same mass and spin as the electron. As a most commonly used positron source in laboratories, radioactive isotope ^{22}Na has a relatively long half-life of 2.6 years and a high positron yield of 90.4%. Positrons are produced via a β^+-decay reaction:

$$^{22}\mathrm{Na} \rightarrow {}^{22}\mathrm{Ne} + e^+ + \nu_e + \gamma$$

With the emission of the positron a 1.27-MeV γ photon is almost simultaneously created. When the obtained positrons penetrate into the material, their energy (with a broad distribution up to 540 keV) will be reduced within a few picoseconds, the so call thermalization. Fig. 4 shows the spectrum of energies and normalized probability of positron produced by Na^{22} [75]. After reaching the thermal energy, the positron diffuses around the material until it collides with an electron. Then the annihilation of the positron-electron pair occurs and two γ photons, with energies of 511 keV converted from the mass of the pair, are emitted. A schematic of the positron annihilation process is shown in the left part of Fig. 5. The time difference between the emission of the 1.27-MeV (birth of positron) and the 511-keV γ photons (annihilation of positron) is defined as the positron lifetime (PLT). The electron density at the annihilation site determines the annihilation rate (λ, the reciprocal of PLT) and thus PLT:

$$\lambda = \frac{1}{\tau} = \pi r_0^2 c \int n_+(r) n_-(r) \Gamma dr$$

where r_0 is the classical electron radius, c the speed of light, $n_+(r)$ the positron density, $n_-(r)$ the electron density, r the position vector, Γ the correlation function describing the electron density increase caused by Coulomb interactions, respectively [76].

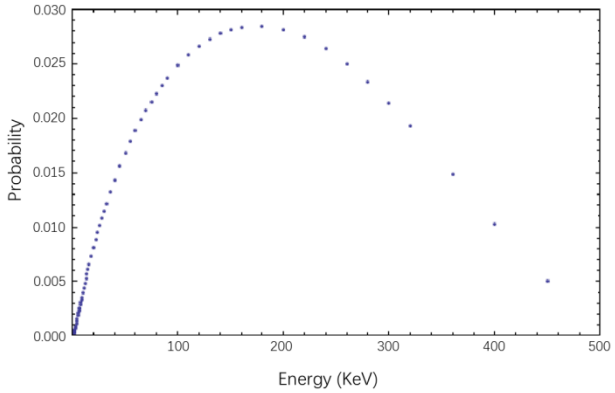

Fig. 4. Na^{22} β^+ positron energy spectrum [75].

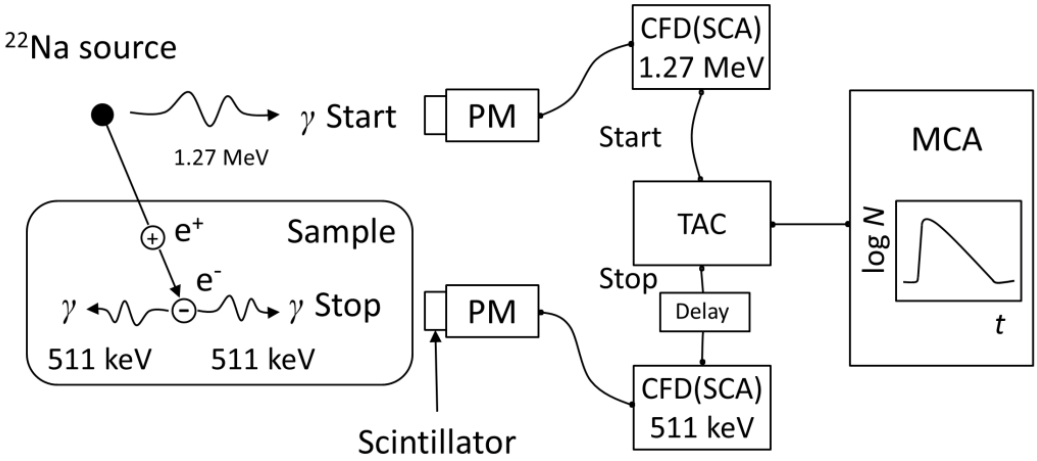

Fig. 5. Schematic of PALS experiment in fast-fast coincidence [76].

In bulk Al, the characteristic PLT is ~160 ps. Because positrons are positively charged, the absence of nuclei, which also have positive charges, makes open-volume defects, e.g. vacancies and dislocations, possible positron traps. The low electron density in such defects results in the longer PLT compared with the bulk material. The characteristic lifetime of positrons that annihilate in a monovacancy in Al is 245–250 ps, while it further increases in vacancy agglomerates (e.g. divacancy ~0.273 ps [77]). In the case of Al-Mg-Si alloys, the trapping of positrons can also take place in solute clusters and precipitates. For solute clusters (i.e. NA and PA clusters) and coherent precipitates (i.e. β''), the trapping mainly arises from the different affinities of Al (-4.41 eV), Mg (-6.18 eV) and Si (-6.95 eV) [78] with the positron wave function spreading over the solute clusters/precipitates. A PLT of 210–220 ps for solute clusters and β'' precipitates has been reported [5,54,55]. For semi-coherent (i.e. β') and in-coherent (i.e. β) precipitates, the interface containing misfit can localize the positron wave function and a higher PLT is expected [79]. The positron wave function Ψ_+ and potentials $V_+(x)$ of possible solute clusters/precipitates are shown in Fig. 6.

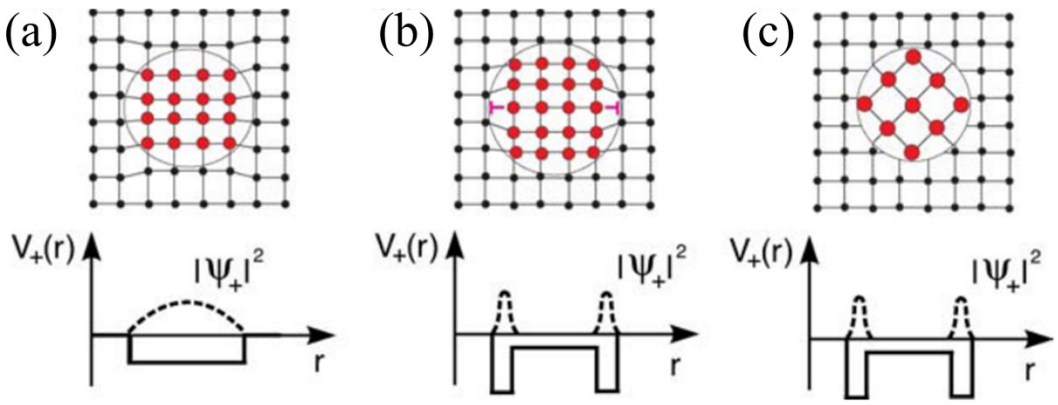

Fig. 6. Localized positron wave function Ψ_+ and potentials $V_+(\mathbf{x})$ of different kinds of solute clusters/precipitates [55]. (a) Coherent solute clusters/precipitates, (b) semi-coherent precipitates and (c) incoherent precipitates.

2.2 Instruments for positron lifetime measurement

As described above, the determination of PLT is made possible by measuring the time difference between the 1.27-MeV birth γ photon (start signal) and one of the 511-keV annihilation γ photons (stop signal) using a fast-fast coincidence system, as shown in Fig. 5.

The activity of the used ^{22}Na source is ~40 μCi, meaning that positrons are emitted every ~700 ns on average. This is much longer than the positron annihilation lifetime in Al alloys (normally < 0.3 ns), which ensures that at most one positron exists in the sample and that the start and stop signals are from the same annihilation event in most cases. A typical sandwich arrangement is used, i.e. the source is inserted between two pieces of Al-Mg-Si samples wrapped up by Al foil. To ensure that most portion of positrons annihilate in the samples, a minimum thickness of 300-500 μm for Al alloy samples is required. We have chosen 1 mm thickness for practical reasons.

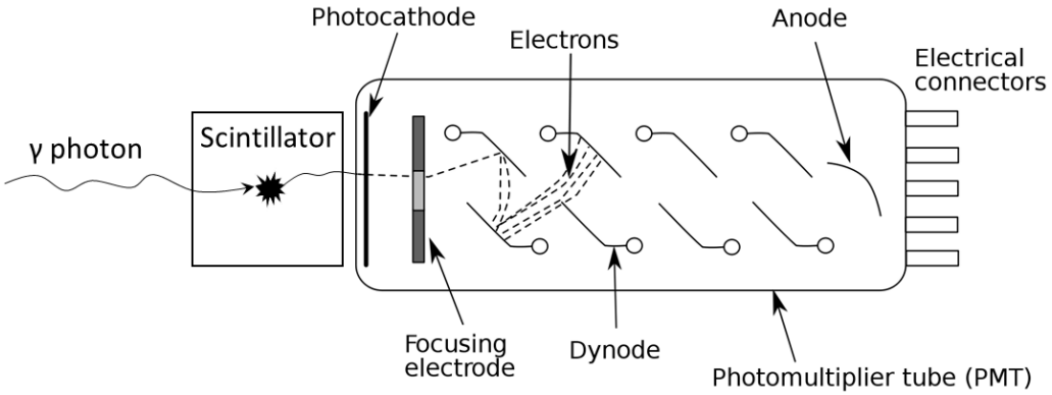

Fig. 7. Schematic view of scintillation counter. Reprinted from [80].

The γ photons are firstly detected by scintillators and excite electron to the excited band. Then photons are emitted with the de-excitation. EJ-232 plastic scintillators with relatively high light output (55%) and a fast response (rise time of 0.35 ns and decay time of 1.6 ns) were used in this

study. These photons are converted into photoelectrons via the photoelectric effect by the photocathodes in photomultiplier tubes (PMT, Hamamatsu H3378-59 in this work), to which scintillators are mounted with silicone grease in between to ensure a good light transmission. These primary electrons are accelerated and focused by an electrode and then multiplied by a sequence of dynodes through secondary emission in the tubes. The schematic view of the detection system is shown in Fig. 7. Electrical output pulses are further processed by a constant fraction discriminator (CFD). If simple threshold triggering was applied, the variation in pulse height would cause a "time walk" effect. However, by implementing the constant-fraction discrimination principle – triggering occurs on a constant fraction of the peak height – trigger times independent of the pulse height can be yielded. Beside as normal CFD, the applied FAST ComTec 7029A model can be simultaneously used as a differential constant fraction discriminator (single-channel analyzer, SCA). The energy window can be adjusted to guarantee the signals from 1.27-MeV (start) and 511-keV (stop) photons are accepted in the correct channels. The resultant pulses from the CFD then start and stop a time-to-amplitude converter (TAC) and the time interval is measured. The output pulses from the TAC with an amplitude proportional to the positron lifetime are scanned and stored in different channels as energy spectrum by a multi-channel analyzer (MCA). A FAST ComTec MCA-3A moiyt55odule is applied. A time resolution of 190-200 ps with a count rate ~500 s^{-1} of the spectrometer is obtained.

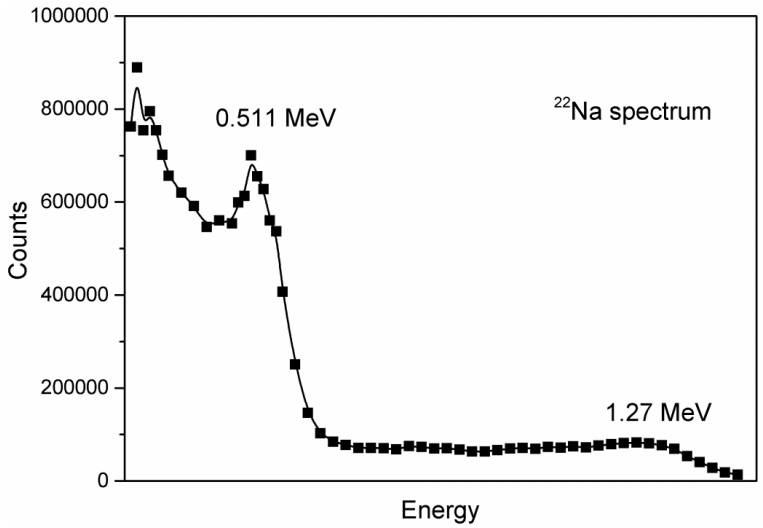

Fig. 8. γ ray spectrum of ^{22}Na measured with plastic scintillators.

Due to the low atomic number (Z) of plastic, photoelectric peaks can be hardly detected and Compton scattering is the dominant interaction of γ photons in the scintillator. The selection of energy window was done by recording the counts of the pulses within a fixed width of energy window, which scans the entire energy range. The γ ray spectrum of ^{22}Na measured with plastic scintillators is shown in Fig. 8.

2.3 Data acquisition and treatment

A pair of well annealed pure Al (99.9999%) was used to determine the source corrections (Kapton foil: ~11 %, ~0.4 ns and positronium formation: <1 %, ~3 ns). Software LT9 was used for data analysis that included subtraction of source contributions and background. Samples after various heat treatments were measured at RT and data collection was done every 2 min (~60000 counts). The spectra are firstly analyzed with a one-component fit, obtaining one-component positron lifetimes (τ_{1C}), which represent the mixed lifetime of all positron components. This fast date acquisition (FDA) mode has been shown to be feasible for one-component analysis [4,7]. Therefore, in situ positron lifetime measurements on the ageing kinetics are made possible by the short accumulation time. Moreover, for samples containing more than one type of positron lifetime components, additional components can be added in the analysis with an improved fit variance. A better statistics ready for lifetime decomposition can be obtained by summing up the period of constant positron lifetime. Certain experiments were also carried out at low temperatures (-60 °C, -120 °C and -180 °C), where the ageing kinetics of Al-Mg-Si alloys are suppressed and thus at least 2×10^6, normal data acquisition (NDA) mode counts are accumulated to ensure a reliable analysis.

3. Other methods employed

3.1 Hardness measurements

To quantify the alloys' mechanical property, both Vickers and Brinell hardness tests were used. Vickers hardness measurements were carried out on well-polished alloy surfaces with tester MHT-10 (load force of 100 gf increasing with 10 gf/s; dwell time: 10 s). For Brinell hardness measurements on samples ground with sandpaper (grit size P4000), a Qness 60M tester with a 1 mm indenter, 10 kg load and 10 s loading time was employed. For both methods, the average value of 10 indentations for each sample was used.

3.2 Differential scanning calorimetry

Differential scanning calorimetry (DSC) measurements were carried out with samples (1 mm thick, 5 mm in diameter, mass ~50 mg) in a Netzsch 204 F1 Phoenix. A baseline was obtained with two empty Al crucibles. For all measurements, pure Al (99.999 %) with roughly equivalent weight as the samples to be analyzed was used as a reference sample. To avoid the influence of storage at RT during transportation, samples were immersed in liquid nitrogen immediately after various heat treatments. After being held for 5 min in the pre-cooled (0 °C) chamber, DSC analyses were performed from 0 °C to 400 °C with a scanning rate of 10 K/min. Then, the baseline was subtracted from the measured curve.

3.3 Electrical resistivity

Sample wires (usually 500 mm long, 0.82 mm in diameter) were made into coils for electrical resistivity measurements. A four point probe system with an alternating current of 100 mA was applied for in-situ measurements. The assembly of the samples normally took 2–3 min after heat treatments. Samples were then kept in an oil bath running at 20 °C during the measurements.

3.4 Transmission electron microscopy

A transmission electron microscope (TEM), a Cs-corrected ETEM (FEI, Titan G2) operated at 300 kV, was used to visualize the precipitates formed after certain AA treatments. Samples for TEM measurements were firstly ground to a thickness of ~0.15 mm with sandpaper. An electrolyte consisting of 24 vol.% HNO_3 and 76 vol.% methanol was then used for the electrolytic thinning at –30 °C.

4. References

[1] G. Gottstein, Physical Foundations of Materials Science, Springer Berlin Heidelberg, 2004.

[2] M. Madanat, M. Liu, J. Banhart, Reversion of natural ageing in Al-Mg-Si alloys, Acta Mater. 159 (2018) 163–172.

[3] V. Fallah, B. Langelier, N. Ofori-Opoku, B. Raeisinia, N. Provatas, S. Esmaeili, Cluster evolution mechanisms during aging in Al-Mg-Si alloys, Acta Mater. 103 (2016) 290–300.

[4] M. Liu, Clustering Kinetics in Al-Mg-Si Alloys Investigated by Positron Annihilation Techniques, Technische Universität Berlin, 2014.

[5] M. Liu, J. Čížek, C.S.T. Chang, J. Banhart, Early stages of solute clustering in an Al-Mg-Si alloy, Acta Mater. 91 (2015) 355–364.

[6] J. Banhart, C.S.T. Chang, Z.Q. Liang, N. Wanderka, M.D.H. Lay, A.J. Hill, Natural aging in Al-Mg-Si alloys - A process of unexpected complexity, Adv. Eng. Mater. 12 (2010) 559–571.

[7] J. Banhart, M.D.H. Lay, C.S.T. Chang, A.J. Hill, Kinetics of natural aging in Al-Mg-Si alloys studied by positron annihilation lifetime spectroscopy, Phys. Rev. B. 83 (2011) 14101.

[8] M. Liu, B. Klobes, J. Banhart, Positron lifetime study of the formation of vacancy clusters and dislocations in quenched Al, Al-Mg and Al-Si alloys, J. Mater. Sci. 51 (2016) 7754–7767.

[9] K. Matsuda, H. Gamada, K. Fujii, Y. Uetani, T. Sato, A. Kamio, S. Ikeno, High-resolution electron microscopy on the structure of Guinier-Preston zones in an Al-1.6 mass Pet Mg2Si alloy, Metall. Mater. Trans. A Phys. Metall. Mater. Sci. 29 (1998) 1161–1167.

[10] S. Pogatscher, H. Antrekowitsch, H. Leitner, T. Ebner, P.J. Uggowitzer, Mechanisms controlling the artificial aging of Al-Mg-Si Alloys, Acta Mater. 59 (2011) 3352–3363.

[11] F.R. Fickett, Aluminum–1. A review of resistive mechanisms in aluminum, Cryogenics (Guildf). 11 (1971) 349–367.

[12] C. Panseri, T. Federighi, A Resistometric Study of Preprecipitation in an Aluminium-1.4 Percent Mg2Si Alloy, J. Inst. Met. London. 94 (1966) 99–197.

[13] I. Kovaćs, J. Lendvai, E. Nagy, The mechanism of clustering in supersaturated solid solutions of A1-Mg2Si alloys, Acta Metall. 20 (1972) 975–983.

[14] H. Seyedrezai, D. Grebennikov, P. Mascher, H.S. Zurob, Study of the early stages of clustering in Al-Mg-Si alloys using the electrical resistivity measurements, Mater. Sci. Eng. A. 525 (2009) 186–191.

[15] H.S. Zurob, H. Seyedrezai, A model for the growth of solute clusters based on vacancy trapping, Scr. Mater. 61 (2009) 141–144.

[16] C.S.T. Chang, J. Banhart, Low-temperature differential scanning calorimetry of an Al-Mg-Si alloy, Metall. Mater. Trans. A Phys. Metall. Mater. Sci. 42 (2011) 1960–1964.

[17] A. Serizawa, S. Hirosawa, T. Sato, Three-Dimensional Atom Probe Characterization of Nanoclusters Responsible for Multistep Aging Behavior of an Al-Mg-Si Alloy, Metall. Mater. Trans. A. 39 (2008) 243–251.

[18] J.H. Kim, H. Tezuka, E. Kobayashi, T. Sato, Effects of Cu and Ag addition on nanocluster formation behavior in Al-Mg-Si alloys, Korean J. Mater. Res. 22 (2012) 329–334.

[19] M.W. Zandbergen, Q. Xu, A. Cerezo, G.D.W. Smith, Data analysis and other considerations concerning the study of precipitation in Al-Mg-Si alloys by Atom Probe Tomography, Data Br. 5 (2015) 626–641.

[20] C.S.T. Chang, I. Wieler, N. Wanderka, J. Banhart, Positive effect of natural pre-ageing on precipitation hardening in Al-0.44 at% Mg-0.38 at% Si alloy, Ultramicroscopy. 109 (2009) 585–592.

[21] M.W. Zandbergen, Q. Xu, A. Cerezo, G.D.W. Smith, Study of precipitation in Al-Mg-Si alloys by Atom Probe Tomography I. Microstructural changes as a function of ageing temperature, Acta Mater. 101 (2015) 136–148.

[22] L. Cao, P.A. Rometsch, M.J. Couper, Clustering behaviour in an Al-Mg-Si-Cu alloy during natural ageing and subsequent under-ageing, Mater. Sci. Eng. A. 559 (2013) 257–261.

[23] Y. Aruga, M. Kozuka, Y. Takaki, T. Sato, Formation and reversion of clusters during natural aging and subsequent artificial aging in an Al-Mg-Si alloy, Mater. Sci. Eng. A. 631 (2015) 86–96.

[24] F. De Geuser, W. Lefebvre, D. Blavette, 3D atom probe study of solute atoms clustering during natural ageing and pre-ageing of an Al-Mg-Si alloy, Philos. Mag. Lett. 86 (2006) 227–234.

[25] M. Murayama, K. Hono, Pre-precipitate clusters and precipitation processes in Al-Mg-Si alloys, Acta Mater. 47 (1999) 1537–1548.

[26] M. Torsæter, H.S. Hasting, W. Lefebvre, C.D. Marioara, J.C. Walmsley, S.J. Andersen, R. Holmestad, The influence of composition and natural aging on clustering during preaging in Al-Mg-Si alloys, J. Appl. Phys. 108 (2010).

[27] Y. Aruga, M. Kozuka, Y. Takaki, T. Sato, Evaluation of Solute Clusters Associated with Bake-Hardening Response in Isothermal Aged Al-Mg-Si Alloys Using a Three-Dimensional Atom Probe, Metall. Mater. Trans. A Phys. Metall. Mater. Sci. 45 (2014) 5906–5913.

[28] P. Dumitraschkewitz, S.S.A. Gerstl, P.J. Uggowitzer, J.F. Löffler, S. Pogatscher, Atom Probe Tomography Study of As-Quenched Al-Mg-Si Alloys, Adv. Eng. Mater. 19 (2017) 1600668.

[29] J.H. Kim, C. Daniel Marioara, R. Holmestad, E. Kobayashi, T. Sato, Effects of Cu and Ag additions on age-hardening behavior during multi-step aging in Al-Mg-Si alloys, Mater. Sci. Eng. A. 560 (2013) 154–162.

[30] Y. Yan, Investigation of the negative and positive effects of natural aging on artificial aging

response in Al-Mg-Si alloys, Technische Universität Berlin, 2014.

[31] S. Pogatscher, H. Antrekowitsch, P.J. Uggowitzer, Influence of starting temperature on differential scanning calorimetry measurements of an Al-Mg-Si alloy, Mater. Lett. 100 (2013) 163–165.

[32] C.D. Marioara, S.J. Andersen, J. Jansen, H.W. Zandbergen, The influence of temperature and storage time at RT on nucleation of the beta'' phase in a 6082 Al-Mg-Si alloy, Acta Mater. 51 (2003) 789–796.

[33] L. Cao, P.A. Rometsch, M.J. Couper, Effect of pre-ageing and natural ageing on the paint bake response of alloy AA6181A, Mater. Sci. Eng. A. 571 (2013) 77–82.

[34] Y.X. Lai, B.C. Jiang, C.H. Liu, Z.K. Chen, C.L. Wu, J.H. Chen, Low-alloy-correlated reversal of the precipitation sequence in Al-Mg-Si alloys, J. Alloys Compd. 701 (2017) 94–98.

[35] M. Saga, Y. Sasaki, M. Kikuchi, Z. Yan, M. Matsuo, Effect of pre-aging temperature on the behavior in the early stage of aging at high temperature for Al-Mg-Si alloy, Mater. Sci. Forum. 217–222 (1996) 821–826.

[36] Y. Birol, Pre-aging to improve bake hardening in a twin-roll cast Al-Mg-Si alloy, Mater. Sci. Eng. A. 391 (2005) 175–180.

[37] A.I. Morley, M.W. Zandbergen, A. Cerezo, G.D.W. Smith, The Effect of Pre-Ageing and Addition of Copper on the Precipitation Behaviour in Al-Mg-Si Alloys, Mater. Sci. Forum. 519–521 (2009) 543–548.

[38] W.F. Miao, D.E. Laughlin, Effects of Cu content and preaging on precipitation characteristics in aluminum alloy 6022, Metall. Mater. Trans. A. 31 (2000) 361–371.

[39] L. Zhen, S.B. Kang, The effect of pre-aging on microstructure and tensile properties of Al-Mg-Si alloys, Scr. Mater. 36 (1997) 1089–1094.

[40] C.D. Marioara, S.J. Andersen, J. Jansen, H.W. Zandbergen, Atomic model for GP-zones in a 6082 Al-Mg-Si system, Acta Mater. 49 (2001) 321–328.

[41] J. Buha, P.R. Munroe, R.N. Lumley, A.G. Crosky, A.J. Hill, Positron Studies of Precipitation in 6061 Aluminium Alloy, in: Proc. 9th Int. Conf. Alum. Alloy., 2004: pp. 1028–1033.

[42] L. Ding, Y. Weng, S. Wu, R.E. Sanders, Z. Jia, Q. Liu, Influence of interrupted quenching and pre-aging on the bake hardening of Al-Mg-Si Alloy, Mater. Sci. Eng. A. 651 (2016) 991–998.

[43] Y. Yan, Z.Q. Liang, J. Banhart, Influence of Pre-Straining and Pre-Ageing on the Age-Hardening Response of Al-Mg-Si Alloys, Mater. Sci. Forum. 794–796 (2014) 903–908.

[44] J. Buha, R.N. Lumley, A.G. Crosky, K. Hono, Secondary precipitation in an Al-Mg-Si-Cu alloy, Acta Mater. 55 (2007) 3015–3024.

[45] K. Yamada, T. Sato, A. Kamio, Effects of Quenching Conditions on Two-Step Aging

Behavior of Al-Mg-Si Alloys, Mater. Sci. Forum. 331–337 (2000) 669–674.

[46] S. Pogatscher, H. Antrekowitsch, H. Leitner, D. Pöschmann, Z.L. Zhang, P.J. Uggowitzer, Influence of interrupted quenching on artificial aging of Al-Mg-Si alloys, Acta Mater. 60 (2012) 4496–4505.

[47] M.A. Madanat, Microscopic Aspects of Ageing in Al-Mg-Si Alloys, Technische Universität Berlin, 2018.

[48] A. Falahati, P. Lang, E. Kozeschnik, Precipitation in Al-alloy 6016 – the role of excess vacancies, Mater. Sci. Forum. 706–709 (2012) 317–322.

[49] G.A. Edwards, K. Stiller, G.L. Dunlop, M.J. Couper, The precipitation sequence in Al-Mg-Si alloys, Acta Mater. 46 (1998) 3893–3904.

[50] H.W. Zandbergen, S.J. Andersen, J. Jansen, Structure determination of Mg5Si6:particles in Al by dynamic electron diffraction studies, Science. 277 (1997) 1221–1225.

[51] W.F. Miao, D.E. Laughlin, Precipitation hardening in aluminum alloy 6022, Scr. Mater. 40 (1999) 873–878.

[52] S. Esmaeili, X. Wang, D.J. Lloyd, W.J. Poole, On the precipitation-hardening behavior of the Al-Mg-Si-Cu alloy AA6111, Metall. Mater. Trans. A. 34 (2003) 751–763.

[53] S.J. Andersen, H.W. Zandbergen, J. Jansen, C. Træholt, U. Tundal, O. Reiso, The crystal structure of the β″ phase in Al-Mg-Si Alloys, Acta Mater. 46 (1998) 3283–3298.

[54] L. Resch, G. Klinser, E. Hengge, R. Enzinger, M. Luckabauer, W. Sprengel, R. Würschum, Precipitation processes in Al-Mg-Si extending down to initial clustering revealed by the complementary techniques of positron lifetime spectroscopy and dilatometry, J. Mater. Sci. 53 (2018) 14657–14665.

[55] T.E.M. Staab, R. Krause-Rehberg, U. Hornauer, E. Zschech, Study of artificial aging in AlMgSi (6061) and AlMgSiCu (6013) alloys by Positron Annihilation, J. Mater. Sci. 41 (2006) 1059–1066.

[56] L. Zhen, S.B. Kang, DSC analyses of the precipitation behavior of two Al-Mg-Si alloys naturally aged for different times, Mater. Lett. 37 (1998) 349–353.

[57] R. Vissers, M.A. van Huis, J. Jansen, H.W. Zandbergen, C.D. Marioara, S.J. Andersen, The crystal structure of the β′ phase in Al-Mg-Si alloys, Acta Mater. 55 (2007) 3815–3823.

[58] K. Matsuda, Y. Sakaguchi, Y. Miyata, Y. Uetani, T. Sato, A. Kamio, S. Ikeno, Precipitation sequence of various kinds of metastable phases in Al-1.0mass% Mg2Si-0.4mass% Si alloy, J. Mater. Sci. 35 (2000) 179–189.

[59] S. Esmaeili, D. Vaumousse, M.W. Zandbergen, W.J. Poole, A. Cerezo, D.J. Lloyd, A study on the early-stage decomposition in the Al-Mg-Si-Cu alloy AA6111 by electrical resistivity and three-dimensional atom probe, Philos. Mag. 87 (2007) 3797–3816.

[60] S. Esmaeili, D.J. Lloyd, W.J. Poole, Effect of natural aging on the resistivity evolution during artificial aging of the aluminum alloy AA6111, Mater. Lett. 59 (2005) 575–577.

[61] C.H. Liu, Y.X. Lai, J.H. Chen, G.H. Tao, L.M. Liu, P.P. Ma, C.L. Wu, Natural-aging-induced reversal of the precipitation pathways in an Al-Mg-Si alloy, Scr. Mater. 115 (2016) 150–154.

[62] C.D. Marioara, H. Nordmark, S.J. Andersen, R. Holmestad, Post-β″ phases and their influence on microstructure and hardness in 6xxx Al-Mg-Si alloys, J. Mater. Sci. 41 (2006) 471–478.

[63] P. Lang, Y. V. Shan, E. Kozeschnik, The life-time of structural vacancies in the presence of solute trapping, Mater. Sci. Forum. 794–796 (2014) 963–970.

[64] H.K. Hardy, The effect of small quantities of Cd, In, Sn, Sb, Tl, Pb or Bi on the ageing characteristics of cast and heat-treated Al-4%Cu-0.15%Ti alloy, J. Inst. Met. 78 (1950) 169–194.

[65] J.M. Silcock, The effect of quenching on the formation of G.P. zones and θ′ in Al Cu-alloys, Philos. Mag. 4 (1959) 1187–1194.

[66] R. Nagai, S. Tanigawa, M. Doyama, Study of aging of Al-Cu and Al-Cu-Sn alloys by positron annihilation, Scr. Metall. 10 (1976) 529–531.

[67] S.P. Ringer, K. Hono, T. Sakurai, The effect of trace additions of Sn on precipitation in Al-Cu alloys: An atom probe field ion microscopy study, Metall. Mater. Trans. A. 26 (1995) 2207–2217.

[68] J.. Silcock, H.. Flower, Comments on a comparison of early and recent work on the effect of trace additions of Cd, In, or Sn on nucleation and growth of θ′ in Al-Cu alloys, Scr. Mater. 46 (2002) 389–394.

[69] L. Bourgeois, C. Dwyer, M. Weyland, J.F. Nie, B.C. Muddle, The magic thicknesses of θ′ precipitates in Sn-microalloyed Al-Cu, Acta Mater. 60 (2012) 633–644.

[70] S. Pogatscher, H. Antrekowitsch, M. Werinos, F. Moszner, S.S.A. Gerstl, M.F. Francis, W.A. Curtin, J.F. Löffler, P.J. Uggowitzer, Diffusion on demand to control precipitation aging: Application to Al-Mg-Si alloys, Phys. Rev. Lett. 112 (2014).

[71] S. Muromachi, T. Mae, On the two-step aging behavior of Al-1.3 wt%Mg2Si alloy, J. Jap. Inst. Met. 38 (1974) 130–138.

[72] M. Werinos, H. Antrekowitsch, T. Ebner, R. Prillhofer, W.A. Curtin, P.J. Uggowitzer, S. Pogatscher, Design strategy for controlled natural aging in Al-Mg-Si alloys, Acta Mater. 118 (2016) 296–305.

[73] M. Werinos, H. Antrekowitsch, E. Kozeschnik, T. Ebner, F. Moszner, J.F. Löffler, P.J. Uggowitzer, S. Pogatscher, Ultrafast artificial aging of Al-Mg-Si alloys, Scr. Mater. 112 (2016) 148–151.

[74] C. Liu, P. Ma, L. Zhan, M. Huang, J. Li, Solute Sn-induced formation of composite β′/β″ precipitates in Al-Mg-Si alloy, Scr. Mater. 155 (2018) 68–72.

[75] R.C. Slaughter, Positron Annihilation Ratio Spectroscopy (PsARS) Applied to Positronium

Formation Studies, (2010).

[76] R. Krause-Rehberg, H.S. Leipner, Positron annihilation in semiconductors: defect studies, Springer-Verlag, Heidelberg, 1999.

[77] M.J. Puska, R.M. Nieminent, Defect spectroscopy with positrons: a general calculational method, 1983.

[78] M.J. Puska, P. Lanki, R.M. Nieminen, Positron affinities for elemental metals, J. Phys. Condens. Matter. 1 (1989) 6081–6093.

[79] G. Dlubek, S. Krause, H. Krause, A.L. Beresina, V.S. Mikhalenkov, K. V Chuistov, Positron studies of precipitation phenomena in Al-Li and in Al-LI-X (X=Cu, Mg or Sc) alloys, J. Phys. Condens. Matter. 4 (1992) 6317–6328.

[80] "Photomultipliertube." https://upload.wikimedia.org/wikipedia/commons/thumb/5/52/Photomultipliertube.svg/2000px-Photomultipliertube.svg.png.

5. Published parts of work

5.1 Paper I

Effect of Sn and In on the natural ageing kinetics of Al-Mg-Si alloys

Meng Liu[a, b, 1, *], Xingpu Zhang[b, 1], Benedikt Körner[b], Mohamed Elsayed[c, d], Zeqin Liang[e], David Leyvraz[e], John Banhart[a, b]

[a] Institute of Applied Materials, Helmholtz Centre Berlin for Materials and Energy, 14109 Berlin, Germany
[b] Department of Materials Science and Technology, Technical University of Berlin, 10623 Berlin, Germany
[c] Department of Physics, Martin Luther University Halle, 06120 Halle, Germany
[d] Department of Physics, Faculty of Science, Minia University, 61519 Minia, Egypt
[e] Novelis Research and Technology Center Sierre, 3960 Sierre, Switzerland

[1] Equal contribution of the authors

*corresponding author: meng.liu@helmholtz-berlin.de

DOI: 10.1016/j.mtla.2019.100261.

URL: https://www.sciencedirect.com/science/article/pii/S2589152919300572

Abstract

The deleterious effect of natural ageing (NA) on subsequent artificial ageing (AA) of Al–Mg–Si alloys can be markedly reduced by adding small amounts of impurities such as Sn or In owing to their strong interactions with vacancies. The retarding effect of Sn on clustering after quenching and during NA was verified in this study. The largest effect was found in a solute-lean Al–Mg–Si alloy containing 70 ppm Sn and solutionised at 570 °C. Employing the same strategy, the delayed clustering kinetics was also observed in alloys in which Sn was replaced by In. Based on the data obtained from positron annihilation lifetime, hardness and electrical resistivity experiments, we introduce some concepts describing the mechanisms of NA cluster formation in the presence of Sn or In based on vacancy-solutes interactions.

Keywords: Al–Mg–Si alloys; Cluster formation; Natural ageing kinetics; Sn addition; In addition; Positron annihilation lifetime spectroscopy

1. Introduction

Al–Mg–Si alloys (so called 6XXX series) have a wide range of applications and owe their strength to the hardening phase β'' that is formed during artificial ageing (AA) usually around 180 °C. The strengthening response, however, can be significantly and often "negatively" affected by the logistically unavoidable storage and corresponding natural ageing (NA) of the semi-manufactured products at "room temperature" (RT) prior to AA [1,2]. Researchers have attributed the slower and

less pronounced increase in hardness, which is directly correlated to the variation in number density and size of β'', to the formation of "deleterious" solute clusters during RT storage [3]. Although the exact details of the underlying microscopic processes remain unknown, a lot of effort has been spent on overcoming the adverse effect of NA and some efficient and effective methods have been developed including: (1) pre-ageing (PA) directly after quenching at an intermediate temperature such as 100 °C to form "favorable" PA clusters acting as nuclei for β'' [4,5]; (2) pre-straining (PS) to accelerate β'' formation through faster solute diffusion and nucleation on dislocations created by PS [6,7]; (3) the combination of PA and PS [8,9]; (4) reversion annealing after NA at temperatures above 225 °C for a short time to dissolve the NA clusters [10–12]; (5) employing interrupted quenching to inhibit the formation of "unfavorable" NA clusters by reducing the quenched-in vacancy concentration and possibly also the solute supersaturation [13]; (6) suppressing NA clustering by storing the material at temperatures below –40 °C [14]. Alternatively, there might be a much simpler and more cost-effective way to prevent excess vacancy-mediated diffusion during NA and to facilitate such diffusion during AA by adding just a few tens of ppm of micro-alloying elements such as Sn [15] or In. The strong binding energy between a vacancy and a Sn atom was proposed to explain the notable effect of Sn (and other elements) on NA/AA kinetics [16], without however providing the details of how Sn atoms influence NA clustering kinetics. Before applying this new design strategy for controlled NA in Al–Mg–Si alloys to real industrial production it is essential to make further efforts to investigate the controlling factors for clustering kinetics in considerable depth. In this work, positron annihilation lifetime spectroscopy (PALS), hardness (HV) and electrical resistivity measurements were applied to follow the microstructural changes during NA in a series of Al–Mg–Si alloys with or without Sn or In addition with the aim of improving the understanding of the mechanisms involved.

2. Experiments

Sn-containing pure ternary Al–Mg–Si alloys and Sn or In-containing commercial AA6014/AA6061 alloys were prepared by Novelis Research and Technology Center Sierre. Three further alloys – 6061(A), 6061–40Sn(A) and 6061–70Sn(A) – were provided by Stefan Pogatscher (results see supplementary material). After homogenization (10 h at 550 °C) and rolling, samples (10 × 10 × 1 mm^3 plates for PALS and HV, ø 0.82 mm wires for resistivity) were solutionized at 540 °C or 570 °C for 1 h, followed by ice-water quenching. Subsequent polishing (only for hardness measurements to achieve a mirror surface), cleaning, drying and assembling usually took 1 min to 2 min for PALS and resistivity and 5 min for hardness experiments. If not otherwise stated, the samples were naturally aged for various times and measured at 20 ± 2 °C. The chemical compositions were determined by atomic emission spectroscopy (AES) and inductively coupled plasma optical emission spectrometry (ICP-OES), as shown in Table 1.

Table 1. Composition of the alloys investigated (Sn and In in ppm, all others in at.%, * from Ref. [16], ** nominally as 6061(A)).

Designation	Mg	Si	Sn	In	Cu	Fe	Mn	Results in Fig.
4-4	0.44	0.37				0.03		1, 3, 5, S1, S2, S3
4-4-40Sn	0.49	0.39	40			0.03		1, 3, 5, S1, S2
4-4-70Sn	0.48	0.37	70			0.03		5, S2, S3
6-8	0.67	0.77	-			0.03		1, 2, 3, 4, 5, 7, S2, S3
6-8-40Sn	0.70	0.75	40			0.03		1, 2, 3,4, 5, 7, S2
6-8-70Sn	0.69	0.74	70			0.03		3, 4, 5, 7, S2, S3
6061(A)*	0.90	0.59			0.09	0.28	0.05	S4
6061-40Sn(A)	**	**	40		**	**	**	S4
6061-70Sn(A)	**	**	70		**	**	**	S4
6061	0.92	0.48			0.11	0.03		S3, S4
6061-70Sn	0.96	0.51	70		0.10	0.03		S3, S4
6014	0.72	0.58			0.05	0.09	0.04	8, S3
6014-40Sn	0.79	0.56	40			0.12	0.04	8
6014-70Sn	0.81	0.54	70			0.12	0.04	8, S3
6014-225In	0.83	0.58		225		0.13	0.04	8
6014-450In	0.81	0.58		450		0.13	0.04	8

Non-destructive positron annihilation lifetime spectroscopy was employed in this study to follow the formation and growth of solute clusters directly from the onset of NA after quenching and to benefit from its unique sensitivity to open volume defects such as quenched-in vacancies as one of the most important factors that affect diffusional processes in these alloys. To determine the positron lifetime (PLT) spectrum, the spectrometer described in a previous paper [17] was used. The fast data acquisition outlined in Refs. [17–19] was adopted in order to resolve clustering kinetics. After subtracting the background and contributions from the source itself, data were analyzed using the software LT9 [20]. The time resolution of the spectrometer is always sufficient for an analysis with only one-component positron lifetime τ_{1C} (as a rough measure of the weighted average PLT $\bar{\tau}$) and sometimes also suitable for constraint-free two-component fitting [19]. Whenever two lifetimes lie closer together, one of them should be fixed (yielding the so-called restricted two-component or 1½ component analysis) to minimize the uncertainties caused by decomposition [17]. In addition to PALS, hardness tests were also performed on an Anton Paar MHT-10 micro-hardness tester. A load of 0.98 N was applied for 10 s for each of ten indentations that were eventually averaged. The evolution of electrical resistivity was recorded in-situ using a standard 4-point method. The results are presented as the normalized increase of resistivity $\Delta\rho/\rho_0$ as a function of NA time. The curves were averaged/smoothed to show the trend in a clearer manner.

3. Results

3.1. Positron lifetime

3.1.1. One-component analysis

When commercial alloys are studied, the presence of impurities other than Sn complicates the situation. Therefore, it is essential to minimize the disturbance caused by such impurities in order to clarify the single effect of Sn on solute clustering. For doing this, pure Al-Mg-Si(Sn) alloys were used.

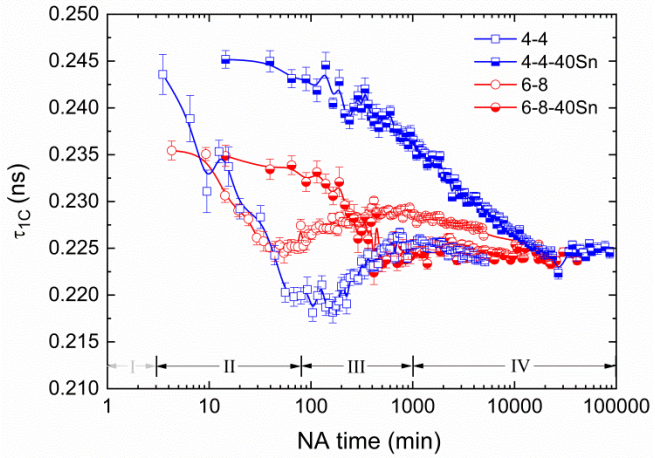

Fig. 1. Influence of 40 ppm Sn on the evolution of the one-component positron lifetime τ_{1C} in pure ternary 4-4 and 6-8 alloys during NA after quenching. The 4 different PLT stages in alloy 4-4 are marked.

The evolution of τ_{1C} is shown in Fig. 1 as a function of NA time. Both the alloys without Sn additions exhibit characteristic stages that had been previously observed [17,21,22] as explained in the discussion section. Sn addition markedly retards NA. Taking the transition time $t_{II\rightarrow III}$ between stages II to III as a measure, the NA kinetics for alloy 6-8-40Sn is ~10 times slower than for pure alloy 6-8 ($t_{II\rightarrow III}$ ~600 min vs. ~60 min). For alloy 4-4-40Sn, the retardation effect is even stronger, namely by a factor of 313 (25000 min vs. 80 min). Another observation is that Sn hardly affects the initial τ_{1C} for both sets of measurements as the curves start at τ_{1C} ~0.244 ns for alloys low in Mg and Si and at τ_{1C} ~0.235 ns for the other two. Moreover, the increase of τ_{1C} during stage III is much less pronounced in the two Sn-containing alloys.

The temperature dependence of τ_{1C} was studied since it yields additional information. It is known that τ_{1C} always decreases for decreasing measurement temperatures regardless of NA time in alloy 4-4. In terms of relative changes of τ_{1C} with respect to a reference temperature, e.g. −60 °C, $\Delta\tau_{1C}(T)$ shows the biggest variations after 5 min of NA [17]. The evolution of $\Delta\tau_{1C}(T)$ measured here for alloys 6-8 and 6-8-40Sn appears similar to that for 4-4 and compared to each other. Just the

NA times at which the variations of $\Delta\tau_{1C}(T)$ are maximal vary: 2 min for 6-8 and 100 min for 6-8-40Sn (see arrows in Fig. 2).

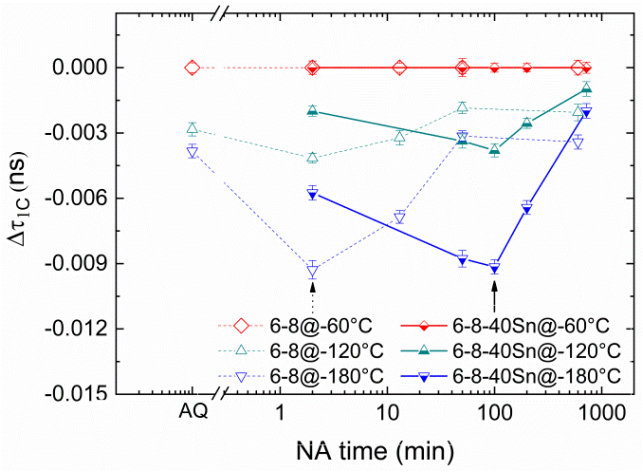

Fig. 2. Temperature dependence of τ_{1C} during NA of 6-8(40Sn) alloys. Low-temperature measurements were performed at 3 different temperatures (-60 °C, -120 °C, -180 °C) after previous NA for a time that can be read from the x-axis. The data for the 3 different measurement temperatures is presented as a difference to the values measured at -60 °C, i.e. $\Delta\tau_{1C}(T) = \tau_{1C}(T) - \tau_{1C}(-60\,°C)$. "AQ" denotes a sample that was solid-state quenched and was kept at low temperature throughout processing to avoid any exposure to "room temperature" [23].

3.1.2. Restricted two-component analysis

τ_{1C} represents a mixture of various lifetime components which we try to separate to improve the understanding of the interactions between Sn, Mg, Si and vacancies from the perspective of positrons. In this work, two competing lifetime components are separated, accordingly related to the presence of vacancy-solute complexes characterised by τ_v and I_v on the one hand and a mixture of solute clusters and free positron annihilation in the bulk characterised by τ_{f+s} and I_{f+s} on the other, see discussion section. None of the defects is distributed densely enough for saturated positron trapping, which is why the separation is possible. Fixing the component τ_v allows for a decomposition despite the low number of counts in the in-situ experiments.

Qualitatively, a similar evolution of decomposed positron lifetimes and intensities is observed in all the alloys: The component τ_{f+s} increases from an initial value well below 0.165 ns to ~0.210 ns (typical lifetime for solute clusters) and then levels off after a certain NA time. With the now improved spectrometer some new characteristics related to vacancies and solute clusters are found, namely, one can still observe some weak trends after the initial increase, e.g. a slight decrease and re-increase of τ_{f+s}after ~100 min of NA in alloy 4-4, see Fig. 3). The corresponding intensities I_{f+s} show at least 3 stages (increase, decrease and re-increase). $I_v = 1 - I_{f+s}$ for the vacancy component varies concurrently. As this has not been reported previously we repeated the experiment on various alloys 4-4 and 4-4-40Sn and found good reproducibility. Moreover, an experiment was carried out

using a spectrometer with a higher resolution and a higher count rate at the University of Halle. Beside the same analysis as for the data shown in Fig. 3, we also varied some of the assumptions for data analysis to confirm the decrease of cluster fraction, see Figs. S1 – S3.

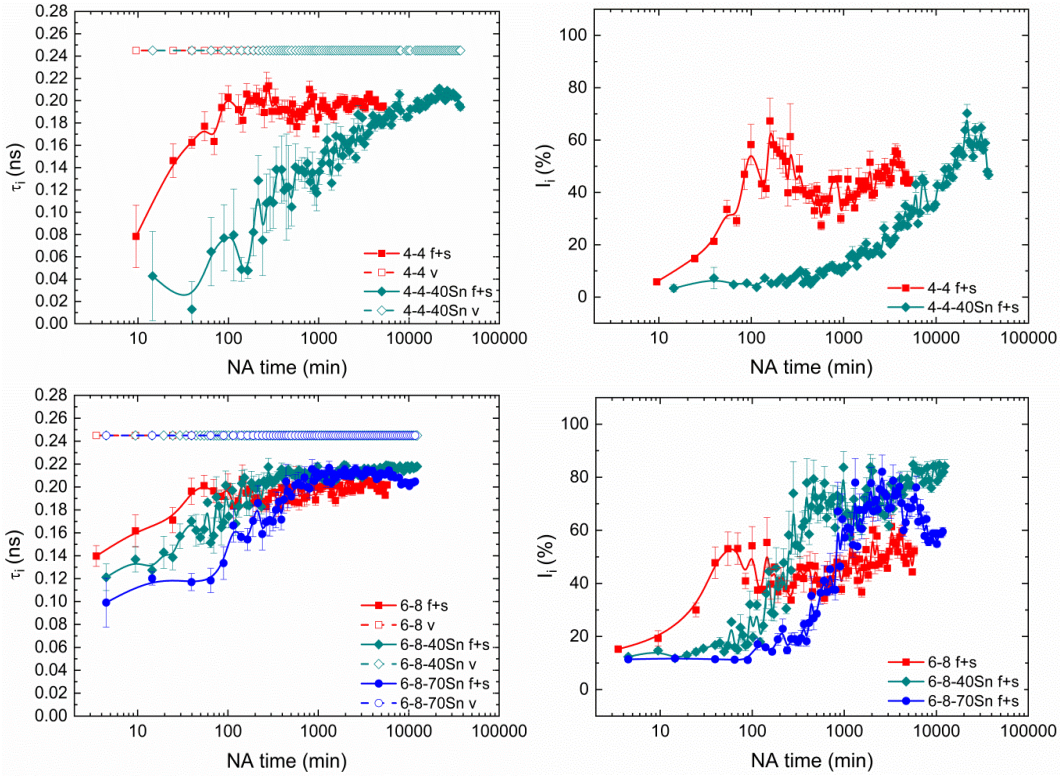

Fig. 3. Evolution of decomposed lifetime components τ_i (left column) and corresponding intensities I_i (right column) in 4-4 and 4-4-40Sn (upper row) or 6-8 and 6-8-40/70Sn (lower row) alloys during NA after quenching. Due to the limited time resolution of the spectrometer used, the lifetimes related to vacancy-type defects were fixed to 0.245 ns. All intensities $I_v = 1 - I_{f+s}$ were not shown in order to present I_{f+s} in a clearer manner.

With Sn added, τ_{f+s} starts with a lower initial value (pointing at a relatively higher annihilation in the bulk) and it requires much more time to reach the final level of PLT. The differences in ageing kinetics between these alloys are also clearly reflected by the intensity variations, e.g. the time at which I_{f+s}starts to decrease of alloys 6-8-40Sn and 6-8-70Sn are ~600 min and ~2500 min, resp., much longer than the one in alloy 6-8 (~60 min). These times roughly correspond to the transition times $t_{II \rightarrow III}$ in Fig. 1. The same holds for the 4-4 and 4-4-40Sn alloys.

The evolution of τ_{f+s} and I_{f+s} as a function of NA time appears different in Fig. 3 for the different Sn contents, but when displaying τ as a function of I (thus eliminating NA time) qualitatively the same pattern is found in all cases, see Fig. 4.

3.2. Hardness and resistivity

It was found that the retardation effect of Sn is stronger if the solution heat treatment (SHT) temperature and/or the Sn content is high as reported previously [16,24], see the evolution of hardness as shown in Fig. S5. Fig. 5 shows that in very early stages of NA, measurable changes in resistivity are observed for all the alloys, implying that clustering already sets in also in the Sn-containing alloys (e.g. alloys 4-4-40/70Sn) although no hardness increase is observed during this period. There is no sign of acceleration of resistivity increase throughout NA on a linear time scale (see Fig. S6a), indicating that ageing proceeds continuously and resistivity changes at the highest rate directly after quenching.

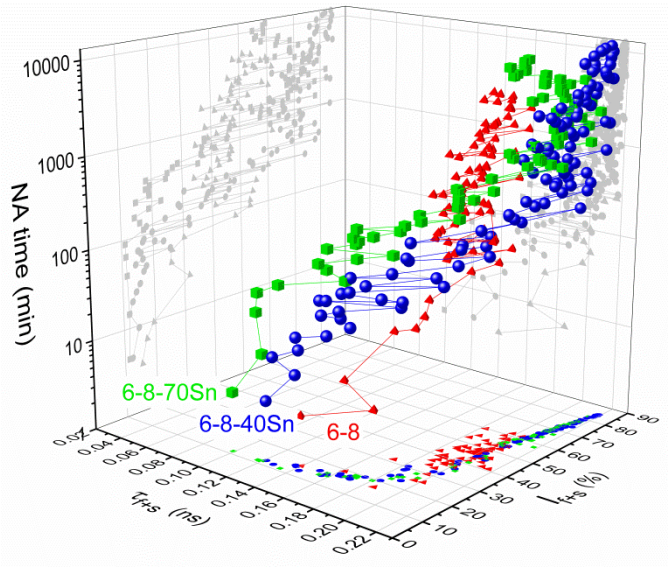

Fig. 4. 3D representation of the evolution of decomposed PLT components in alloys 6-8 and 6-8-40/70Sn during NA. PLTs τ_{f+s} are shown as a function of their corresponding intensities I_{f+s}.

Despite of the individual sensitivity of the methods applied, the general retardation effect due to increasing Sn-content as observed by resistivity and hardness measurements is analogous to the PALS observations: For alloy 4-4, an increase from 40 ppm to 70 ppm Sn delays the increase in resistivity and hardness by approximately the same factor of 7, while for alloy 6-8, this factor is 2. This also confirms that Sn addition just slows down clustering while the general characteristics are maintained.

Moreover, some one-component lifetimes of Fig. 1 are compared to the averages calculated from Fig. 3 in Fig. S4.

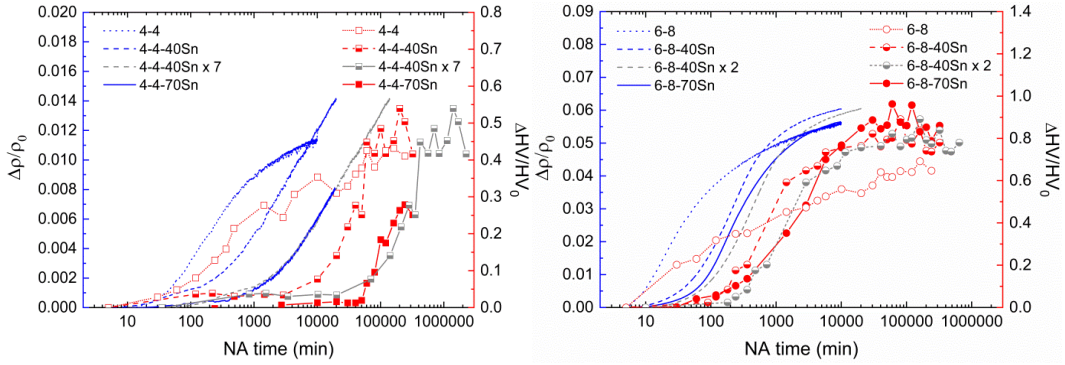

Fig. 5. Influence of Sn content (40 and 70 ppm) on resistivity (blue curves) and hardness (red symbols, same data as in Fig. S5) evolution of 4-4-40/70Sn (l.h.s.) and 6-8-40/70Sn (r.h.s.) alloys during NA (SHT temperature = 570 °C). The values for Sn-free 4-4 and 6-8 alloys are also given for comparison. Grey curves/symbols are resistivity/hardness curves of 4-4-40Sn/6-8-40Sn alloys delayed by a factor given in the legend. They overlap with the undelayed ones of 4-4-70Sn/6-8-70Sn alloys. No scatter bars are shown to present the data in a clearer manner.

4. Discussion

4.1. Mechanism of cluster formation and growth

After and possibly during quenching solute clusters form and grow via diffusion of solutes aided by vacancies. The rate of such processes depends on both the vacancy concentration and the activation energy of solute migration Vacancies transport solute atoms to other atoms to form solute clusters, and after spending a certain time at or in the clusters they eventually detach to diffuse to new solute atoms, an idea called the "vacancy-pump model" [25]. A vacancy may be repeatedly trapped by and released from a cluster. The probability for a vacancy to escape from a cluster and re-enter the matrix in the simplest model scales with $\exp(-ncE_b/kT)$, with n the number of atoms in that cluster, c a constant and E_b the binding energy between a vacancy and a solute atom [26], which explains the fast formation of clusters during early stages of NA, followed by a stage of slower cluster growth as vacancies are bound in clusters and lost to sinks. Because the fraction of vacancies is so low compared to that of solute atoms and clusters most clusters are vacancy-free at any time and contain vacancies only temporarily [17,21].

4.2. General interpretation of PLT evolution in Al, Al-Mg/Si and Al-Mg-Si alloys

It has been reported that a fraction of ~2×10^{-5} atom^{-1} (theoretically up to 1.4×10^{-4} atom^{-1} [27]) of mono-vacancies are preserved in as-quenched pure aluminium [19]. Vacancies will partially diffuse to the nearest sinks and disappear during NA [28,29], the rest form small but stable vacancy clusters (~3 on average as estimated from [19] or more according to calculations [30]) but the exact nature of inter-vacancy interaction forces is still disputed [31-33].

In binary Al-Mg and Al-Si alloys, vacancy–solute complexes and/or clusters containing various vacancies are formed after quenching, depending on the type of solute and its content [19]. This can

be explained by the interactions between vacancies and solute atoms. Solute clustering is weak due to calculated repulsive interactions between Mg-Mg and Si-Si (binding energies of –0.037 eV and –0.025 eV, respectively, Table. 2) [34,35] and experimental data [19,36,37].

For ternary Al-Mg-Si alloys, clustering is more complicated. Binding between Mg-Si appears favourable from atomistic calculations [34]. Taking into account the mentioned repulsive interactions between Mg-Mg and Si-Si, solute-vacancy complexes and Mg-Si clusters will be formed in ternary Al-Mg-Si alloys during NA, while vacancies can hardly aggregate not only due to the strong binding with the now also formed Si-Mg clusters but also due to the very high solute/vacancy ratio. Such processes were observed by PALS [21] and the characteristic stages of alloy 4-4 are also shown in Fig. 1. It was postulated that the complex pattern of τ_{1C} evolution observed is the result of interactions between vacancies and solute atoms or clusters, more specifically, the decrease, increase and re-decrease of positron lifetime during stages II, III and IV is correlated with the formation, growth and coarsening or ordering of solute clusters, respectively. In the light of the present new measurements based on a higher resolution spectrometer, stages II and III shall be discussed below.

4.2.1. PALS stage II

τ_{1C} during PALS stage II evolves due to at least two types of competing positron traps, vacancy-solute complexes and vacancy-free coherent solute clusters [17]. Initially formed solute clusters contribute only little to τ_{1C}. As more clusters form and grow during stage II, they increasingly gain the capability to trap positrons and I_{f+s} increases at the cost of I_v, as shown in Fig. 3, augmented also by the increasing binding energies with positrons. The decrease of τ_{1C} upon cooling in Fig. 2 is caused by the different positron trapping properties of vacancy-solute complexes and initial (small) solute clusters. While trapping in vacancy-related defects is strong at any temperature, and that in clusters is higher at low temperatures where positrons have lowered energies and are less likely to escape the trap. Immediately after quenching, trapping is mostly in vacancies and only the small temperature dependence for the as-quenched alloy 6-8 (less for 4-4) indicates that some clusters must have formed during quenching. During ensuing NA the formation of solute clusters is responsible for the increasing temperature dependence, which peaks after an intermediate NA time, after which the temperature variations get smaller again due to the increasing dominance of solute clusters in trapping positrons at any temperature.

4.2.2. PALS stage III

How vacancies and solute clusters further evolve during PALS stage III is not known with certainty. Based on atom probe measurements [38], ^{25}Mg-NMR [39], Doppler broadening spectroscopy and

PALS observations [23] as well as our Kinetic Monte Carlo calculations (unpublished) and Phase Field Crystal calculations [40], incorporation of Mg into previously formed Si-Mg clusters appears plausible. The associated higher Mg/Si ratio of the clusters together with the larger atomic size and lower electron density of Mg atoms than Si leads to the increase of τ_{1C} with corresponding PLTs approaching ~0.220 ns. The closer this component lies together with the one of vacancy-type defects (0.245 ns), the more likely they appear as one component. Thus, because of insufficient time resolution, we previously failed to decompose the PLT spectra for stage III, i.e. just one component was found.

As the absolute concentration of vacancy-type defects cannot increase during NA, the course of intensities in Fig. 3 must arise from the decrease in cluster site fraction – large clusters consuming smaller clusters already formed in their vicinity. As a result, fewer but larger clusters are formed. As the site fraction of clusters decreases one expects a decrease of τ_{f+s} since it represents an average of annihilation in clusters and free positron annihilation in the bulk. This is what we see in Fig. 3 between 150 min and 700 min for alloy 4-4 (decrease from about 0.203 ns to 0.185 ns) and for alloy 4-4-40Sn (similar decrease from 8000 min onward).

The decrease of cluster site fraction has been confirmed by Monte Carlo calculations [41] and by more elaborate Phase Field Crystal (PFC) calculations [40]. However, most atom probe measurements [42,43] do not show coarsening with the exception of a Cu-containing alloy 6111 in which after 100 hours a slight decrease of number density of Mg-Si clusters has been measured [44]. One reason is that PALS is more sensitive than APT to very small clusters, which are more prone to coarsen than larger ones and also to the fact that APT data is rarely available for short NA times. Therefore, the increase of positron lifetime in stage III is caused by two mechanisms, enrichment of Mg and coarsening of the cluster population.

Clusters or precipitates are potential positron traps provided that a critical size has been reached. The positron wave function is spread over the entire trap. However, if a cluster or precipitate contains open volume defects such as a vacancy, then positrons will be strongly localized at the site of the vacancy. Thus, the annihilation parameters will exhibit the characteristic signals of this inner defect due to the strong confinement of the positron wave function [45]. At the early stage of NA, most of the solute clusters are vacancy-free at a given time, but a vacancy-free solute cluster can temporarily turn into a vacancy-containing one, after which it converts back into a vacancy-free cluster. Some vacancies will be almost permanently trapped by clusters after a certain NA time. In this case, these clusters will be more “vacancy”-type and can no longer be regarded as pure solute clusters, which will also contribute to the decrease in number density of the “real” clusters (decreasing I_{f+s}).

4.3. Effects of Sn on the early stage of clustering

To discuss the effect of Sn on clustering, knowing the binding energies between a vacancy and various kinds of solutes and between solutes is useful. We adopt the values given in Table 2 in this study that were determined on an equal footing by using first-principles analysis [46].

The interaction energy between a vacancy and a Sn atom is ~10 times higher than with either Mg or Si. Although Si, Ge and Sn all belong to group IV of the periodic table, i.e. the same effective valence, the binding energy of V-Sn and V-Ge is much higher than V-Si, which might be a size effect [47].

The solute-solute interactions Si-Si, Mg-Mg, and Si-Sn in Al were found to be all negative (repulsive) or neutral, while for Si-Mg and Mg-Sn, attractive interactions were calculated, see Table 2.

Table 2. Interaction energies (eV) for solute-solute [34] and vacancy-solute [46] complexes. Note that the exact values differ between various sources and that for V-Mg even a repulsive interaction has been claimed) [48].

Solute-solute	Si-Si	Mg-Mg	Si-Mg	Si-Sn	Mg-Sn	Sn-Sn
Interaction energy	–0.025	–0.037	+0.042	0	+0.1	n.a.

Vacancy-solute	V-Si	V-Mg	V-Sn
Interaction energy	+0.033	+0.026	+0.281

4.3.1. Cluster formation in the presence of Sn

The task now is to set up a scenario of how Sn atoms suppress clustering on the basis of PALS, hardness and resistivity experiments in analogy to the influence of Cu on NA kinetics in Al-Mg-Si alloys discussed earlier [18].

- **Sn-free clusters** (green routes in Fig. 6)

The formation of solute clusters is much faster in pure Al-Mg-Si alloys than in Sn-containing ones (see the green route 1-2-3-4 in Fig. 6). In the presence of Sn, a considerable fraction of the vacancies preferentially bind with Sn atoms, forming V-Sn complexes in addition to V-Si and V-Mg. Such vacancies will be immobilised by Sn atoms due to the much stronger interaction energy between V-Sn than V-Si and V-Mg and only a limited amount of vacancies are able to bind with Si/Mg atoms and to assist their migration and Mg-Si clustering will be sluggish. Even if all vacancies bound with Si and Mg atoms (the content of Si and Mg is much higher than Sn) and assisted them in forming Sn-free Si-Mg clusters, the migration of V-Si and V-Mg complexes would be notably slowed down if a Sn atom was located in their vicinity as a result of the attractive

binding between V-Sn and Mg-Sn (see the interaction field of the Sn atom in Fig. 6). This is highly likely since the distances between vacancies and solutes atoms or clusters are small in the initial stage of NA. Each vacancy has to repeatedly transport Si and Mg atoms to the cluster. Thus, the influence of Sn on clustering would be much larger than expected from its low concentration because every time a vacancy detaches from a cluster it can be temporarily trapped by a Sn atom with a certain probability.

- **Sn-containing clusters (orange routes in Fig. 6)**

Not only Sn but also Cu (and Au [49]) exhibit a similar effect in trapping vacancies and retarding NA of Al alloys as found by PALS [18], electrical resistivity [50] and hardness measurement [51]. The common feature among these solute additions is that they all have stronger binding energies with vacancies [34,46,48] than the main alloying elements. A difference is that the vacancy can still escape from a Cu atom or Cu-containing cluster and further assist solute diffusion in a reasonable time, while for Sn, the release of vacancies is more unlikely due to their even stronger interactions with Sn (0.281 eV) than with Cu (0.124 eV [52]). This is supported by the suppressed formation of Cu clusters or GP zones in an Al-Cu-Sn alloy [53]. Furthermore, although the interaction between Si-Cu is repulsive (–0.038 eV [34]), considerable amounts of Cu-containing Si-Cu, Mg-Cu and Si-Mg-Cu in addition to pure Si-Mg clusters were identified after 2 h of NA in an Al-Mg-Si alloy using atom probe tomography [44]. In analogy, except for Mg-Mg, Si-Si (repulsive) and Si-Sn (neutral), all other solute-solute (Mg-Si and Mg-Sn)/vacancy-solute (V-Mg and V-Si) interaction energies were found to be attractive, thus, pointing at the possibility of also Sn incorporation into clusters in Al-Mg-Si-Sn alloys. Such Sn-containing clusters might be even stronger containment of vacancies than single Sn atoms. The probability of "permanent" trapping of vacancies increases with the number of Sn atoms (also Mg and Si) in the clusters. Therefore, to simplify the discussion in this study, we firstly assume that once a vacancy is bound to a Sn atom or Sn-containing clusters, it cannot detach thereafter to transport the next solute atom as a bare vacancy (see dashed arrow iii in Fig. 6), i.e. V-Sn complexes have very limited capacity in returning a vacancy to the matrix, i.e. vacancy pumping is inhibited.

All processes involving Sn are shown as orange routes in Fig. 6 (i-ii-iii, 1-2′, 1-2″-5, 1-2-3-4-1′ and 1-2-3-4-1″-ii). Step iii is clearly the rate-limiting process. The time needed for step ii depends on the mobility of Sn-vacancy complexes. The diffusion coefficient D of Sn in Al matrix is known to be ~18 times higher than that of Al at ~344 °C [31,54], but extrapolation to 20 °C is not possible. If the mobility was low at 20 °C step ii would further reduce the clustering rate, otherwise Sn-vacancy complexes would capture Mg or Si atoms and then become immobile.

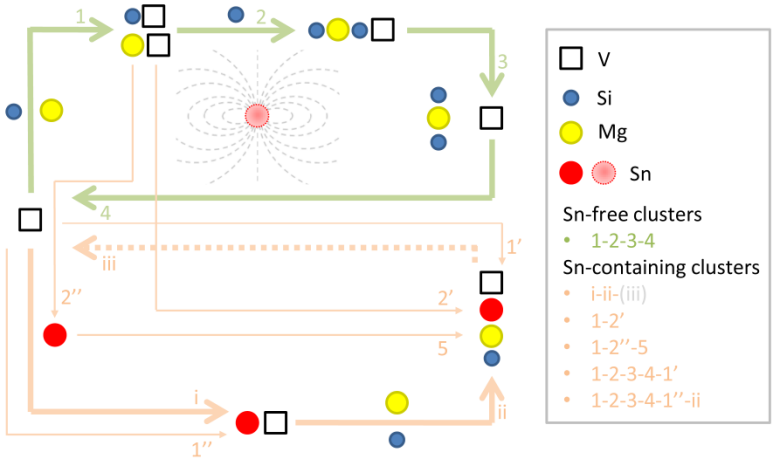

Fig. 6. Schematic illustration of the formation processes of Sn-free (green, vacancy-pump effective) and Sn-containing (orange, vacancy-pump delayed) clusters. Blue, yellow and red spheres accordingly denote Si, Mg and Sn atoms, while black open squares correspond to vacancies. The main clustering processes are indicated by the large green (Sn-free) and orange (Sn-containing) arrows, while the interaction between a vacancy/vacancy-solute complex and a Sn atom/Sn-containing cluster during or after the formation of Sn-free clusters is indicated by the small orange arrow. The potential influence induced by Sn (other than forming a vacancy-Sn complex, light red sphere) is illustrated by gray dashed field lines. The exact number of solute atoms which are associated to the vacancy or clusters cannot be specified in this figure. To simplify the discussion, the formation of 2V-Sn will not be addressed in this work.

The above propositions clearly imply that at RT, the combined effects of "permanent" trapping of vacancies by Sn atoms or Sn-containing clusters, the plausible slow diffusivity of V-Sn complexes at RT and the reduced migration rate of vacancies (V-Si/Mg complexes) due to the neighbouring Sn atoms would certainly give rise to a reduced rate of clustering. As a result, small vacancy-containing Si-Mg-Sn and Si-Mg clusters are slowly formed in the presence of Sn, since each vacancy can only transport very limited amount of solutes to form clusters [55]. Thus, based on the similar clustering characteristics among such alloys as shown in Fig. 2, it appears that Sn additions merely and continuously influence clustering kinetics from the onset of NA. However, Sn addition cannot prohibit clustering during quenching, as indicated by the similar T-dependences for both as-quenched samples as shown in Fig. 2, since the binding between the vacancies and Sn atoms becomes much weaker at elevated temperatures during quenching.

4.3.2. Comparison between low-T ageing and micro-alloying element addition

The key to suppress NA clustering lies in controlling vacancy-assisted diffusion of solute atoms. Beside by adding Sn, this can also be achieved, for instance, by processing an alloy at low temperatures. As shown in Fig. 7, ageing alloy 6-8 at 0 °C is almost equivalent to adding 40 ppm or 70 ppm Sn, pointing at the fact that both methods seem to affect solute clustering in an identical manner.

The normalized resistivity changes at low temperatures are smaller than those aged at high temperatures, but after certain ageing times, this trend is reversed, see crossovers in Fig. 7, an effect noted before [57]. According to Ref. [58,59] and to a study of precipitate evolution in Al-Zn alloys by first-principles [60], at a given time, ageing an alloy at lower temperatures gives rise to smaller but more densely distributed precipitates than at higher temperature. As electrons are more efficiently scattered by many small clusters than from fewer and larger ones, the crossovers shown in Fig. 7 appear plausible. Extending this picture to the case of Sn addition we suspect that Sn not only delays clustering but also leads to a higher number density of smaller clusters after a long NA time in both 4-4 and 6-8 based alloys.

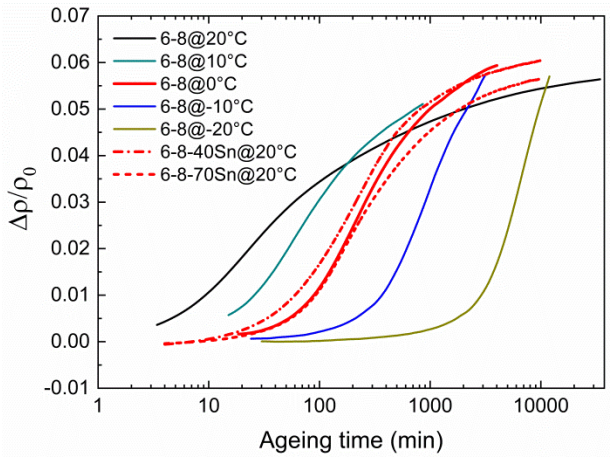

Fig. 7. Comparison between the effects of ageing temperature (solid lines) and Sn additions (dashed lines) on normalized resistivity changes in alloys 6-8, 6-8-40Sn and 6-8-70Sn. Resistivity data is taken from Ref. [56].

4.3.3. Influence of Mg/Si ratio, main alloying element content and impurities

In addition to Sn content and SHT temperature as reported by [16,24], there are other factors which may directly/indirectly influence the retardation effect of Sn on solute clustering including, but not limited to, Mg/Si ratio, Mg and Si content as well as impurities such as Fe and Mn. A comparison is made using both pure alloys and commercial alloys to clarify their respective effects on cluster formation, see Fig. S6 and Fig. S7.

4.4. NA kinetics of In-containing Al-Mg-Si alloys

In atoms in an aluminium matrix bind strongly with vacancies (~0.2 eV [48]), and the diffusion properties are similar to Sn [31], while the solubility of In in Al is even higher than Sn. Therefore, In should retard natural ageing too. Three 6014 alloys – with and without In additions – were investigated, see Fig. 8.

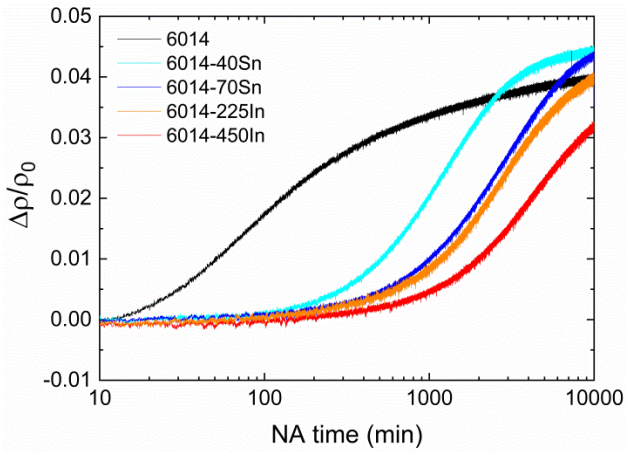

Fig. 8. Evolution of normalized resistivity changes in 6014 alloys with and without In addition, as compared to Sn-added ones.

Resistivity data shows that NA kinetics in 6014 alloy is delayed for >1 day (determined by the time where an increase of $\Delta\rho/\rho_0 = 0.005$ has been reached) with 225/450 ppm of In addition. Our results are supported by a recent study on a 6061 alloy containing both Sn and In, where a slower evolution in HV was observed than in the Sn-added one [58]. Compared to Sn, the effect of 225 ppm In is even stronger than both 40 ppm and 70 ppm Sn. It is highly likely that a much larger fraction of the quenched-in vacancies is trapped by In atoms than by Sn due to the higher site fraction of solutes. Fig. 8 also shows crossover of the resistivity curves with and without In. The reasons for this should be the same as for Sn.

5. Conclusions

We investigate various Sn and In-containing Al-Mg-Si alloys by applying positron annihilation lifetime spectroscopy (PALS), hardness and electrical resistivity measurement and find:

- Even small additions of Sn or In retard clustering kinetics in Al-Mg-Si alloys during NA by sometimes orders of magnitudes in accordance with the literature.
- Positron lifetime measurements show that Sn does not change the basic clustering path. Especially clustering shortly after quenching is simply delayed in Sn-containing alloys. Only in later stages, deviations occur, for example, stage III is less pronounced when Sn is present.
- It is found that in stage III cluster coarsening takes place in addition to the earlier postulated enrichment of clusters in Mg. This, however, is not reflected by published atom probe data.
- In all alloys, resistivity increases before hardness during natural ageing, indicating that the first clusters formed are too small to influence hardness but already scatter electrons.
- Sn addition to an alloy has a similar retarding effect on clustering as lowering the ageing temperature. Smaller but more densely distributed clusters are formed both due to Sn addition and to lowered temperature.

Acknowledgements

The Deutsche Forschungsgemeinschaft (DFG) funded this project (Ba 1170/22). Xingpu Zhang thanks the China Scholarship Council (CSC) for a research fellowship. Support from Prof. S. Pogatscher (Montanuniversität Leoben) and Prof. R. Krause-Rehberg (University Halle) is gratefully acknowledged.

References

[1] M.L.V. Gayler, G.D. Preston, The age-hardening of some aluminium alloys, J. I. Met. 41 (1929) 191–247.

[2] D.W. Pashley, J.W. Rhodes, A. Sendorek, Delayed ageing in aluminium-magnesium-silicon alloys: effect on structure and mechnical properties, J. I. Met. 94 (1966) 41–49.

[3] I. Kovács, J. Lendvai, E. Nagy, The mechanism of clustering in supersaturated solid–solutions of Al-Mg2Si alloys, Acta Metall 20 (1972) 975–983.

[4] H. Suzuki, M. Kanno, G. Itoh, A consideration of the two-step ageing process in Al-Mg-Si alloys, Aluminium 57 (1981) 628–629.

[5] L. Zhen, S.B. Kang, The effect of pre-aging on microstructure and tensile properties of Al-Mg-Si alloys, Scripta Mater 36 (1997) 1089–1094.

[6] R.S. Yassar, D.P. Field, H. Weiland, The effect of cold deformation on the kinetics of the beta" precipitates in an Al-Mg-Si alloy, Metall. Mater. Trans. A 36A (2005) 2059–2065.

[7] Y. Birol , Pre-straining to improve the bake hardening response of a twin-roll cast Al-Mg-Si alloy, Scripta Mater 52 (2005) 169–173.

[8] T. Masuda, Y. Takaki, T. Sakurai, S. Hirosawa, Combined effect of pre-straining and pre-aging on bake-hardening behavior of an Al-0.6 mass%Mg-1.0 mass%Si alloy, Mater. Trans. 51 (2010) 325–332.

[9] Y. Yan, Z.Q. Liang, J. Banhart, Influence of pre-straining and pre-ageing on the age hardening response of Al-Mg-Si alloys, Mater. Sci. Forum 794-796 (2014) 903–908.

[10] C. Haase, H. Wurst, Zur Frage der Kalt- und Warmaushärtung bei Aluminium-Mag- nesium-Silizium-Legierungen, Z. Metallkd. 33 (1941) 399–403.

[11] Y. Birol, Restoration of the bake hardening response in a naturally aged twin-roll cast AlMgSi automotive sheet, Scripta Mater 54 (2006) 2003–2008.

[12] M. Madanat, M. Liu, J. Banhart, Reversion of natural ageing in Al-Mg-Si alloys, Acta Mater 159 (2018) 163–172.

[13] S. Pogatscher, H. Antrekowitsch, H. Leitner, D. Poschmann, Z.L. Zhang, P.J. Uggowitzer, Influence of interrupted quenching on artificial aging of Al-Mg-Si alloys, Acta Mater 60 (2012) 4496–4505.

[14] J. Royset, T. Stene, J.A. Seater, O. Reiso, The effect of intermediate storage temper- ature and time on the age hardening response of Al-Mg-Si alloys, Mater. Sci. Forum 519-521 (2006) 239–244 .

[15] S. Muromachi, T. Mae, On the two-step aging behavior of Al-1.3 wt%Mg2Si alloy, J. Jpn. I. Met. 38 (1974) 130–138.

[16] S. Pogatscher, H. Antrekowitsch, M. Werinos, F. Moszner, S.S.A. Gerstl, M.F. Francis, W.A. Curtin, J.F. Löffler, P.G. Uggowitzer, Diffusion on demand to control precipitation aging: application to Al-Mg-Si alloys, Phys. Rev. Lett. 112 (2014) 225701.

[17] M. Liu, J. Či ž ek, C.S.T. Chang, J. Banhart, Early stages of solute clustering in an Al-Mg-Si alloy, Acta Mater 91 (2015) 355–364.

[18] M. Liu, J. Banhart, Effect of Cu and Ge on solute clustering in Al-Mg-Si alloys, Mater. Sci. Eng. A 658 (2016) 238–245.

[19] M. Liu, B. Klobes, J. Banhart, Positron lifetime study of the formation of vacancy clusters and dislocations in quenched Al, Al-Mg and Al-Si alloys, J. Mater. Sci. 51 (2016) 7754–7767.

[20] J. Kansy, Microcomputer program for analysis of positron annihilation lifetime spectra, Nucl. Instru. Meth. Phys. Res. A 374 (1996) 235–244.

[21] J. Banhart, M.D.H. Lay, C.S.T. Chang, A.J. Hill, Kinetics of natural aging in Al-Mg-Si alloys studied by positron annihilation lifetime spectroscopy, Phys. Rev. B 83 (2011) 014101.

[22] J. Banhart, C.S.T. Chang, Z.Q. Liang, N. Wanderka, M.D.H. Lay, A.J. Hill, Natural aging in Al-Mg-Si alloys - A process of unexpected complexity, Adv. Eng. Mater. 12 (2010) 559–571.

[23] M. Liu, Clustering kinetics in Al-Mg-Si alloys investigated by positron annihilation techniques Ph.D. thesis, Technische Universität, Berlin, 2014 .

[24] M. Werinos, H. Antrekowitsch, T. Ebner, S. Pogatscher, Design strategy for controlled natural aging in Al-Mg-Si alloys, Acta Mater 118 (2016) 296–305.

[25] I.A. Girifalco, H. Herman, A model for growth of Guinier-Preston zones - Vacancy pump, Acta Metall 13 (1965) 583–590.

[26] H.S. Zurob, H. Seyedrezai, A model for the growth of solute clusters based on vacancy trapping, Scripta Mater 61 (2009) 141–144.

[27] G. Gottstein, Physical Foundations of Materials Science, Springer-Verlag, Berlin, Heidelberg, 2004 .

[28] F.D. Fischer, J. Svoboda, F. Appel, E. Kozeschnik, Modeling of excess vacancy annihilation at different types of sinks, Acta Mater 59 (2011) 3463–3472.

[29] C. Panseri, T. Federighi, Isochronal annealing of vacancies in aluminium, Philos. Mag. 3 (1958) 1223–1240.

[30] H. Wang, D. Rodney, D.S. Xu, R. Yang, P. Veyssière, Defect kinetics on experimental timescales using atomistic simulations, Philos. Mag. 93 (2013) 186–202.

[31] P. Ehrhart, P. Jung, H. Schultz, H. Ullmaier, Atomic Defects in Metals, Landolt-Börnstein, New Series, Group III, Springer-Verlag, Berlin, 1991.

[32] V. Gavini, K. Bhattacharya, M. Orti, Vacancy clustering and prismatic dislocation loop formation in aluminum, Phys. Rev. B 76 (2007) 180101.

[33] G. Ho, M.T. Ong, K.J. Caspersen, E.A. Carter, Energetics and kinetics of vacancy diffusion and aggregation in shocked aluminium via orbital-free density functional theory, Phys. Chem. Chem. Phys. 9 (2007) 4951–4966.

[34] S. Hirosawa, F. Nakamura, T. Sato, First-principles calculation of interaction energies between solutes and/or vacancies for predicting atomistic behaviors of microalloying elements in aluminum alloys, Mater. Sci. Forum 561-565 (2007) 283–286.

[35] Z.Q. Liang, C.S.T. Chang, C. Abromeit, J. Banhart, J. Hirsch, The kinetics of clustering in Al-Mg-Si alloys studied by Monte Carlo simulation, Int. J. Mater. Res. 103 (2012) 980–986.

[36] A.K. Gupta, D.J. Lloyd, Study of precipitation kinetics in a super purity Al-0.8 Pct Mg-0.9 Pct Si alloy using differential scanning calorimetry, Metall. Mater. Trans. A 30 (1999) 879–884.

[37] G. Thomas, Quenching defects in binary aluminium alloys, Philos. Mag. 4 (1959) 1213–1228 .

[38] A. Serizawa, S. Hirosawa, T. Sato, Three-dimensional atom probe characterization of nanoclusters responsible for multistep aging behavior of an Al-Mg-Si alloy, Metall. Mater. Trans. A 39A (2008) 245–251.

[39] M.D.H. Lay, H.S. Zurob, C.R. Hutchinson, T.J. Bastow, A.J. Hill, Vacancy behavior and solute cluster growth during natural aging of an Al-Mg-Si alloy, Metall. Mater. Trans. A 43A (2012) 4507–4513 .

[40] V. Fallah, B. Langelier, N. Ofori-Opoku, B. Raeisinia, N. Provatas, S. Esmaeili, Cluster evolution mechanisms during aging in Al-Mg-Si alloys, Acta Mater 103 (2016) 290–300.

[41] Z.Q. Liang, Clustering and precipitation in Al-Mg-Si alloys Ph.D. thesis, Technische Universität, Berlin, 2012 .

[42] Y. Aruga, M. Kozuka, Y. Takaki, T. Sato, Formation and reversion of clusters during natural aging and subsequent artificial aging in an Al-Mg-Si alloy, Mater. Sci. Eng. A 631 (2015) 86–96.

[43] M.W. Zandbergen, Q. Xu, A. Cerezo, G.D.W. Smith, Study of precipitation in Al-Mg-Si alloys by atom probe tomography I. Microstructural changes as a function of ageing temperature, Acta Mater 101 (2015) 136–148.

[44] R.K.W. Marceau, A. de Vaucorbeil, G. Sha, S.P. Ringer, W.J. Poole, Analysis of strengthening in AA6111 during the early stages of aging: Atom probe tomography and yield stress modelling, Acta Mater 61 (2013) 7285–7303 .

[45] R. Krause-Rehberg, H.S. Leipner, Positron Annihilation in Semiconductors, Springer-Verlag, Heidelberg, 1999.

[46] P. Lang, Y.V. Shan, E. Kozeschnik, The life-time of structural vacancies in the presence of solute trapping, Mater. Sci. Forum 794-796 (2014) 963–970.

[47] F. Hashimoto, M. Ohta, Interaction between a vacancy and a Si, Ge, Sn atom in Al-10wt.%Zn alloy, J. Phys. Soc. Jpn. 19 (1964) 1331–1336.

[48] C. Wolverton, Solute-vacancy binding in aluminum, Acta Mater 55 (2007) 5867–5872.

[49] B. Klobes, O. Balarisi, M. Liu, T.E.M. Staab, K. Maier, The effect of microalloying additions of Au on the natural ageing of Al-Cu, Acta Mater 58 (2010) 6379–6384.

[50] D.K. Chatterjee, K.M. Entwistle, Study of effect of magnesium loss and of addition of copper on aging of aluminum-magnesium-silicon alloys, J. I. Met. 101 (1973) 53–59.

[51] J.H. Kim, C.D. Marioara, R. Holmestad, E. Kobayashi, T. Sato, Effects of microalloying elements (Cu, Ag) on nanocluster formation and age-hardening behavior in Al-Mg-Si alloys, in: Proceedings of the ICAA-13, Pittsburgh, 2012, pp. 1057–1062.

[52] P. Lang, T. Weisz, M.R. Ahmadi, E. Povoden-Karadeniz, A. Falahati, E. Kozeschnik, Thermo-kinetic simulation of the yield strength evolution of AA7075 during natural ageing, Adv. Mat. Res. 922 (2014) 406–411.

[53] H. Kimura, R.R. Hasiguti, Interactions of vacancies with Sn atoms and the rate of G-P zone formation in an Al-Cu-Sn alloy, Acta Mater 9 (1961) 1076–1078.

[54] G. Erdélyi, K. Freitag, H. Mehrer, Diffusion of tin implanted in aluminium, Philos. Mag. 63 (1991) 1167.

[55] T. Federighi, G. Thomas, The interaction between vacancies and zones and the ki- netics of pre-precipitation in Al-rich alloys, Philos. Mag. 7 (1961) 127–131.

[56] J. Kühn, Investigation of clustering in Al-Mg-Si alloys by resistivity measurement Master thesis, Technische Universität, Berlin, 2013.

[57] C. Panseri, T. Federighi, A resistometric study of preprecipitation in an aluminium-1.4 percent Mg2Si alloy, J. I. Met. 94 (1966) 99–197.

[58] M. Werinos, H. Antrekowitsch, T. Ebner, R. Prillhofer, P.J. Uggowitzer, S. Pogatscher, Hardening of Al-Mg-Si alloys: Effect of trace elements and prolonged natural aging, Mater. Design. 107 (2016) 257–268.

[59] S.N. Kim, J.H. Kim, H. Tezuka, E. Kobayashi, T. Sato, Formation behavior of nan- oclusters in Al-Mg-Si alloys with different Mg and Si concentration, Mater. Trans. 54 (2013) 297–303.

[60] S. Müller , L.-W. Wang, A. Zunger, First-principles kinetics theory of precipitate evolution in Al-Zn alloys, Model. Simul. Mater. Sci. 10 (2002) 131–145.

Supplementary Material (SM)

Effect of Sn and In on the natural ageing kinetics of Al-Mg-Si alloys

Meng Liu[a, b, 1, *], Xingpu Zhang[b, 1], Benedikt Körner[b], Mohamed Elsayed[c, d], Zeqin Liang[e], David Leyvraz[e], John Banhart[a, b]

[a] Institute of Applied Materials, Helmholtz Centre Berlin for Materials and Energy, 14109 Berlin, Germany
[b] Department of Materials Science and Technology, Technical University of Berlin, 10623 Berlin, Germany
[c] Department of Physics, Martin Luther University Halle, 06120 Halle, Germany
[d] Department of Physics, Faculty of Science, Minia University, 61519 Minia, Egypt
[e] Novelis Research and Technology Center Sierre, 3960 Sierre, Switzerland

[1] Equal contribution of the authors

Tests of restricted two-component analysis ("1½ component" analysis)

Restricted two-component analysis involves fixing one of the positron lifetime components, in our case the longer one (τ_v) associated to vacancy-related defects. Thus, reliable knowledge about this component is required because with a wrong change the analysis will go wrong. We base our choice of the value of τ_v on:

- Results of three-component decompositions that yield an almost unchanged value of 0.245 ns for the first 70 min of NA [1].
- Theoretical data on positron lifetimes in various defects (summary in Ref. [2]).

In order to assess the reliability of the analysis presented in Fig. 3, especially the fact that $I_{f+s} = 1 - I_v$ decreases after about 100 min of NA in alloy 4-4, we add the following experiments and analyses:

- An experiment with a high-resolution (0.135 ns) digital spectrometer set up at the University of Halle, data analysis assuming τ_v=0.245 ns as for Fig. 3, see Fig. S1,
- Assuming not only τ_v=0.245 ns, but also τ_v=0.240 ns and τ_v=0.250 ns, see Fig. S2,
- Assuming a non-constant τ_v that decreases or increases by 0.005 ns, see Fig. S3.

All the measurements and analyses show a decrease of τ_{f+s} and a decrease of I_{f+s} in stage III. There are small quantitative differences in the analyses, which however, do not affect the basic conclusions.

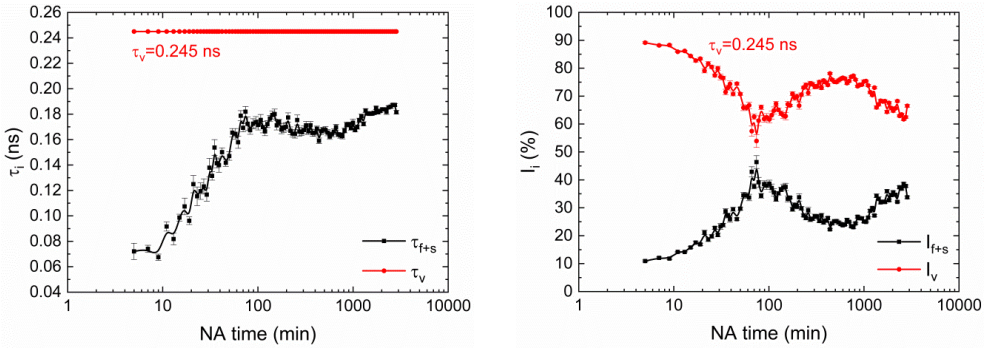

Fig. S1. Positron lifetime measurement on alloy 4-4 and a restricted two-component analysis in analogy to Fig. 3 (τ_v= 0.245 ns).

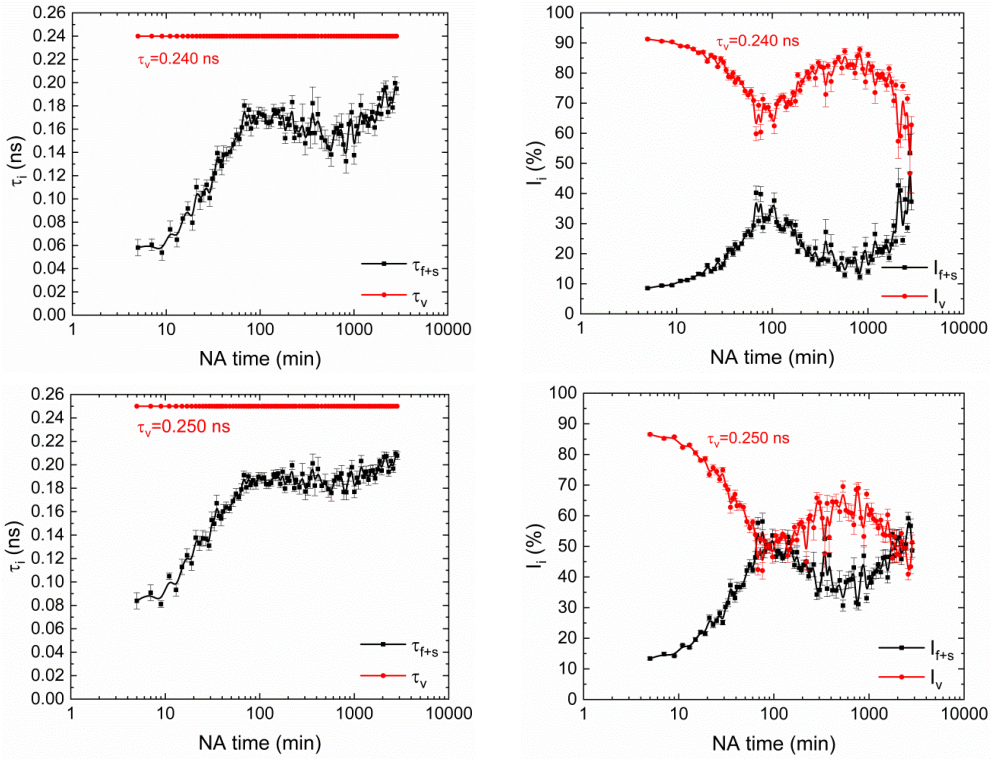

Fig. S2. As Fig. S1, but with a lifetime component τ_v of 0.240 ns (upper line) or 0.250 ns (lower line).

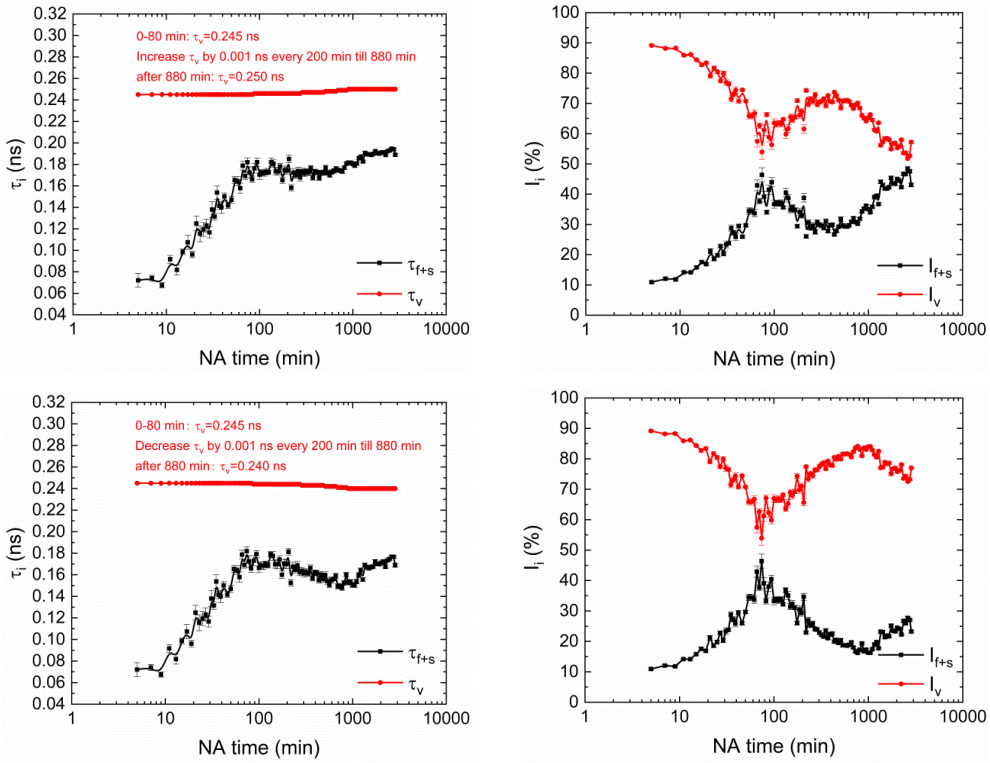

Fig. S3. As Fig. S2, but with the lifetime component τ_v increasing (upper line) or decreasing (lower line) from 0.245 ns to 0.250 ns or 0.240 ns, respectively.

Comparison between τ_{1C} and $\bar{\tau}$

The one-component PLT τ_{1C} is not equal to the lifetime $\bar{\tau}$ averaged from individual components although the two terms are often used in a synonymous way. Fig. S4 compares τ_{1C} and $\bar{\tau}$ for alloys 4-4 and 4-4-40Sn. The general course is found to be very similar, with minor deviations for 4-4-40Sn, where $\bar{\tau}$ is slightly lower than τ_{1C}. Especially for short ageing times where the vacancy-related component is strong, characterising a spectrum that contains more than one PLT by just one parameter τ_{1C} leads to this artefact. The discussion of the ageing kinetics, however, is not affected. Thus, the PLT in the quenched alloys can be reasonably described by τ_{1C}.

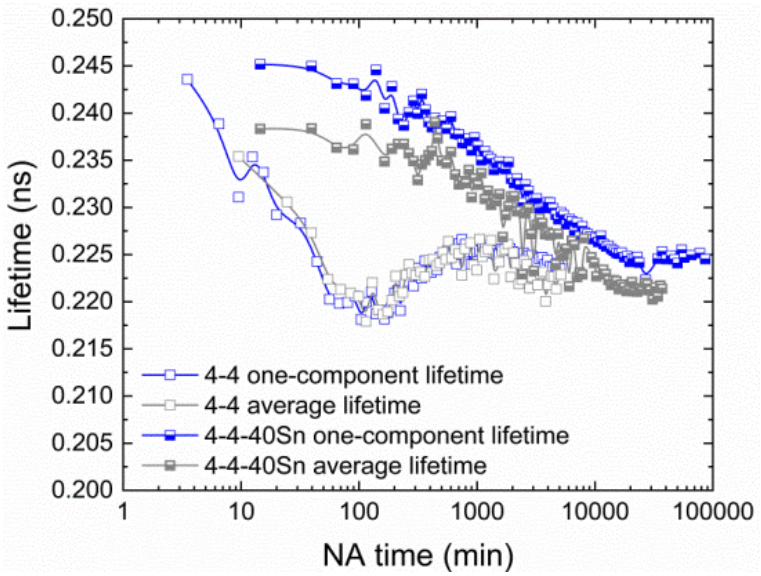

Fig. S4. Comparison between the one-component positron lifetime (from Fig. 1) and the average lifetime (calculated from Fig. 3). No scatter bars are shown to present the data in a clearer manner.

Influence of SHT temperature and Sn content on NA kinetics

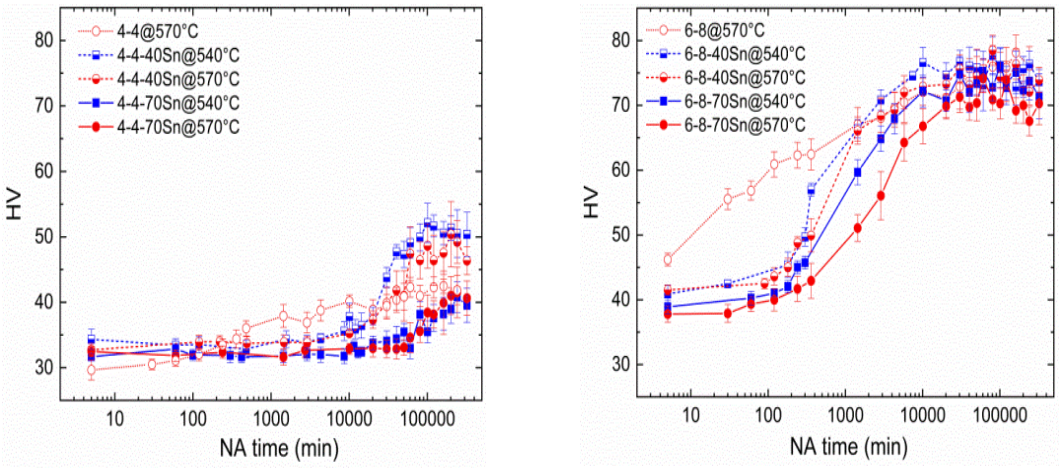

Fig. S5. Influence of SHT temperature (540 °C and 570 °C) and Sn content (40 ppm and 70 ppm) on hardness evolution of a) 4-4-40/70Sn and b) 6-8-40/70Sn alloys during NA.

The evolution of hardness shown in Fig. S5 also reveals the retardation effect of Sn on NA observed by PALS. In addition to Fig. 5, the influence of SHT temperature and Sn content on suppressing NA as reported in Ref. [3] is studied. For alloy 4-4, hardness remains constant up to 3 d/5 w for 40 ppm/70 ppm Sn addition, respectively, while for 6-8-40/70Sn alloys, stabilisation times are much shorter, i.e. ~90 min/200 min, respectively, i.e. higher Sn content leads to longer retardation of NA for both alloys. After this "stabilisation period", an increase in hardness is observed. The increase of solutionising temperature from 540 °C to 570 °C has very little effect on NA kinetics of 4-4-40/70Sn alloys, other than on the one observed for alloys 6-8-40/70Sn, see Fig. S5, where NA is more delayed for 570 °C solutionising temperature. This has been explained by the higher Sn-

solubility for lower Mg or Si content. Accordingly, in the alloys leaner in Mg and Si, a given amount is easier to dissolve and requires lower temperatures [4].

Influence of Mg/Si ratio, main alloying element content and impurities

In addition to Sn content and SHT temperature as reported by [3,5], there are other factors which may directly or indirectly influence the retardation effect of Sn on solute clustering including, but not limited to, Mg/Si ratio, Mg and Si content as well as impurities such as Fe and Mn. Comparisons are made by using some pure alloys and commercial alloys with and without Sn and measuring the electrical resistivity as a measure for clustering, see Fig. S6.

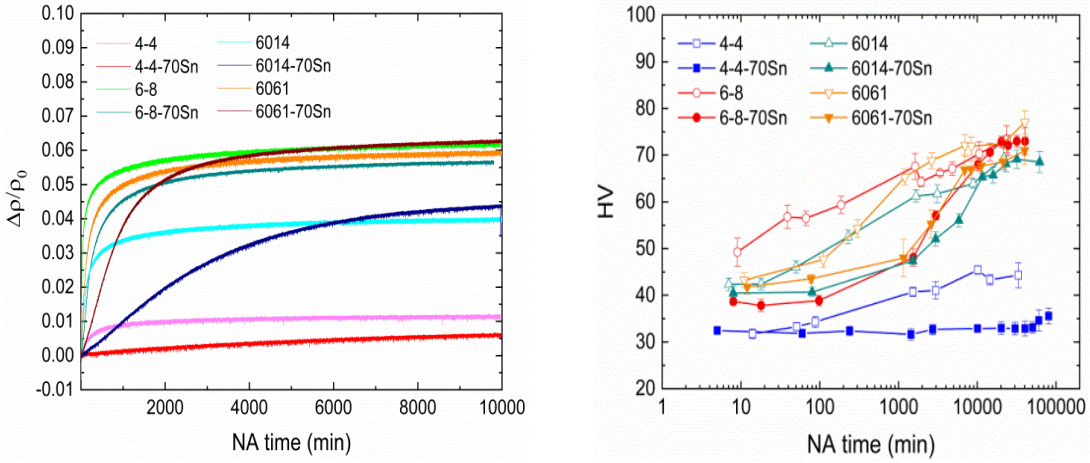

Fig. S6. a) Comparison between normalized resistivity changes in various alloys during NA on a linear time scale; b) the corresponding hardness evolutions on a logarithmic time scale.

- Mg/Si ratio, Mg and Si content

The retardation effect of Sn is found to be less pronounced in alloys 6-8-70Sn and 6061-70Sn, moderate in 6014-70Sn, but largest in 4-4-70Sn according to resistivity data shown in Fig. S6. No direct correlation between the Mg/Si ratio and the retardation effect is found, see alloy 4-4-70Sn with an intermediate Mg/Si ratio (1.25) but the largest effect for instance. However, taking into account the impact of the main alloying elements on Sn solubility [5], the marked differences in solute content between these alloys should be noticed in the first place. It was reported that for a given SHT temperature, Si strongly reduces the solubility of Sn in fcc Al, while for Mg, this effect is smaller [4]. This implies that the effect of Sn on clustering should be weaker in alloys with high Si (Mg) content. Taking alloys 6-8-70Sn and 4-4-70Sn as an example, the former has a considerably higher Si (Mg) content than the latter, which should and does, in turn, give rise to a significant reduction in the number of soluble Sn atoms, i.e. only a smaller fraction of quenched-in vacancies will bind with Sn and more Sn-free solute clusters should be formed in alloy 6-8-70Sn than in 4-4-70Sn. Apart from this, it can be reasonably assumed that the clustering kinetics is comparatively faster in alloy 6-8-70Sn. This is because on the one hand the distances between solutes/clusters

(high solute content) are smaller, and on the other, the diffusion of vacancy-solute complexes and bare vacancies would be affected to less extent due to fewer Sn atoms in their surroundings. Thus, the dissolved Sn atoms determine the total effect of retardation and this is small if only a limited amount of Sn is soluble.

- Impurities

6061 and 6061-70Sn alloys with a composition corresponding to alloys 6061(A) and 6061-70Sn(A) used by S. Pogatscher for their studies [3] were intended to reproduce a comparable effect of Sn. In fact, however, Sn exhibits only qualitatively but not quantitatively the effect in prohibiting NA, e.g. the clustering kinetics in 6061-70Sn is even faster than in 6061-40Sn(A) alloy, see Fig. S7.

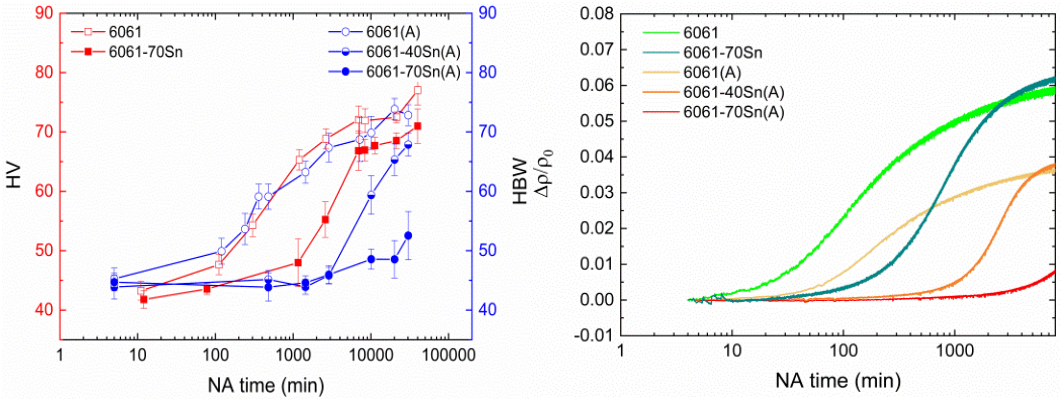

Fig. S7. a) Hardness evolution and b) normalized resistivity changes of the two types of 6061(Sn) alloys investigated during NA. Hardness data of 6061(A) and 6061-40/70Sn(A) alloys (blue spheres) were taken from [3].

It is known that a certain amount of Si will be retained in the Fe-rich intermetallics, which are always present in commercial aluminium alloys and cannot be fully dissolved during and after SHT. Thus, we intentionally reduced the Si content in alloy 6061-70Sn (~0.1%) while keeping Fe as low as possible, aiming at ensuring a similar NA behaviour for 6061-70Sn and 6061-70Sn (A) alloys. But still it seems that the reduction in Si content may not be sufficient, since the Fe/Si ratio of such intermetallics in an Al-0.37Mg-1.02Si-0.26Fe alloy (wt.%) approximately equals 1 as determined by EDX composition analysis [6]. Therefore, the higher retardation potential of Sn in the alloys investigated in Ref. [3] might be due to hitherto differences in alloy processing.

References

[1] M. Liu, J. Čižek, C.S.T. Chang, J. Banhart, Early stages of solute clustering in an Al-Mg-Si alloy, Acta Mater. 91 (2015) 355-364.

[2] J. Banhart, M.D.H. Lay, C.S.T. Chang, A.J. Hill, Kinetics of natural aging in Al-Mg-Si alloys studied by positron annihilation lifetime spectroscopy, Phys. Rev. B 83 (2011) 014101.

[3] S. Pogatscher, H. Antrekowitsch, M. Werinos, F. Moszner, S.S.A. Gerstl, M.F. Francis, W.A. Curtin, J.F. Löffler, P.G. Uggowitzer, Diffusion on demand to control precipitation aging: application to Al-Mg-Si alloys, Phys. Rev. Lett. 112 (2014) 225701.

[4] M. Werinos, H. Antrekowitsch, W. Fragner, T. Ebner, P.J. Uggowitzer, S. Pogatscher, Influence of Sn-solubility on suppression of natural aging in an AA6061 aluminum alloy, in: (Eds.), Proceedings of the Materials Science & Technology (MS&T) Pittsburgh, USA, 2014, pp. 1283-1290.

[5] M. Werinos, H. Antrekowitsch, T. Ebner, S. Pogatscher, Design strategy for controlled natural aging in Al-Mg-Si alloys, Acta Mater. 118 (2016) 296-305.

[6] Z.Q. Liang, Clustering and precipitation in Al-Mg-Si alloys (Ph.D. thesis), Technische Universität Berlin, 2012.

5.2 Paper II

Influence of Sn on the age hardening behavior of Al-Mg-Si alloys at different temperatures

Xingpu Zhang[a], Meng Liu[a,b,*], Haiming Sun[c], John Banhart[a,b]

[a] Technische Universität Berlin, Hardenbergstraße 36, 10623 Berlin, Germany
[b] Helmholtz-Zentrum Berlin für Materialien und Energie, Hahn-Meitner-Platz 1, 14109 Berlin, Germany
[c] Clean Nano Energy Center, State Key Laboratory of Metastable Materials Science and Technology, Yanshan University, 066004 Qinhuangdao, People's Republic of China

*corresponding author: meng.liu@helmholtz-berlin.de

DOI: 10.1016/j.mtla.2019.100441.

URL: https://www.sciencedirect.com/science/article/pii/S2589152919302376

Abstract

Addition of minute amounts of Sn to Al-Mg-Si alloys is known to have a pronounced effect on their age-hardening characteristics. In this study, the influence of Sn addition on the ageing behavior of lean and concentrated alloys at five different temperatures was studied. Hardness, positron annihilation lifetime spectroscopy and transmission electron microscopy measurements complemented by differential scanning calorimetry yield information that allow one to assess the microscopic mechanisms that govern ageing. It is found that Sn slows down the ageing kinetics at 100 °C and 140 °C but accelerates the kinetics and enhances the hardening response at 210 °C and 250 °C. At the standard artificial ageing temperature of 180 °C, the effect of Sn on ageing varies depending on the alloy composition. The observed different ageing kinetics can be explained by the different vacancy behaviors in the presence of Sn. Moreover, the activation energy analysis reveals that the ageing process in Sn-added alloys is controlled by both the separation of Sn-vacancy complexes and the migration of solute-vacancy complexes.

Keywords: Al-Mg-Si alloys; Sn addition; Vacancies; Ageing; Positron annihilation lifetime spectroscopy

1. Introduction

Al-Mg-Si (6xxx) alloys are extensively used for many applications including automotive body panels, where they are age-hardened in the final processing step simultaneously with paint baking. For this alloy, the decomposition of supersaturated solid solution involves the appearance of various precipitates [1]: atomic clusters (possibly different types) → GP zones → β'' → β' → β, where the

arrows denote a sequence as given either by progressing time or rising temperature. Clustering of Si and Mg at 'room temperature' (RT) has been reported to be a complex process involving distinct stages [2] and to have a big influence on the subsequent precipitation at elevated temperatures [3]. The next phase formed at higher temperatures around 100 °C has been named GP zone [1,4,5], pre-ageing (PA) cluster [6], cluster (2) [7] or pre-β'' [8], probably referring to the same or similar structures that are not well explored. The term 'PA cluster' will be used as the only notation in this paper. The following coherent β'' precipitate has the appearance of a needle and is believed to be the most effective strengthening phase, while the rod-like β' precipitate is semi-coherent and appears mostly in overaged alloys. The incoherent β is the final equilibrium phase in Al-Mg-Si alloys.

For practical reasons, Al-Mg-Si alloys have to be stored at RT for a certain time after solutionising and quenching prior to final paint baking. However, clusters formed during natural ageing (NA) cannot act as nuclei of β'' precipitates but instead cause a reduction in hardening rate and baking response [2], the so-called 'negative effect'. To overcome the adverse influence of NA, many methods have been developed, including pre-ageing [9,10], pre-straining [11] and interrupted quenching [12,13], etc. Among all these methods, the simple approach of microalloying with Sn has shown advantages due to its easy operability and cost-effectiveness. More than 60 years ago, the potential of Sn addition in delaying GP zone formation was first discovered in Al-Cu alloys [14]. Muromachi and Mae further investigated the feasibility in suppressing NA in Al-Mg-Si alloys by adding Sn [15] without, however, providing an in-depth explanation of the mechanism. Recently, more detailed studies [16,17] regarding the factors influencing the performance of Sn at RT were carried out and a thermodynamic model that Sn atoms trap vacancies during NA but release them during artificial ageing (AA) was proposed [18]. The promoting effect of Sn at high temperatures (210 °C - 250 °C) has also attracted some attention [19,20]. However, a systematic study on the influence of Sn on the ageing behavior in the temperature range from 100 °C to 250 °C (even at the standard AA temperature of 180 °C) is missing so far.

In this work, we combine hardness measurement, positron annihilation lifetime spectroscopy (PALS), transmission electron microscopy (TEM) and differential scanning calorimetry (DSC) to characterize the microstructure evolution of Al-Mg-Si (Sn) alloys after various heat treatments. In particular, PALS is applied because the lifetime of positrons in alloys is correlated to the electron density of the positron annihilation site and, therefore, allows us to distinguish between vacancy-related defects and other phases formed in Al-Mg-Si alloys such as solute clusters [21] and precipitates [22]. Altogether, this provides more information on the vacancy behavior in lean and concentrated alloys (with/without Sn) aged at different temperatures.

2. Experiments

Sn-free and Sn-containing (70 ppm) pure ternary Al-Mg-Si alloys and commercial alloys 6014 were prepared by the Novelis Research and Technology Center Sierre. Another pure binary Al-Sn alloy was provided by the University of Halle. The chemical compositions of the alloys were determined by atomic emission spectroscopy (AES) and inductively coupled plasma optical emission spectrometry (ICP-OES) as listed in Table 1.

Table 1. Chemical compositions of the alloys investigated.

Designation	Mg (at.%)	Si (at.%)	Sn (ppm)	Fe (at.%)	Mn (at.%)	Cu (at.%)
4-4	0.44	0.37	-	0.03	-	-
4-4-70Sn	0.48	0.37	70	0.03	-	-
6014	0.72	0.58	-	0.09	0.04	0.05
6014-70Sn	0.81	0.54	70	0.12	0.04	-
Al-50Sn	-	-	50	-	-	-

Samples (10 × 10 × 1 mm^3 plates for hardness measurements and PALS, Ø 5 mm disks with thickness of 1 mm for DSC) were solutionized at 570 °C for 1 h. Normal quenching (NQ) was done in ice water. Subsequent ageing at various temperatures was performed in different heating media. (i) Oil: 100 °C, 140 °C and 180 °C; (ii) Liquid metal (LM) Bi57Sn43: 180 °C, 210 °C and 250 °C. LM gives rise to a much faster heating rate than oil (refer to [23] for more details). Interrupted quenching (IQ) for alloy 4-4-70Sn was carried out in an oil bath at 250 °C for 10 s followed by ice-water quenching. The heat treatment profiles are shown in Fig. 1.

Brinell hardness measurements were performed using a Qness 60M tester with a 1 mm indenter. A load of 10 kg with 10 s loading time was applied. The average value of 10 indentations for each sample was used.

The spectrometer described in [21] (with plastic scintillators type EJ232) was employed for positron lifetime (PLT) experiments. Spectra were analysed with software LT9. The one-component positron lifetime τ_{1C} (which differs only slightly from the averaged lifetime $\bar{\tau}$ [24]) of Al-Mg-Si alloys is used for the interpretation of positron lifetime evolution and is compared to literature values in some cases. In Al-Mg-Si alloys, the characteristic lifetimes of positrons trapped in various types of defects are: ≤ 160 ps for Al bulk with defects, 245~250 ps for mono-vacancy-related defects, 210~215 ps for Mg-Si clusters/GP zones/β''. For β', the corresponding PLT is even higher than for β'' because of the semi-coherency between lattice and precipitate [22,25]. The change of the contribution from an individual component would correspondingly increase/decrease τ_{1C}. For Al-50Sn, the time resolution of the applied spectrometer (195~200 ps) enables us to decompose the positron lifetime spectra into 2 components, with τ_b being the reduced lifetime in Al bulk and τ_d the lifetime in defects such as vacancy-solute complexes, solute clusters and precipitates.

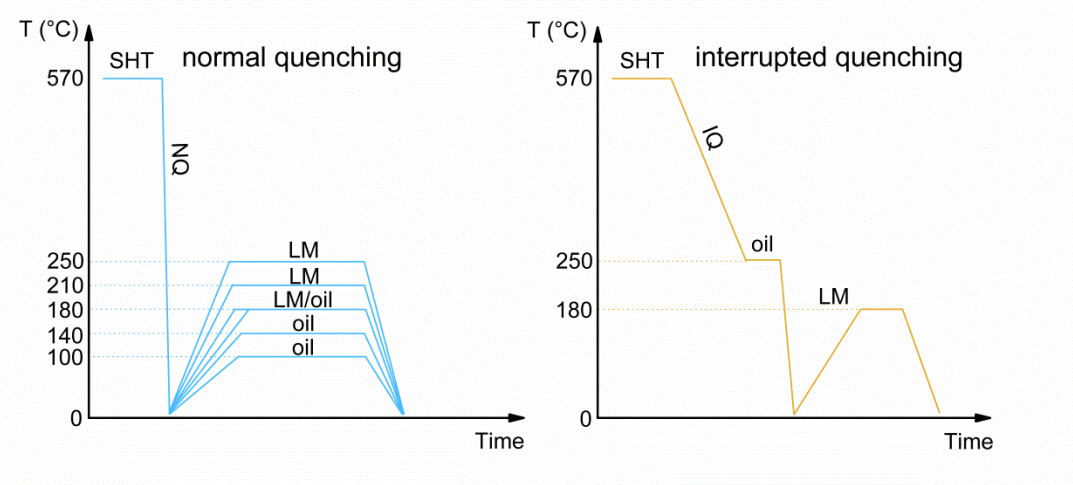

Fig. 1. Heat treatment profiles. 'SHT' stands for solution heat treatment, 'NQ' for normal quenching, 'IQ' for interrupted quenching and 'LM' for liquid metal.

Samples for TEM were ground to a thickness of ~0.15 mm, followed by electrolytic thinning with electrolyte consisting of 24 vol.% HNO_3 and 76 vol.% methanol at −30 °C. The TEM observations were performed with a Cs-corrected ETEM (FEI, Titan G2) operated at 300 kV.

DSC analyses were carried out from 0 °C to 400 °C with a scanning rate of 10 K/min using a Netzsch 204 F1 Phoenix calorimeter.

3. Results

3.1. Ageing at 100 °C and 140 °C

Figs. 2a, c show the hardness evolution in alloys 4-4(Sn) – meaning both Sn-free and Sn-containing alloys – and 6014(Sn) during ageing at 100 °C and 140 °C. At 100 °C, the harnesses of alloys 4-4 and 6014 increase continuously after a roughly constant stage and reach 94 HBW and 114 HBW after ~4 months, respectively. Ageing at 140 °C promotes the hardening kinetics significantly while the final hardness values remain unchanged for all four alloys. At both temperatures, Sn addition delays the hardening kinetics.

Figs. 2b, d compare the evolution of τ_{1C} upon ageing at 100 °C and 140 °C. Directly after solutionising and quenching, different values of τ_{1C} are observed: ~242 ps in alloys 4-4(Sn) and ~231 ps in alloys 6014(Sn). At 100 °C, τ_{1C} in alloy 4-4 drops continuously to 207 ps after 30 min, while hardness only shows a slight increase. Then, τ_{1C} increases to a maximum of 219 ps after 1 d, followed by a re-decrease. A similar τ_{1C} evolution is observed in alloy 6014 aged at 100 °C, namely decrease, increase and re-decrease, but with a faster kinetics and a higher minimum value of 216 ps reached after only 10 s. Apart from a few exceptions (30 s and 1 min in 6014-70Sn), Sn addition leads to higher τ_{1C} values at 100 °C and this effect is more pronounced in alloy 4-4. Moreover, when comparing the transition times of τ_{1C} evolution, the retarding effect of Sn addition on ageing kinetics

is also present (only with the exception of the lowest point for alloys 4-4(Sn)). Compared to 100 °C, τ_{1C} evolution in all alloys aged at 140 °C shows the same trend but the kinetics is much faster. Moreover, the minimum of τ_{1C} in Sn-free alloys is significantly lower at 140 °C than at 100 °C (~14 ps lower in alloy 4-4; ~9 ps in alloy 6014), whereas in Sn-added ones the difference is small.

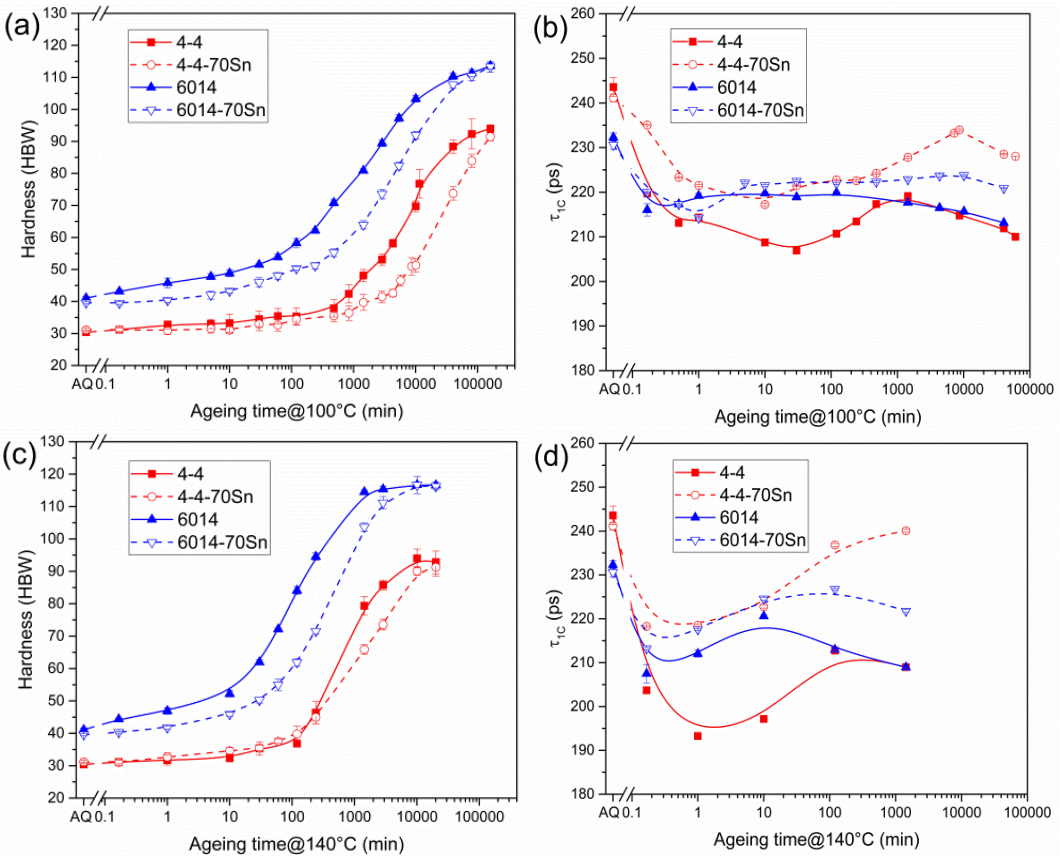

Fig. 2. Evolution of hardness and τ_{1C} during ageing at 100 °C (a, b) and 140 °C (c, d) in oil for alloys 4-4(Sn) and 6014(Sn). The states after solutionising and quenching (AQ) are also given. Lines connecting points are trend lines only.

3.2. Ageing at 180 °C

The hardness evolutions for NQ alloys 4-4(Sn) and 6014(Sn) and for IQ alloy 4-4-70Sn aged at 180 °C in LM are shown in Fig. 3a. For alloy 4-4-70Sn (NQ), accelerated kinetics and increased peak hardness compared to alloy 4-4 are observed (84 HBW after 1 d and 74 HBW after 2 d, respectively). In comparison, Sn addition delays the peak-ageing time from 2 h to 4 h in alloy 6014 without changing the peak hardness. Besides, alloy 4-4-70Sn (IQ) shows notably slower hardening kinetics at 180 °C than alloys 4-4 and 4-4-70Sn (NQ) and its peak hardness is at the same level as in alloy 4-4.

Sn addition also has a pronounced influence on the τ_{1C} evolution for alloys aged at 180 °C in LM, see Fig. 3b. τ_{1C} in alloy 4-4 drops by 72 ps to 171 ps after only 10 s ageing and remains nearly constant up to 5 min. Longer ageing leads to a continuous increase in τ_{1C} to 230 ps after 2 d. For

alloy 6014, 10 s ageing reduces τ_{1C} by 37 ps to 194 ps. Then, τ_{1C} increases to 210 ps after 1 min and remains constant till 2 h. Upon longer ageing, τ_{1C} increases further and reaches 232 ps after 4.5 d. In the peak-aged condition (green dashed boxes), τ_{1C} in alloy 6014 is 20 ps lower than in alloy 4-4. With Sn addition, the decrease of τ_{1C} after 10 s ageing is much smaller (only 26 ps in alloy 4-4-70Sn (NQ) and 14 ps in alloy 6014-70Sn). Moreover, 4-4-70Sn (NQ) exhibits not only an earlier increase of τ_{1C} (after 30 s) than 4-4 but also a higher maximum value (248 ps) after only 30 min. The general trend of τ_{1C} evolution in 6014-70Sn is found similar to 6014 but the corresponding values are noticeably higher. In addition, τ_{1C} in 4-4-70Sn (IQ) starts from 173 ps and increases at a higher rate than in 4-4 during the following ageing. After 1 week of ageing at 180 °C, a τ_{1C} value of 247 ps is reached for 4-4-70Sn (IQ).

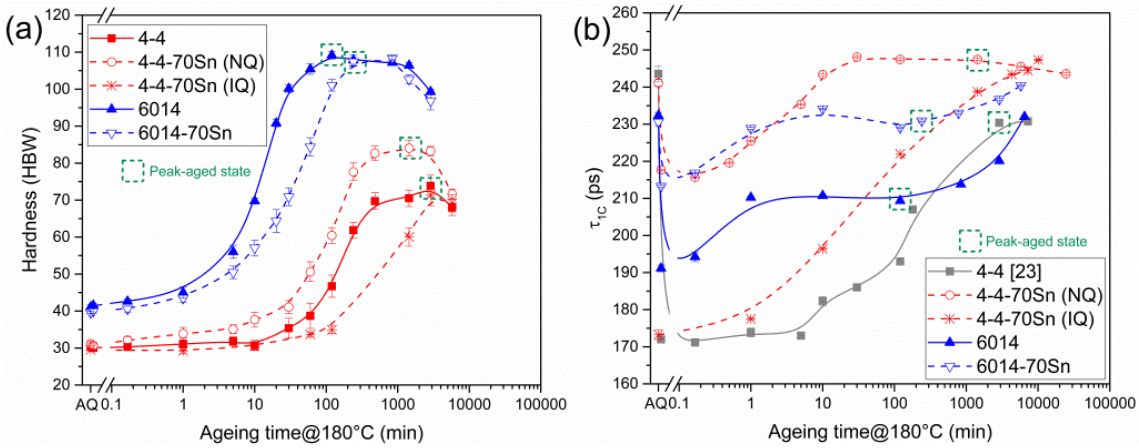

Fig. 3. (a) Hardness curves for normally quenched alloys 4-4(Sn) and 6014(Sn) and interrupted quenched alloy 4-4-70Sn aged at 180 °C in LM. (b) Corresponding τ_{1C} evolution. τ_{1C} data for alloy 4-4 are taken from Ref. [23]. The peak-aged states chosen for TEM analyses are marked with green dashed boxes.

The low-magnification TEM images of precipitates formed in the peak-aged alloys 4-4(Sn) and 6014(Sn) at 180 °C are shown in Fig. 4. At least 100 precipitates are measured to estimate the average length. Sparsely distributed coarse precipitates with an average length of 98 ± 85 nm (standard deviation) are observed in alloy 4-4 (Fig. 4a), while Sn addition refines the microstructure markedly and reduces the average length to 30 ± 23 nm (Fig. 4b). For alloy 6014, denser precipitates with an average length of 13 ± 6 nm are found (Fig. 4c). However, there is no further refinement in alloy 6014-70Sn as the average length of precipitates (13 ± 4 nm) is the same as in 6014 (Fig. 4d).

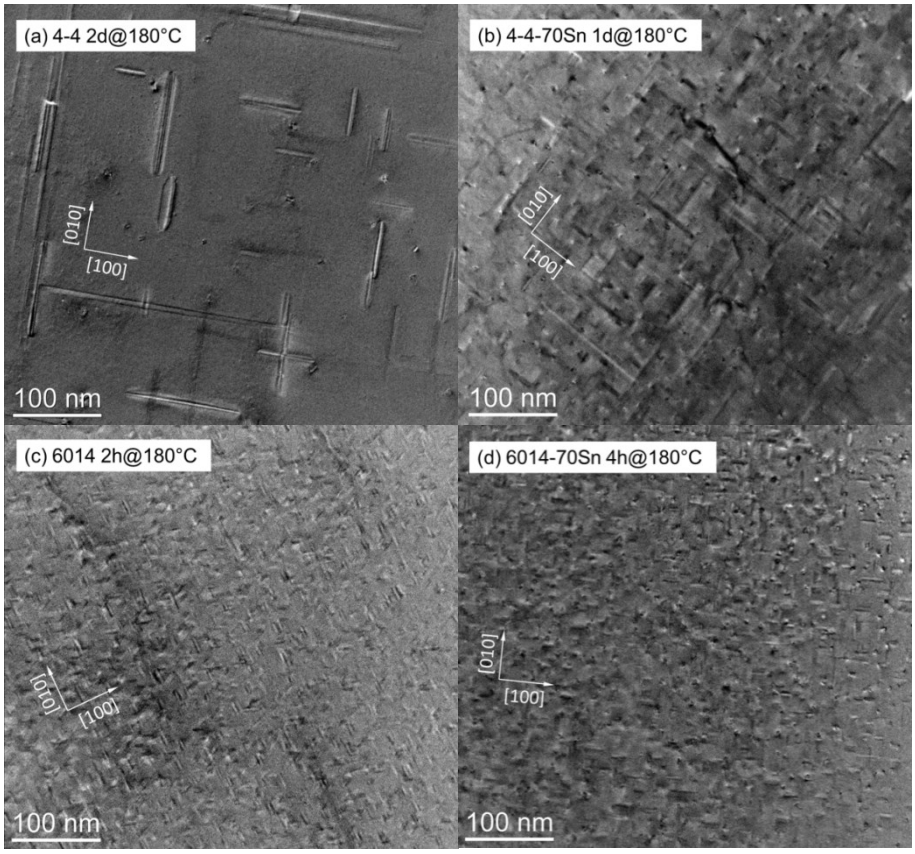

Fig. 4. Low-magnification TEM images of alloys peak-aged at 180 °C: (a) alloy 4-4, (b) 4-4-70Sn, (c) 6014, (d) 6014-70Sn.

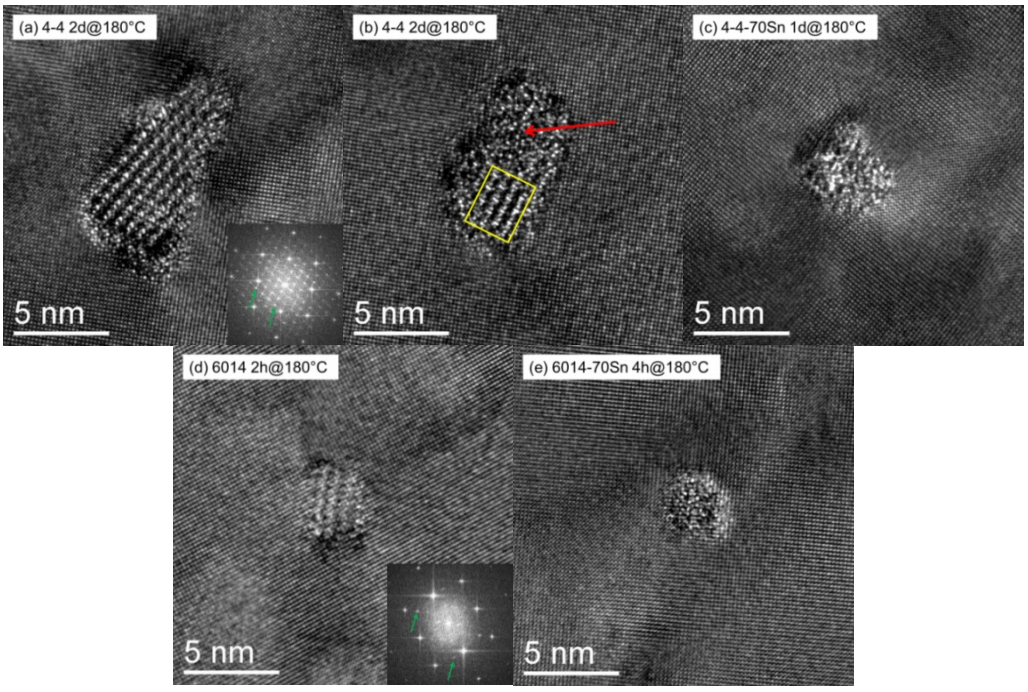

Fig. 5. Representative HRTEM images of peak-aged alloys at 180 °C: (a, b) alloy 4-4, (c) 4-4-70Sn, (d) 6014 and (e) 6014-70Sn. (b) shows the occasionally found precipitate consisting of a periodic structure (yellow box) and a disordered phase (red arrow) in alloy 4-4. Corresponding FFT patterns in alloys 4-4 (a) and 6014 (d) are given in the insets (green arrows indicate the diffraction spots associated with the precipitates).

The representative microstructure of precipitates in alloys 4-4(Sn) and 6014(Sn) peak-aged at 180 °C is also characterized by high-resolution TEM (HRTEM) as shown in Fig. 5. Average cross-sections are calculated based on at least 20 precipitates. Precipitates in 4-4 exhibit much larger average cross-section (35 ± 15 nm^2) than in 6014 (8 ± 2 nm^2). For 4-4, besides the dominating periodic structure (Fig. 5a and the area marked with the yellow box in Fig. 5b), a disordered phase is also observed occasionally (see red arrow in Fig. 5b), while for 6014 all precipitates show visible periodicity (Fig. 5d). The *d* value measured by fast Fourier transform (FFT) pattern associated with precipitates showing a periodic structure agrees well with the calculated one from lattice constants of monoclinic β'' given in the literature (*a*=1.516 nm, *b*=0.405 nm, *c*=0.674 nm, *β*=106° [26]). The average cross-section in alloy 4-4 is reduced markedly to 9 ± 4 nm^2 by adding Sn (Fig. 5c), while in alloy 6014-70Sn the average cross-section (8 ± 3 nm^2) is similar to that in 6014 (Fig. 5e). Moreover, Sn addition clearly introduces disorder into the precipitates, especially in 4-4-70Sn.

3.3. Ageing at 210 °C and 250 °C

Figs. 6a, c show hardness curves for alloys 4-4(Sn) and 6014(Sn) during ageing at 210 °C and 250 °C. In contrast to at 100 °C and 140 °C (Figs. 2a, c), Sn addition generates a faster ageing kinetics (except for alloy 6014 at 210 °C) along with improved hardening response at 210 °C and 250 °C. In addition, it is evident that higher temperature (250 °C) accelerates the hardness increase but results in reduced peak hardness.

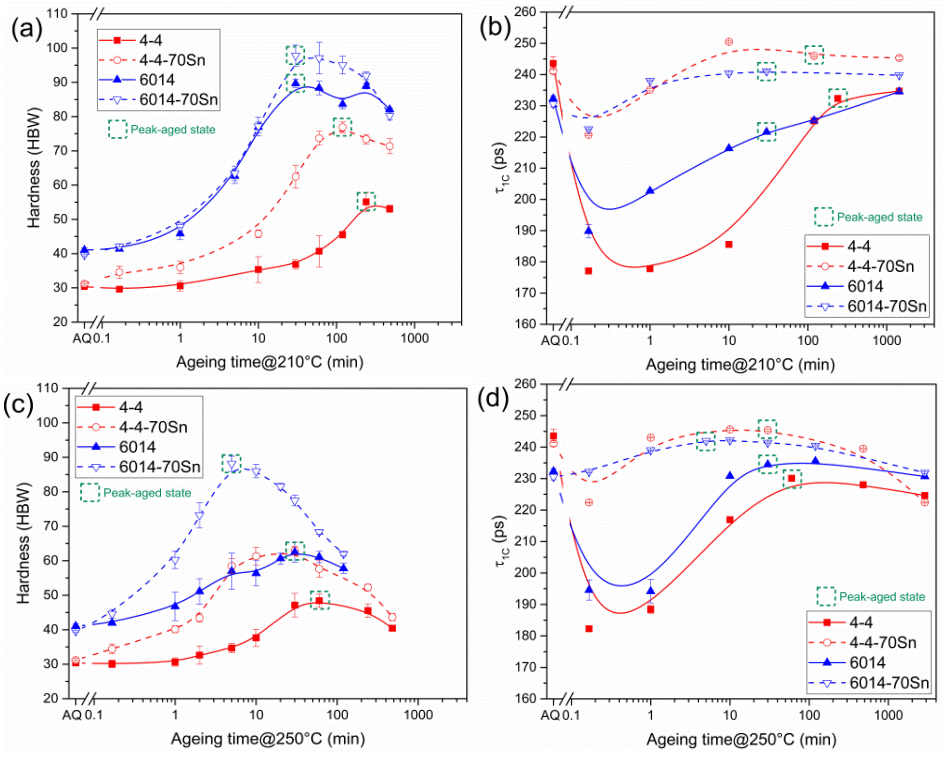

Fig. 6. Influence of Sn addition on the evolution of hardness and τ_{1C} during ageing at 210 °C (a, b) and 250 °C (c, d) in alloys 4-4(Sn) and 6014(Sn). Peak-aged states are marked with green dashed boxes.

The evolutions of τ_{1C} during ageing at 210 °C and at 250 °C are shown in Figs. 6b, d, respectively. At 210 °C, 10 s ageing reduces τ_{1C} to 177 ps in alloy 4-4. Then, it starts to increase after 1 min and reaches 234 ps after 1 d. For alloy 6014, τ_{1C} decreases to 190 ps after 10 s and rises continuously to 234 ps within 1 d without showing the distinct plateau observed at 180 °C (Fig. 3b). After adding 70 ppm Sn, the decrease in τ_{1C} during the first 10 s in both alloys is diminished notably. Upon longer ageing, τ_{1C} increases and reaches a nearly constant value above 240 ps. At 250 °C, τ_{1C} for all four alloys increases in a similar manner as at 210 °C. Unlike for ageing at 210 °C, a re-decrease in τ_{1C} can be clearly observed after 20 – 30 min. At both 210 °C and 250 °C, τ_{1C} in the peak-aged Sn-free alloys (green dashed boxes) appear to be higher than at 180 °C

3.4. τ_{1C} after 10 s ageing in oil/LM at different temperatures

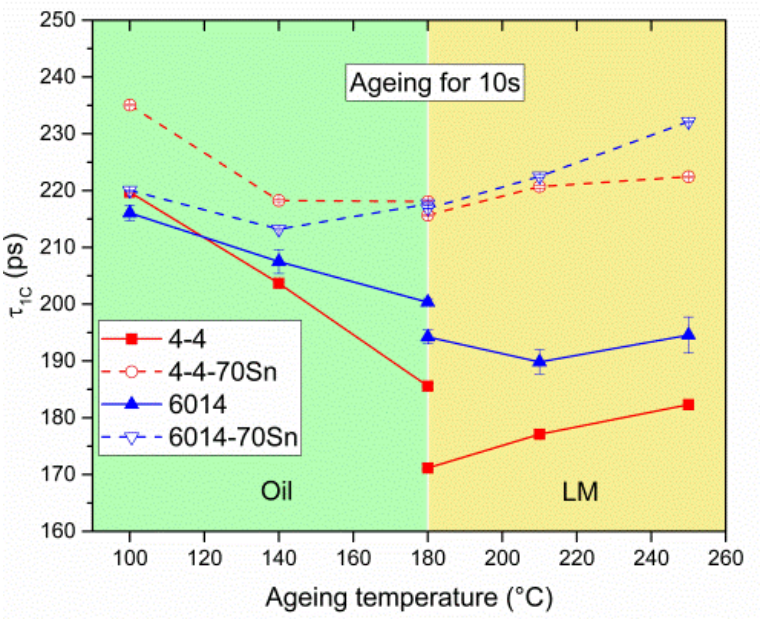

Fig. 7. τ_{1C} for alloys 4-4(Sn) and 6014(Sn) after 10 s ageing at different temperatures. Two different heating media were used: Oil for 100 °C, 140 °C and 180 °C (l.h.s.) and LM for 180 °C, 210 °C and 250 °C (r.h.s.).

The influence of short ageing (10 s) at different temperatures on τ_{1C} is shown in Fig. 7. For alloys 4-4 and 6014 aged in oil, τ_{1C} decreases with rising temperature in the temperature range from 100 °C to 180 °C. At 180 °C, τ_{1C} is reduced remarkably by changing the heating medium to LM. At higher temperatures in LM, τ_{1C} increases again in 4-4 while it remains roughly constant in 6014. In general, τ_{1C} in 4-4 is lower than that in 6014 except for 100 °C. Furthermore, Sn addition increases τ_{1C} considerably in both alloys. Different heating media at 180 °C hardly show an effect on τ_{1C} in Sn-added alloys.

3.5. Differential scanning calorimetry

Fig. 8 shows DSC traces of NQ alloys 4-4(Sn) and 6014(Sn) and the IQ alloy 4-4-70Sn. 3 exothermic peaks (‘1’, ‘2’ and ‘3’) accordingly related to the formation of clusters, β’’ and β’ [27] can be observed in alloys 6014(Sn). Compared to 6014, Sn addition reduces the area of peak ‘1’ and shifts the peak to a higher temperature. The peak temperatures of ‘2’ and ‘3’ are also influenced by Sn addition and are shifted to higher and lower temperatures, respectively. In alloy 4-4, peak ‘1’ is invisible while ‘2’ and ‘3’ overlap at ~320 °C. With Sn addition, peaks ‘2’ and ‘3’ are shifted to lower temperatures and seem to move apart. After IQ for 4-4-70Sn, the overlap of ‘2’ and ‘3’ emerges again.

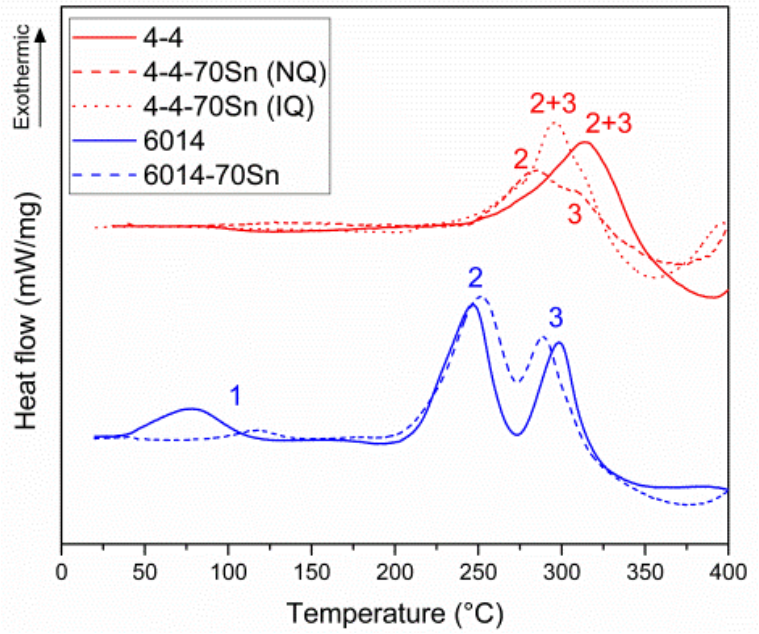

Fig. 8. DSC curves of NQ alloys 4-4(Sn) and 6014(Sn) and the IQ alloy 4-4-70Sn. ‘1’, ‘2’ and ‘3’ refer to the reaction peaks at different temperatures.

4. Discussion

Different ageing behaviors of Al-Mg-Si (Sn) alloys were observed depending on the ageing temperature and on the alloy composition. In the following sections, we attempt to clarify the clustering and precipitation processes at different temperatures based on experimental observations.

4.1. Ageing at 100 °C and 140 °C

- **Sn-free**

For alloy 4-4 directly after solutionising and quenching, it was proposed that over 85% of the positrons annihilate in solute-monovacancy complexes [21], which explains the starting τ_{1C} value of 242 ps in this study (Fig. 2b). The relatively lower τ_{1C} of 231 ps observed for as-quenched 6014

indicates the additional formation of some solute clusters during quenching due to the higher solute concentration in alloy 6014 [28].

The increase of hardness of alloys 4-4 and 6014 upon ageing at 100 °C and 140 °C (Figs. 2 a, c) indicates the formation of PA clusters, which have been reported to take place at 70 °C and above and to be beneficial for the subsequent artificial ageing response [10,29,30]. The faster hardening kinetics and larger hardening response observed in alloy 6014 than in alloy 4-4 are in agreement with the larger peak 1 in alloy 6014 (Fig. 8), implying that PA clusters can form faster at these temperatures in concentrated alloys. τ_{1C} evolutions during ageing at 100 °C and 140 °C (Figs. 2 b, d) were found to be similar to that during NA [2,28], where the measured trend was interpreted by the interaction between vacancies and solute atoms/clusters. According to previous studies, only (PA) clusters are formed at 80 °C [6] and 100 °C [8] and the formation of β'' from PA clusters was only observed after 2 d at 150 °C [8]. Therefore, it is likely that the competition between vacancies and PA clusters also controls the positron lifetime evolution at 100 °C and probably also in the early stage of ageing at 140 °C:

(1) Decrease of τ_{1C}: during ageing, vacancies keep exchanging sites with neighboring atoms and assist in the diffusion of solutes and the formation of clusters [31]. Then, vacancies detach from clusters and repeat this process until they eventually go to sinks, the so-called 'vacancy pump' idea. As a result, the formed clusters gain increasing importance in trapping positrons, which brings down τ_{1C}. Possibly some of the positrons also annihilate in the bulk, which will further shorten the lifetime, provided that trapping is not saturated, see τ_{1C} of 193 ps in 4-4 aged at 140 °C in Fig. 2d as an example. The earlier appearance of a minimum τ_{1C} in 6014 than in 4-4 is caused by the more efficiently formed clusters due to the higher solute concentration. Moreover, vacancies are lost faster at higher temperatures because they diffuse faster to sinks on the one hand and because their binding to the clusters is weaker on the other [23]. This explains the lower τ_{1C} after 10 s ageing (Fig. 7) as well as the lower minimum τ_{1C} (Figs. 2b, d) observed at 140 °C than at 100 °C for both alloys.

(2) Increase of τ_{1C}: vacancies annihilate further during continued ageing, the corresponding τ_{1C}, however, increases subsequently. Previous PALS experiments on alloys with a varying Mg content [28] have revealed that the τ_{1C} increase at RT occurs only in the presence of a sufficient amount of Mg and point at the incorporation of Mg atoms into the already formed Si-rich clusters ($\tau_{Mg} > \tau_{Si}$). At elevated temperatures, the diffusivity of Si in aluminium is 2.5 times (at 80 °C) or 2 times (180 °C) higher than Mg [6], which gives rise to the preferential formation of Si-rich Si-Mg clusters, i.e. larger Si depletion than Mg during the initial clustering stage where τ_{1C} decreases. Therefore, in the ensuing stage, the less mobile Mg atoms start to get involved more in clustering and lift τ_{1C}. In addition, it was proposed that cluster coarsening can also contribute to the increase of τ_{1C} [17].

(3) Re-decrease of τ_{1C}: the reason for this is still inconclusive. The ordering phenomenon within clusters found by Matsuda in Al-Mg-Si at 70 °C by HRTEM [32] may be the reason for this.

- **Sn-added**

Since Mg and Si atoms (clusters) complicate the situation, pure binary Al-Sn is considered first. For as-quenched Al-0.02 at.% Sn alloy, Čížek et.al [33] observed a τ_d (decomposed PLT in defect) value of 235 ps and related this to Sn-monovacancy complexes based on atomic superposition (ATSUP) calculations [34]. In our alloy with a much lower Sn content (50 ppm), however, a higher τ_d of 250 ps was found (Fig. 9a). This value rather agrees with those from Refs. [35-37], which were explained by the rapid formation of Sn-divacancy complexes during quenching [36] enabled by the strong interaction energy of 0.281 eV between Sn atoms and vacancies [38].

In the case of ternary alloys 4-4 and 6014 with Sn addition, the initial τ_{1C} values after quenching are found similar to the Sn-free ones (Fig. 2b), indicating that Sn addition can hardly retard the formation of solute clusters during quenching [17]. During the following ageing at 100 °C and 140 °C, the hardening kinetics for both alloys are markedly delayed (Figs. 2a, c). In addition, DSC also shows the potential of Sn in suppressing clustering (Fig. 8). Given the same initial solute supersaturation, the retarding effect of Sn can only be attributed to the lower available vacancy concentration for solute diffusion. Previous works have shown that Sn atoms can suppress solute clustering at RT in Al-Mg-Si alloys by reducing the number of available vacancies for solute diffusion due to the strong Sn-vacancy binding [17,18]. Moreover, because of the higher characteristic PLT in a vacancy than in a cluster, the observed notable higher τ_{1C} in Sn-added alloys (Figs. 2b, d) points at vacancies retained by Sn. This is supported by the two-component analysis of alloy Al-50Sn. As shown in Fig. 9, the drop of τ_d to 232 ps with a roughly constant I_d after 1 d annealing at 100 °C indicates the transformation from Sn-divacancy complexes formed during quenching to Sn-monovacancy complexes, while the subsequent stable τ_d upon longer ageing confirms the existence of Sn-monovacancy complexes up to 1 week. Isochronal annealing of the same alloy also shows that Sn-vacancy binding is strong enough to survive up to 150 °C [37]. These vacancies trapped by Sn can barely contribute to the diffusion of Mg and Si atoms – the formation of PA clusters in 4-4-70Sn and 6014-70Sn is thus suppressed. In addition, the formation of Sn-containing clusters, which might have even stronger binding with vacancies than single Sn atoms, can further hinder the migration of vacancies [17].

In general, the clustering/precipitation characteristics in Sn-added Al-Mg-Si alloys aged at various temperatures share in some ways many similarities, but are dissimilar in certain respects: during ageing at low temperatures including but not limited to RT [16-18], 100 °C and 140 °C, the strong binding between Sn atoms and vacancies leads to a notable decrease in the amount of vacancies

available for solute diffusion – a retarded clustering kinetics is observed. However, at elevated temperatures, on the one hand the binding between Sn and vacancy becomes progressively weaker, and another factor – the alloy composition comes into play at temperatures ≥ 180 °C. Accordingly, the combined effects complicate the situation and will be discussed in the following.

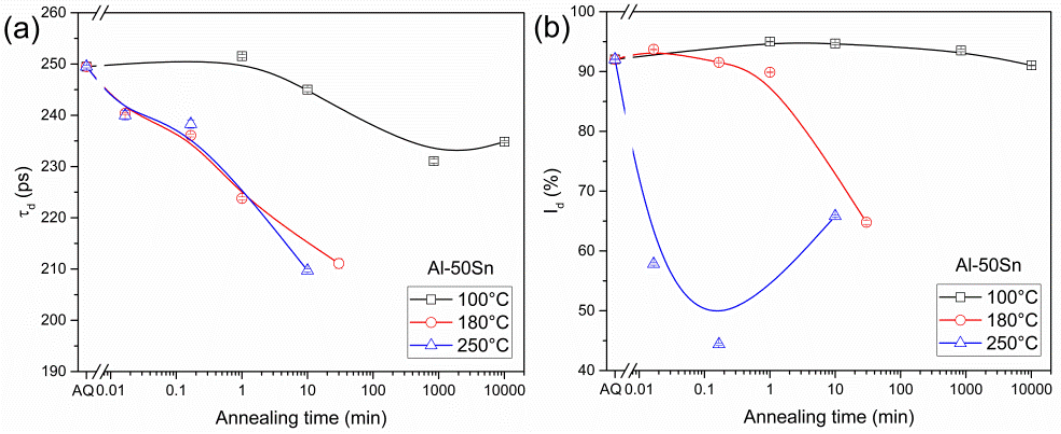

Fig. 9. Evolution of decomposed positron lifetime components: (a) lifetime τ_d, (b) corresponding intensity I_d of Al-50Sn annealed at 100 °C, 180 °C and 250 °C.

4.2. Ageing at 180 °C

- **Sn-free**

At 180 °C, the trend observed for lower temperatures is seen to continue in that even more vacancies anneal out very fast without forming too many clusters, which gives rise to a very low τ_{1C} of 171 ps in alloy 4-4 after 10s in LM (Fig. 3b). However, under equal condition, the more efficiently formed clusters and thus more vacancies retained by clusters in the concentrated alloy 6014 lead to a higher τ_{1C} value of 193 ps. For alloy 6014, the subsequent increase in τ_{1C} between 10 s and 1 min indicates the formation of precipitates which gradually reduces the bulk contribution. With longer ageing time, precipitates continue to form and grow, resulting in the sharp hardness increase to ~110 HBW (Fig. 3a). However, τ_{1C} stays roughly constant at ~210 ps up to 2 h. This might be a consequence of saturated positron trapping in precipitates in which the positron lifetimes are similar. The low-magnification TEM image after 2 h ageing at 180 °C (Fig. 4c) indeed confirms a dense distribution of precipitates in 6014, which are identified as β'' by the FFT pattern (Fig. 5d). Miao and Laughlin [39] have also reported that β'' is the main strengthening phase in a concentrated alloy (6022) aged at 175 °C. Therefore, the τ_{1C} value around 210 ps in the peak-aged alloy 6014 (Fig. 3b) should correspond to positron annihilation in β'' phase. This is also supported by the combined positron lifetime and dilatometry measurements in alloy 6060 [40], where a $\bar{\tau}$ ~214 ps associated with the β'' phase was observed. Even longer ageing leads to a further increase in τ_{1C} to 232 ps after 4.5 d but a decrease in hardness. The transformation from coherent β'' to semi-coherent β' explains this change. On the other hand, due to the considerably lower solute and

vacancy concentration in alloy 4-4 than in alloy 6014, the precipitation kinetics is slower and no increase is observed either in hardness or in τ_{1C} until 10 min or 5 min, respectively (Figs. 3a, b). Thereafter, τ_{1C} in alloy 4-4 increases continuously without a constant stage and reaches 230 ps in the peak-aged state after 2 d – 20 ps higher than that of peak-aged 6014. Considering the overlap of β'' and β' peaks in the DSC curve for 4-4 (Fig. 8), it is possible that β' already forms and coexists with β'' (or even totally replaces β'' [41]) before peak hardness is reached, which leads to a higher τ_{1C} due to its semi-coherency. The exact correlation between the observed disorder via HRTEM (Fig. 5b) and β' phase is not clear, but a disordered phase was also found in a peak-aged Al-0.36 at.% Mg-0.36 at.% Si alloy and was attributed to post-β'' phases (β', U2 or B') [42]. In addition to PALS, the observed more sparsely distributed coarse precipitates in peak-aged 4-4 compared to 6014 (Figs. 4a, c) limit the hardening kinetics and age hardening potential of alloy 4-4.

- **Sn-added**

For alloy 4-4, Sn addition accelerated the ageing kinetics and hardening response at 180 °C, as revealed by hardness (Fig. 3a), PALS (Fig. 3b), DSC (Fig. 8) and TEM (Figs. 4a, b). Two plausible reasons may apply:

Firstly, because of the crucial role of vacancies in AA [43], the positive effect of Sn on promoting precipitation may arise from a higher amount of retained vacancies. Since the comparable site fractions of vacancies in as-quenched Al-Mg-Si alloy (10^{-5} [44]) and Sn atoms (7×10^{-5}) are much higher than that of vacancy sinks (8×10^{-10} [24], mainly dislocation jogs in our case), Sn-vacancy complexes will be formed involving most Sn atoms after quenching. Moreover, the roughly constant I_d (τ_d > 236 ps) up to 10 s at 180 °C in Al-50Sn validates the survival of Sn-monovacancy complexes after short annealing (red curves in Fig. 9). Therefore, compared to the fast vacancy loss in 4-4, more vacancies should remain in 4-4-70Sn, resulting in the largely suppressed decrease of τ_{1C} after short ageing (10 s) as shown in Fig. 7. Later, as shown in Fig. 9, τ_d in Al-50Sn starts to decrease and reaches 211 ps after 30 min of ageing at 180 °C. This value is much lower than the characteristic positron lifetime in Sn-monovacancy complexes (~235 ps), but agrees well with the one in Sn precipitates formed during slow cooling [33]. This can be explained by the separation of Sn-vacancy complexes and the subsequent loss of the detached vacancies as well as by the formation of Sn precipitates. Both vacancy-related defects and Sn precipitates contribute to the defect intensity I_d, but the rate of vacancy loss is higher than the formation of Sn precipitates in the initial stage of ageing. Thus, a pronounced decrease in I_d from 91% to 65% is observed. Thereafter, the concentration of vacancies gradually approaches the thermal equilibrium at the ageing temperature, while Sn precipitates continuously form and grow. Moreover, the loss of vacancies and formation of Sn precipitates also occur at 250 °C, and the faster formation of Sn precipitates at higher temperature results in the re-increase in I_d after ageing for 10 min (blue curves in Fig. 9). In

alloy 4-4-70Sn, the separation of Sn-vacancy complexes can be assumed in a similar manner. The gradually detaching vacancies enhance the diffusion of Mg and Si atoms and correspondingly accelerate precipitation. In order to examine this assumption, 10 s IQ on alloy 4-4-70Sn was performed at 250 °C in an oil bath. Coming from 540 °C, the sample cools down to 250 °C and spends some time in between. This facilitates annealing out of vacancies as binding with Sn is weak at temperatures ≥ 250 °C, supported by the obtained low τ_{1C} value of 173 ps for 4-4-70Sn directly after IQ (Fig. 3b). During the following ageing at 180 °C, 4-4-70Sn (IQ) shows a largely reduced hardening kinetics and can only reach the same peak hardness as 4-4 (Fig. 3a), confirming the beneficial effect of more excess vacancies on precipitation in alloy 4-4-70Sn.

Secondly, Sn atoms may act as heterogeneous nucleation sites for precipitates. A comparable behavior of Sn has been found previously in Al-Cu alloys, where Sn clusters are seen to act as nucleation sites for θ' [45,46]. Direct evidence for the existence of Sn clusters cannot be obtained in the current study applying TEM, but it has been reported that Sn clusters can hardly be detected using atom probe tomography in a Sn-containing AA6061 alloy naturally aged for 2 weeks and artificially aged at 170 °C for 12 h [18]. Moreover, by considering the attractive interaction between Mg-Sn (0.1 eV [47]) and Mg-Si (0.042 eV [47]), it is highly unlikely for a Sn atom, which is surrounded and "shielded" by hundreds of Mg and Si atoms in its vicinity, to diffuse to the next Sn atom, i.e. Sn clustering can be reasonably excluded in the investigated Sn-containing Al-Mg-Si alloys. Still, Sn atoms might contribute to nucleation. For lean Al-Mg-Si alloy with Ge addition aged at 180 °C, Mørtsell et al. [42] reported that the chemical similarity between Ge and Si enables Ge to substitute Si in precipitates and form the same atomic structure as Si, however, disordered. Since Sn, Ge and Si belong to the same IVA group in the periodic table, the replacement of Si by Sn can also occur and be the reason for the disorder occurring in the precipitate's structure (Fig. 5c). Because the interaction energy between Mg-Sn is larger than between Mg-Si [47], attachment of Mg to precipitates with embedded Sn atoms would be facilitated, which in turn promotes the nucleation reaction.

Interestingly, an opposite effect of Sn on the hardening kinetics of 6014 is observed, i.e., hardening in 6014 is delayed by adding Sn. This corresponds to the retarded formation of β'', see also the higher DSC peak temperature of β'' in 6014-70Sn (Fig. 8). As stated above, the higher solute concentration in 6014 than in 4-4 promotes the formation of clusters during quenching from solutionising and heating to 180 °C. These clusters might play the same role as Sn atoms in retarding vacancy loss during heating, and then these retained vacancies will detach from clusters and assist in the diffusion of solutes, resulting in the formation of fine and densely distributed β'' precipitates. Therefore, refinement caused by Sn addition no longer occurs (Fig. 4e) and the same peak hardness is obtained. Although the exact binding energy between above mentioned clusters and vacancies is unknown, due to the higher vacancy concentration in 6014-70Sn than in 6014 after

short time at 180 °C as reflected by the higher τ_{1C} (Fig. 3b) – a faster ageing kinetics is expected – but delayed hardening kinetics, a more difficult detachment of vacancies from Sn atoms than from these clusters in 6014 seems to be a reasonable explanation.

It is noteworthy that τ_{1C} in Sn-added alloys is notably higher than in Sn-free ones throughout the entire ageing period (Fig. 3b). The initial higher τ_{1C} after short ageing is explicitly caused by the vacancies bound by Sn, while the formation of new phases during longer ageing makes the explanation for the later stages more complicated. The possibility of excess vacancies still captured by Sn atoms can be examined with the designed IQ experiment. For alloy 4-4-70Sn directly after IQ, τ_{1C} appears much smaller than for alloy 4-4-70Sn (NQ) but similar to alloy 4-4 after 10 s ageing at 180 °C, indicating that the extra lifetime contribution linked to excess vacancies bound by Sn atoms can be removed by IQ. In other words, IQ should be able to eliminate the τ_{1C} difference between long-time aged alloys 4-4 and 4-4-70Sn if the above-mentioned notably higher τ_{1C} during ageing at 180 °C resulted from vacancies retained by Sn atoms. However, after 1 week ageing at 180 °C τ_{1C} for alloy 4-4-70Sn (IQ) still reaches 247 ps as for alloy 4-4-70Sn (NQ). Consequently, excess vacancies trapped by Sn atoms can be excluded as a reason for the high PLT and therefore, considering the slower hardness but faster τ_{1C} increase in alloy 4-4-70Sn (IQ) compared to alloy 4-4 aged at 180 °C, the prolonged τ_{1C} must reflect the longer characteristic PLT in Sn-modified precipitates. The atomic radius of Sn (0.145 nm) is larger than that of Si (0.110 nm) and when Si atoms in the precipitates are replaced by Sn atoms a lattice expansion of precipitates may contribute to this longer characteristic PLT. Moreover, the disordered structure (Figs. 5c, e) triggered by the participation of Sn in the formation of precipitates could be another reason.

It is also found that τ_{1C} for alloys 4-4 and 6014 after 10 s ageing at 180 °C are obviously increased by changing the heating medium from LM to oil (Fig. 7). This has been linked to more retained vacancies because the slower heating rate in oil results in a longer dwell time at low temperatures and enables the formation of more clusters, which can, in turn, prevent the further loss of vacancies [23]. However, Sn-added alloys are barely influenced by the heating rate. This may originate from the largely hindered vacancy loss by Sn even in LM (higher heating rate).

4.3. Ageing at 210 °C and 250 °C

- **Sn-free**

The influence of short ageing (10 s) in LM at high temperatures on alloys without Sn addition will be discussed first (Fig. 7). For alloy 4-4, τ_{1C} increases when the temperature rises from 180 °C, suggesting the formation of precipitates. Since the equilibrium vacancy concentration is ~7×10^{-7} at 250 °C [24], which is slightly above the detection limit, the contribution of such vacancies on PLT is only marginal in this temperature range. In comparison, due to the more efficiently formed clusters in alloy 6014, τ_{1C} stays above 190 ps even at elevated temperatures.

For longer ageing time at 210 °C and 250 °C, hardness and τ_{1C} start to increases due to the further formation of precipitates for both of 4-4 and 6014 (Fig. 6), whilst the constant stage of τ_{1C} corresponding to β'' formation for 6014 aged at 180 °C is no longer visible. According to Resch et al. [40], who have previously observed a similar increase in $\bar{\tau}$ for Al-Mg-Si alloys aged at 210 °C, the disappearance of the constant stage could be the evidence for the earlier transformation from β'' to β' compared to ageing at 180 °C. Formation of a low number density of β' has also been reported by Liu et al. [48] to be favorable at elevated temperatures, which agrees well with the higher τ_{1C} (> 230 ps) at higher temperatures than at 180 °C in the peak-aged state (Figs. 6b, d). These sparse β' precipitates do not show large hardening potential and cause a pronounced drop in peak hardness at higher temperatures (Figs. 6a, c). In addition, higher temperatures shorten the time to reach peak hardness. Considering the decreased solute super-saturation at higher temperature, the faster ageing kinetics appears to originate from the accelerated mobility of vacancies. It is also notable that even though overageing occurs at all three temperatures (180 °C, 210 °C and 250 °C), a final drop in τ_{1C} is only observed at 250 °C. Because the positron diffusion length in aluminium is ~100 nm, this drop implies that the precipitate spacing is getting larger, i.e. a more pronounced coarsening of precipitates occurs at 250 °C than at lower temperatures.

- **Sn-added**

Sn addition shows the capability to promote the precipitation kinetics and preserve hardening potential at high temperatures, which can be explained by the more available vacancies retained by Sn and the fact that Sn atoms are preferential nucleation sites, in analogy to 4-4(Sn) aged at 180 °C. The higher concentration of excess and probably also equilibrium vacancies in Sn-added Al-Mg-Si alloys can be deduced from the markedly higher τ_{1C} after 10 s ageing (Figs. 6b, d), which is also supported by the intensity ~44% for Sn-monovacancy complexes as observed in Al-50Sn after 10 s annealing at 250 °C (Fig. 9). According to Liu et al. [20], Sn-vacancy complexes can act as preferential nuclei for β' and refine the coarse precipitates formed in Al-Mg-Si alloys at 250 °C. Our observation of the fast increase of τ_{1C} to >235 ps within 1 min of ageing for Sn-added alloys

(Fig. 6) also reflects the fast Sn-assisted nucleation of positron traps with long lifetimes, which should be similar to the disordered precipitates found in 4-4-70Sn and 6014-70Sn alloys aged at 180 °C.

4.4. Activation energy analysis

In the investigated temperature range, the Johnson-Mehl-Avrami equation can be used to describe the precipitation process:

$$f = 1 - \exp^{-(kt)^n},$$

where f is the relative volume fraction of precipitates, t the ageing time, k the temperature-dependent reaction rate and n the Avrami index. Moreover, k can be expressed by the Arrhenius equation:

$$k = k_0 \cdot \exp(-Q/RT).$$

Corresponding to the half maximum hardening state, f is assumed to be a constant. Therefore, it is possible to estimate the activation energies (Q) associated with the ageing process based on the times required for increasing the hardness halfway up to the maximum at various ageing temperatures.

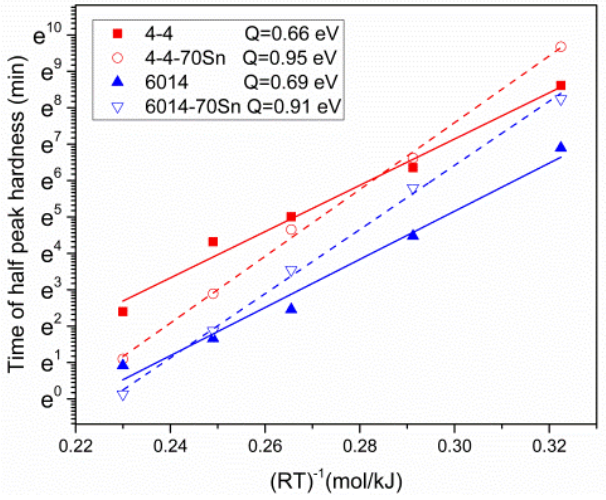

Fig. 10. Arrhenius activation energy analysis for alloys 4-4(Sn) and 6014(Sn). Straight lines are linear fits.

Fig. 10 shows the Arrhenius plot for alloys 4-4(Sn) and 6014(Sn). For Sn-free alloys 4-4 and 6014, the activation energies are 0.66 and 0.69 eV, respectively, which agrees well with the typical migration energies for Mg-vacancy (0.67 eV, [49]) or Si-vacancy (0.64 eV, [50]) complexes in aluminium. Thus the ageing processes in Sn-free alloys are likely to be driven by existing excess vacancies but not by thermal vacancies that would have to be created first – an activation energy up to 1.25 eV should be obtained instead [51]. For 4-4-70Sn and 6014-70Sn alloys, higher Q values of 0.95 eV and 0.91 eV are obtained. Apparently, hardening in Sn-added alloys is governed by some

activation energy that is 0.22~0.29 eV higher than in Sn-free alloys. As described above, Sn atoms influence the ageing behavior by capturing/releasing vacancies at different temperatures. Considering the binding energy of 0.281 eV between Sn and vacancy [38], it is reasonable to assume that in the presence of Sn the ageing process is controlled by a combined activation process: the separation of Sn-vacancy complexes and then the migration of solute-vacancy complexes.

5. Conclusions

In this work, we have investigated the influence of Sn addition on the ageing behavior of both lean and concentrated Al-Mg-Si alloys at five different temperatures and found that Sn addition can either slow down or accelerate the ageing process depending not only on ageing temperature but also on alloy composition. The different vacancy behaviors controlled by Sn are assumed to be the main reason:

- 100 °C and 140 °C: the diffusion of Mg and Si solutes is significantly delayed as vacancies are trapped by Sn and as a result the ageing kinetics is delayed in both alloys.
- 180 °C: in lean alloy, Sn prevents the initial fast vacancy loss, releases vacancies subsequently and acts as nucleation site for precipitation, resulting in the accelerated hardening kinetics and promoted hardening response. In concentrated alloy, clusters formed during quenching can perform in a similar way as Sn in retaining vacancies but the even stronger binding between Sn and vacancies rather leads to a retardation of ageing.
- 210 °C and 250 °C: the beneficial influence of Sn occurs in both alloys with an explanation based on Sn releasing previously retained vacancies and acting as nucleation site.
- Activation energy analysis reveals that the ageing process in Sn-free alloys is controlled by migration of solute-vacancy complexes, but in Sn-added alloys additionally by the required separation of Sn-vacancy complexes.

Acknowledgements

We would like to thank Dr. Zeqin Liang and David Leyvraz of Novelis Research and Technology Center Sierre and Dr. Mohamed Elsayed from University of Halle for providing the alloys, Christiane Förster for TEM samples preparation and Chuihui Liu from Central South University for the fruitful discussion concerning the TEM analysis. The Deutsche Forschungsgemeinschaft (DFG) funded this project (Ba1170/22). Xingpu Zhang thanks the China Scholarship Council (CSC) for a research fellowship.

Declaration of interests

The authors declare that they have no known competing financial interests or personal relationships that could have appeared to influence the work reported in this paper.

References

[1] G.A. Edwards, K. Stiller, G.L. Dunlop, M.J. Couper, The precipitation sequence in Al-Mg-Si alloys, Acta Mater. 46 (1998) 3893-3904.

[2] J. Banhart, C.S.T. Chang, Z.Q. Liang, N. Wanderka, M.D.H. Lay, A.J. Hill, Natural aging in Al-Mg-Si alloys - A process of unexpected complexity, Adv. Eng. Mater. 12 (2010) 559-571.

[3] L. Zhen, S.B. Kang, DSC analyses of the precipitation behavior of two Al-Mg-Si alloys naturally aged for different times, Mater. Lett. 37 (1998) 349-353.

[4] M. Murayama, K. Hono, Pre-precipitate clusters and precipitation processes in Al-Mg-Si alloys, Acta Mater. 47 (1999) 1537-1548.

[5] J. Buha, R.N. Lumley, A.G. Crosky, K. Hono, Secondary precipitation in an Al-Mg-Si-Cu alloy, Acta Mater. 55 (2007) 3015-3024.

[6] M.W. Zandbergen, Q. Xu, A. Cerezo, G.D.W. Smith, Study of precipitation in Al-Mg-Si alloys by atom probe tomography I. Microstructural changes as a function of ageing temperature, Acta Mater. 101 (2015) 136-148.

[7] A. Serizawa, S. Hirosawa, T. Sato, 3DAP Characterization and Thermal Stability of Nano-Scale Clusters in Al-Mg-Si Alloys, Mater. Sci. Forum 519-521 (2006) 245-250.

[8] C.D. Marioara, S.J. Andersen, J. Jansen, H.W. Zandbergen, The influence of temperature and storage time at RT on nucleation of the β" phase in a 6082 Al-Mg-Si alloy, Acta Mater. 51 (2003) 789-796.

[9] L. Zhen, S.B. Kang, The effect of pre-aging on microstructure and tensile properties of Al-Mg-Si alloys, Scripta Mater. 36 (1997) 1089-1094.

[10] Y. Birol, Pre-aging to improve bake hardening in a twin-roll cast Al-Mg-Si alloy, Mat. Sci. Eng. A 391 (2005) 175-180.

[11] Y. Birol, Pre-straining to improve the bake hardening response of a twin-roll cast Al-Mg-Si alloy, Scripta Mater. 52 (2005) 169-173.

[12] S. Pogatscher, H. Antrekowitsch, H. Leitner, A.S. Sologubenko, P.J. Uggowitzer, Influence of the thermal route on the peak-aged microstructures in an Al-Mg-Si aluminum alloys, Scripta Mater. 68 (2013) 158-161.

[13] S. Pogatscher, H. Antrekowitsch, H. Leitner, D. Poschmann, Z.L. Zhang, P.J. Uggowitzer, Influence of interrupted quenching on artificial aging of Al-Mg-Si alloys, Acta Mater. 60 (2012) 4496-4505.

[14] H. Hardy, The effect of small quantities of Cd, In, Sn, Sb, Tl, Pb, or Bi on the ageing characteristics of cast and heat-treated aluminium-4-percent copper-0.15-percent titanium alloy, J. I. Met. 78 (1950) 169-194.

[15] S. Muromachi, T. Mae, On the two-step aging behavior of Al-1.3 wt%Mg2Si alloy, J. Jpn. I. Met. 38 (1974) 130-138 [in Japanese].

[16] M. Werinos, H. Antrekowitsch, T. Ebner, S. Pogatscher, Design strategy for controlled natural aging in Al-Mg-Si alloys, Acta Mater. 118 (2016) 296-305.

[17] M. Liu, X. Zhang, B. Körner, M. Elsayed, Z. Liang, D. Leyvraz, J. Banhart, Effect of Sn and In on the natural ageing kinetics of Al–Mg–Si alloys, Materialia 6 (2019) 100261.

[18] S. Pogatscher, H. Antrekowitsch, M. Werinos, F. Moszner, S.S.A. Gerstl, M.F. Francis, W.A. Curtin, J.F. Löffler, P.G. Uggowitzer, Diffusion on demand to control precipitation aging: application to Al-Mg-Si alloys, Phys. Rev. Lett. 112 (2014) 225701.

[19] M. Werinos, H. Antrekowitsch, E. Kozeschnik, T. Ebner, F. Moszner, J.F. Loffler, P.J. Uggowitzer, S. Pogatscher, Ultrafast artificial aging of Al-Mg-Si alloys, Scripta Mater. 112 (2016) 148-151.

[20] C. Liu, P. Ma, L. Zhan, M. Huang, J. Li, Solute Sn-induced formation of composite β′/β″ precipitates in Al-Mg-Si alloy, Scripta Mater. 155 (2018) 68-72.

[21] M. Liu, J. Čižek, C.S.T. Chang, J. Banhart, Early stages of solute clustering in an Al-Mg-Si alloy, Acta Mater. 91 (2015) 355-364.

[22] T.E.M. Staab, R. Krause-Rehberg, U. Hornauer, E. Zschech, Study of artificial aging in AlMgSi (6061) and AlMgSiCu (6013) alloys by positron annihilation, J. Mater. Sci. 41 (2006) 1059-1066.

[23] M. Madanat, Microscopic aspects of ageing in Al-Mg-Si alloys, (Ph.D. thesis), Technische Universität Berlin, 2018.

[24] M. Madanat, M. Liu, J. Banhart, Reversion of natural ageing in Al-Mg-Si alloys, Acta Mater. 159 (2018) 163-172.

[25] G. Dlubek, S. Krause, H. Krause, A.L. Beresina, V.S. Mikhalenkov, K.V. Chuistov, Positron studies of precipitation phenomena in Al-Li and in Al-Li-X (X = Cu,Mg or Sc) alloys, J. Phys.: Condens. Mat. 4 (1992) 6317-6328.

[26] S.J. Andersen, H.W. Zandbergen, J. Jansen, C. Traeholt, U. Tundal, O. Reiso, The crystal structure of the β " phase in Al-Mg-Si alloys, Acta Mater. 46 (1998) 3283-3298.

[27] C.S.T. Chang, J. Banhart, Low-temperature differential scanning calorimetry of an Al-Mg-Si alloy, Metall. Mater. Trans. A 42A (2011) 1960-1964.

[28] J. Banhart, M.D.H. Lay, C.S.T. Chang, A.J. Hill, Kinetics of natural aging in Al-Mg-Si alloys studied by positron annihilation lifetime spectroscopy, Phys. Rev. B 83 (2011) 014101.

[29] F. De Geuser, W. Lefebvre, D. Blavette, 3D atom probe study of solute atoms clustering during natural ageing and pre-ageing of an Al-Mg-Si alloy, Phil. Mag. Lett. 86 (2006) 227-234.

[30] M. Torsæter, H.S. Hasting, W. Lefebvre, C.D. Marioara, J.C. Walmsley, S.J. Andersen, R. Holmestad, The influence of composition and natural aging on clustering during preaging in Al-Mg-Si alloys, J. Appl. Phys. 108 (2010)

[31] I.A. Girifalco, H. Herman, A model for growth of Guinier-Preston zones - Vacancy pump, Acta Metall. 13 (1965) 583-590.

[32] K. Matsuda, S. Ikeno, H. Gamada, K. Fujii, Y. Uetani, T. Sato, A. Kamio, High-resolution electron microscopy on the structure of Gunier-Preston zones in an Al-1.6 mass Pct Mg2Si alloy, Metall. Mater. Trans. A 29 (1998) 1161-1167.

[33] J. Čižek, O. Melikhova, I. Procházka, Annealing process in quenched Al-Sn alloys: A positron annihilation study, Phys. Rev. B 71 (2005) 064106.

[34] O. Melikhova, J. Kuriplach, J. Čižek, I. Prochazka, Vacancy-solute complexes in aluminum, Appl. Surf. Sci. 252 (2006) 3285-3289.

[35] C. Szeles, K. Suevegh, Z. Homonnay, A. Vertes, Positron lifetime and Mössbauer spectroscopy study of vacancy-tin interaction in dilute Al-Sn alloys, Phys. Status. Solidi. A 103 (1987) 397-401.

[36] C. Szeles, K. Suevegh, Z. Homonnay, A. Vertes, Vacancy trapping at tin atoms during the recovery of a fast-quenched dilute aluminium-tin alloy and its effect on the isomer shift of the ^{119}Sn Mössbauer isotope, J. Phys. Condens. Matter 2 (1990) 3201-3217.

[37] F. Lotter, U. Mühle, M. Elsayed, A.M. Ibrahim, T. Schubert, R. Krause-Rehberg, B. Kieback, T.E.M. Staab, Precipitation Behavior in High Purity Aluminium Alloys with Trace Elements – The Role of Quenched in Vacancies, Phys. Status. Solidi. A 2155 (2018) 1800375.

[38] P. Lang, Y.V. Shan, E. Kozeschnik, The life-time of structural vacancies in the presence of solute trapping, Mater. Sci. Forum 794-796 (2014) 963-970.

[39] W.F. Miao, D.E. Laughlin, Precipitation hardening in aluminum alloy 6022, Scripta Mater. 40 (1999) 873-878.

[40] L. Resch, G. Klinser, E. Hengge, R. Enzinger, M. Luckabauer, W. Sprengel, R. Würschum, Precipitation processes in Al–Mg–Si extending down to initial clustering revealed by the complementary techniques of positron lifetime spectroscopy and dilatometry, J. Mater. Sci. 53 (2018) 14657–14665.

[41] Y.X. Lai, B.C. Jiang, C.H. Liu, Z.K. Chen, C.L. Wu, J.H. Chen, Low-alloy-correlated reversal of theprecipitation sequence in Al-Mg-Si alloys, J. Alloy. Compd. 701 (2017) 94-98.

[42] E.A. Mørtsell, C.D. Marioara, S.J. Andersen, J. Røyset, O. Reiso, R. Holmestad, Effects of germanium, copper, and silver substitutions on hardness and microstructure in lean Al-Mg-Si alloys, Metall. Mater. Trans. A 46 (2015) 4369-4379.

[43] S. Pogatscher, H. Antrekowitsch, H. Leitner, T. Ebner, P.J. Uggowitzer, Mechanisms controlling the artificial aging of Al-Mg-Si Alloys, Acta Mater. 59 (2011) 3352-3363.

[44] A. Falahati, P. Lang, E. Kozeschnik, Precipitation in Al-alloy 6016 - the role of excess vacancies, Mater. Sci. Forum 706-709 (2012) 317-322.

[45] S. Ringer, K. Hono, T. Sakurai, The effect of trace additions of sn on precipitation in Al-Cu alloys: an atom probe field ion microscopy study, Metall. Mater. Trans. A 26 (1995) 2207-2217.

[46] J. Silcock, H. Flower, Comments on a comparison of early and recent work on the effect of trace additions of Cd, In, or Sn on nucleation and growth of θ′ in Al–Cu alloys, Scripta Mater. 46 (2002) 389-394.

[47] S. Hirosawa, F. Nakamura, T. Sato, First-principles calculation of interaction energies between solutes and/or vacancies for predicting atomistic behaviors of microalloying elements in aluminum alloys, Mater. Sci. Forum 561-565 (2007) 283-286.

[48] C. Liu, Y. Lai, J. Chen, G. Tao, L. Liu, P. Ma, C. Wu, Natural-aging-induced reversal of the precipitation pathways in an Al–Mg–Si alloy, Scripta Mater. 115 (2016) 150-154.

[49] S. Rothman, N. Peterson, L. Nowicki, L. Robinson, Tracer diffusion of magnesium in aluminum single crystals, Phys. Status. Solidi. B 63 (1974) K29-K33.

[50] D. Bergner, E. Cyrener, Diffusion of Foreign Elements in Aluminum Solid Solutions. Pt. 3. Investigations Into the Diffusion of Silicon in Aluminum Using the Microprobe, Neue Hütte 18 (1973) 356-361.

[51] Y. Du, Y. Chang, B. Huang, W. Gong, Z. Jin, H. Xu, Z. Yuan, Y. Liu, Y. He, F.-Y. Xie, Diffusion coefficients of some solutes in fcc and liquid Al: critical evaluation and correlation, Mater. Sci. Eng. A 363 (2003) 140-151.

5.3 Paper III

Combined effect of Sn addition and pre-ageing on natural secondary and artificial ageing of Al-Mg-Si alloys

Xingpu Zhang[a,b,*], Meng Liu[a,b], John Banhart[a,b]

[a] Technische Universität Berlin, Hardenbergstraße 36, 10623 Berlin, Germany
[b] Helmholtz-Zentrum Berlin für Materialien und Energie, Hahn-Meitner-Platz 1, 14109 Berlin, Germany

*corresponding author: xingpu.zhang@helmholtz-berlin.de

Submitted to “Materials Science and Engineering: A”.

Abstract

Both Sn addition and pre-ageing (PA) have been shown to be able to maintain the artificial ageing (AA) potential after natural ageing (NA) of Al-Mg-Si alloys. In this study the combined effect of Sn addition and PA at 100 °C or 180 °C on natural secondary ageing (NSA) and subsequent artificial ageing (AA) of alloy AA6014 was investigated using hardness, resistivity and differential scanning calorimetry measurements. It is found that PA can suppress NSA and improve the AA hardening kinetics and response after 1 week of NSA in both alloys with and without Sn addition. The effect of PA at 100 °C is more pronounced in the Sn-free alloy while the combination of PA at 180 °C and adding Sn shows superiority in suppressing NSA and thus avoiding the undesired hardening before AA. Moreover, when a natural pre-ageing (NPA) step up to 8 h is applied before PA, the effect of PA at 100 °C in Sn-added alloy can be improved. The influence of Sn on vacancies at different ageing temperatures is discussed to explain the observed phenomena.

Keywords: Al-Mg-Si alloys; Sn addition; Pre-ageing; Natural secondary ageing; Artificial ageing; Natural pre-ageing

1. Introduction

The age-hardenability of Al-Mg-Si alloys is of great importance for their industrial application in automotive, aircraft, etc. Ideally, artificial ageing (AA) at ~180 °C is carried out immediately after quenching from the solutionising temperature (~540 °C) and the alloys can be largely strengthened. In practice, however, a delay at room temperature (RT) after solutionising treatment is inevitable and leads to the reduced hardening kinetics and achievable strength during following AA [1,2]. Therefore, various methods have been developed over the past decades to compensate the adverse effect of natural ageing (NA).

One viable method by microalloying with Sn has been investigated recently. As the diffusion of solute atoms requires excess vacancies, the desired retardation of NA can be achieved by reducing the available vacancies with Sn atoms that bind vacancies strongly at RT [3]. Upon subsequent AA, Sn-vacancy binding weakens and, thus, trapped vacancies are released [3] and the new thermal vacancies are no longer immobilized, thus, supporting the precipitate formation. As a result, a significant AA hardening potential can still be obtained in Sn-added alloy after a certain period of NA time [4]. However, Sn retards NA sufficiently only at low enough temperatures storage [5] and for alloys with low Mg and Si content because the solubility of Sn in Al-Mg-Si alloy is adversely influenced by the presence of Mg and Si [4,6].

Another commonly used method is pre-ageing (PA), i.e. samples are artificially underaged immediately after solutionising and quenching, which improves the AA response after NA [2,7–11]. Instead of NA clusters, PA clusters, which can further grow into β'' during AA, have been proposed to form above a critical temperature of ~67 °C [12]. Note that the term "PA cluster" is used to designate this phase in this paper, regardless of the different notations found in the literature, including PA cluster [11], cluster (2) [13], GP zone [14,15] and pre-β'' [16]. It has been found that the efficiency of PA shows a temperature dependence and that both the PA temperature and time must be controlled to avoid an excessive PA hardness [10,17]. Moreover, an enhanced PA effect achieved by minor addition of Cu [18,19] or Ag [20] has been demonstrated. Nevertheless, the possibility of combining PA treatment and Sn addition in diminishing the detrimental effect of NA has so far received little attention and only low PA temperatures (80–140 °C) have been considered [21].

In the present work, PA at both low and high temperatures (100 °C and 180 °C) is carried out on Al-Mg-Si alloys with and without Sn addition, aiming to find a good combination of the two approaches in suppressing NA and maintaining good AA response.

2. Experimental

Industrial AA6014 alloys with and without Sn were manufactured by the Novelis Research and Technology Center Sierre and received as sheets of 1 mm thickness. The alloy compositions are given in Table 1. The two alloys differ slightly in Mg, Si and Cu content, but the total amount of solutes is the same (1.35 at. %).

Solution heat treatment (SHT) was performed at 570 °C for 60 min with argon as the protective gas, after which quenching was done in ice water. Samples were then either stored in an incubator running at 20 °C for NA or immersed into an oil bath held at 100 °C or liquid metal (LM) Bi57Sn43 at 180 °C for PA. The same incubator was used for subsequent NSA after PA. Optional natural pre-ageing (NPA) at 20 °C for 4 or 8 h was conducted before PA at 100 °C for alloy 6014-70Sn. Final

AA was carried out in LM at 180 °C after 1 week of NA/NSA. The heat treatment procedures are given in Fig. 1.

Table 1. Chemical compositions of the alloys as determined by atomic emission spectroscopy and inductively coupled plasma optical emission spectrometry.

Alloy code	Mg (at.%)	Si (at.%)	Sn (ppm)	Cu (at.%)	Fe (at.%)	Mn (at.%)
6014	0.72	0.58	-	0.05	0.09	0.04
6014-70Sn	0.81	0.54	70	-	0.12	0.04

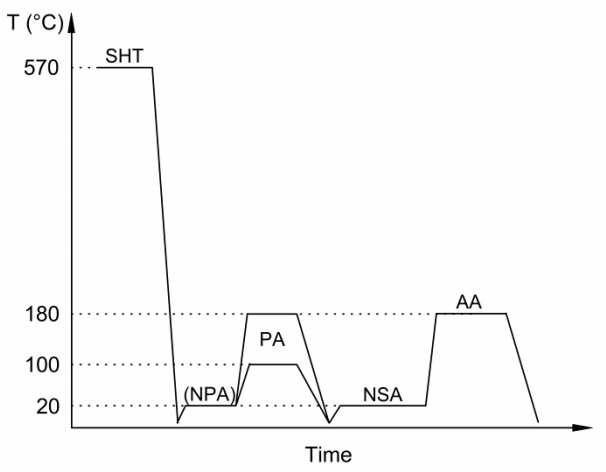

Fig. 1. Heat treatment procedures.

Brinell hardness was measured by employing a Qness 60M tester (1 mm indenter, 10 kg load and 10 s loading time). At least 10 indentations were performed for each sample. The hardness increment during NA/NSA is the value relative to the first measurement carried out after 3–4 min NA/NSA.

In-situ electrical resistivity measurements were performed using a four point probe system with a current of 100 mA. Sample wires (usually 500 mm long, 0.82 mm in diameter) were kept in an oil bath held at 20 °C during the measurements. The change of resistivity ($\Delta\rho$) during NA/NSA is calculated by subtracting the initial value measured after 2–3 min NA/NSA.

DSC measurements were carried out with samples (1 mm thick, 5 mm in diameter) in a Netzsch 204 F1 Phoenix. Pure Al (99.999 %) was used as the reference sample. To avoid storage at RT, samples were stored in liquid nitrogen immediately after quenching. After being held for 5 min in the pre-cooled (0 °C) chamber, DSC analyses were performed from 0 °C to 400 °C with a scanning rate of 10 K/min. The curve obtained with two empty crucibles was used as the baseline.

3. Results

3.1. State during NA/NSA

For alloys 6014(Sn) – meaning both alloys 6014 and 6014-70Sn – after solutionising and quenching, Sn addition delays the hardening kinetics during NA, i.e. alloy 6014 shows a continuous hardness increase, while hardness for alloy 6014-70Sn stays constant for 8 h before the increase (black lines in Fig. 2a, c). A hardness value ~72 HBW is reached after half a year in both alloys. After PA at 100 °C and 180 °C, the hardness of the alloys is increased (more pronounced in alloy 6014 than in 6014-70Sn, see the insets in Fig. 2a, c) and the following hardening during NSA is retarded compared to the alloys without PA (Fig. 2a, c). Stages of constant hardness are also observed in alloy 6014 with PA time ≥ 10 min at 100 °C and ≥ 1 min at 180 °C. Moreover, analysis of the hardness increment shows that after the same PA treatment at 100 °C the increase in alloy 6014-70Sn starts later but surpasses that of alloy 6014 during ensuing NSA (Fig. 2b). The later hardness increase in alloy 6014-70Sn is also observed after PA at 180 °C but no data after long enough NSA time are available to determine the intersection, see Fig. 2d.

Fig. 3a shows the electrical resistivity changes in alloys 6014(Sn) during NA and NSA after PA at 100 °C and 180 °C. During NA, the resistivity increase in alloy 6014 exhibits similar distinct stages on the logarithmic time scale as previously described [22]. Sn addition slows down the resistivity change markedly. After ~1 week of NA, the resistivity increase in the two alloys reaches a comparable value. For both alloys, PA not only slows down the resistivity increase but also reduces the value achieved within 1 week of NSA. As for the hardness increment it was found that after the same PA treatment at 100 °C the resistivity increases later in alloy 6014-70Sn but reaches higher values than in alloy 6014. The rates of resistivity change during NA/NSA are assessed with the derivatives dρ/dt (Fig. 3b). During NA, dρ/dt in alloy 6014 decreases continuously, while in alloy 6014-70Sn it starts with much smaller values and remains constant for longer than 1 d before the final decrease. After PA, the initial dρ/dt values during NSA in both alloys are decreased. PA generates and extends stages with negligible rate change in alloys 6014 and 6014-70Sn, respectively. Differing from the following continuous drop in alloy 6014, a noticeable increase in dρ/dt is found in alloy 6014-70Sn after certain PA times depending on the ageing temperature.

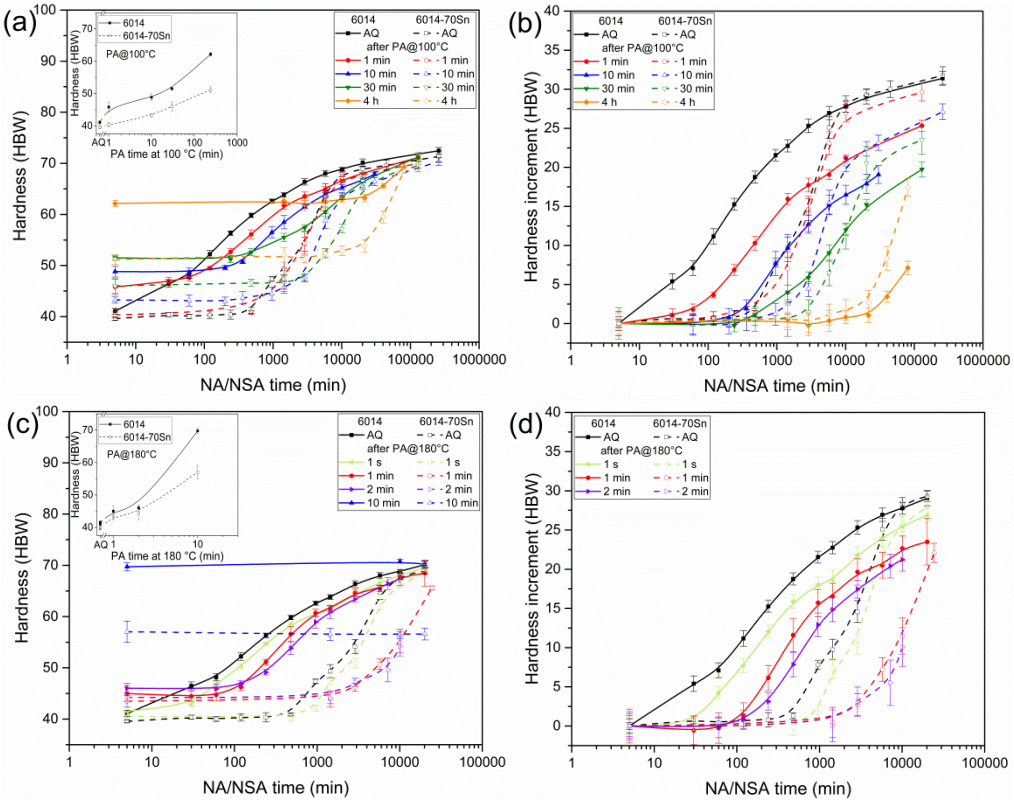

Fig. 2. Hardness evolution and increment during NA and NSA after PA at (a, b) 100 °C and (c, d) 180 °C for alloys 6014(Sn). ‘AQ’ refers to alloys after solutionising and quenching without PA. The hardness increase during PA at (a) 100 °C and (c) 180 °C is given in the insets (more data for longer PA times can be found in [23]).

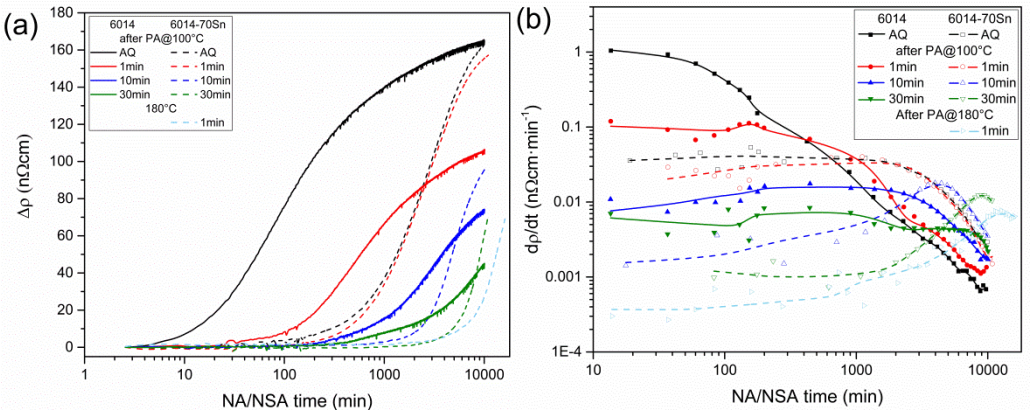

Fig. 3. (a) Changes and (b) derivatives of electrical resistivity in alloys 6014(Sn) during NA/NSA.

3.2. State after 1 week of NA/NSA

DSC analysis of alloys 6014(Sn) after various heat treatments is shown in Fig. 4. Directly after quenching (AQ), alloy 6014 exhibits three exothermic peaks – ‘1’ around 75 °C, ‘3’ around 247 °C and ‘4’ around 298 °C, while alloy 6014-70Sn shows comparable peaks but with strongly suppressed ‘1’ (grey lines in Fig. 4a, b). After 1 week of NA, the exothermic peak ‘1’ can hardly be observed for the two alloys; the endothermic trough ‘2’ appears between 145 °C and 241 °C for alloy 6014 and between 170 °C and 247 °C for alloy 6014-70Sn; the exothermic peaks ‘3’ and ‘4’

are delayed to higher temperatures. PA diminishes the trough '2' and shifts '3' and '4' to lower temperatures with increasing PA times in both alloys.

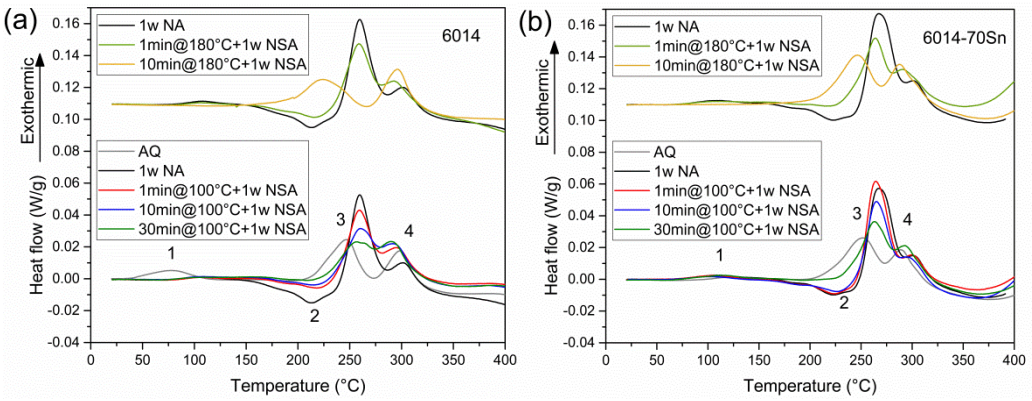

Fig. 4. DSC traces in alloys (a) 6014 and (b) 6014-70Sn after various heat treatments measured at a scanning rate of 10 K/min.

3.3. State during AA

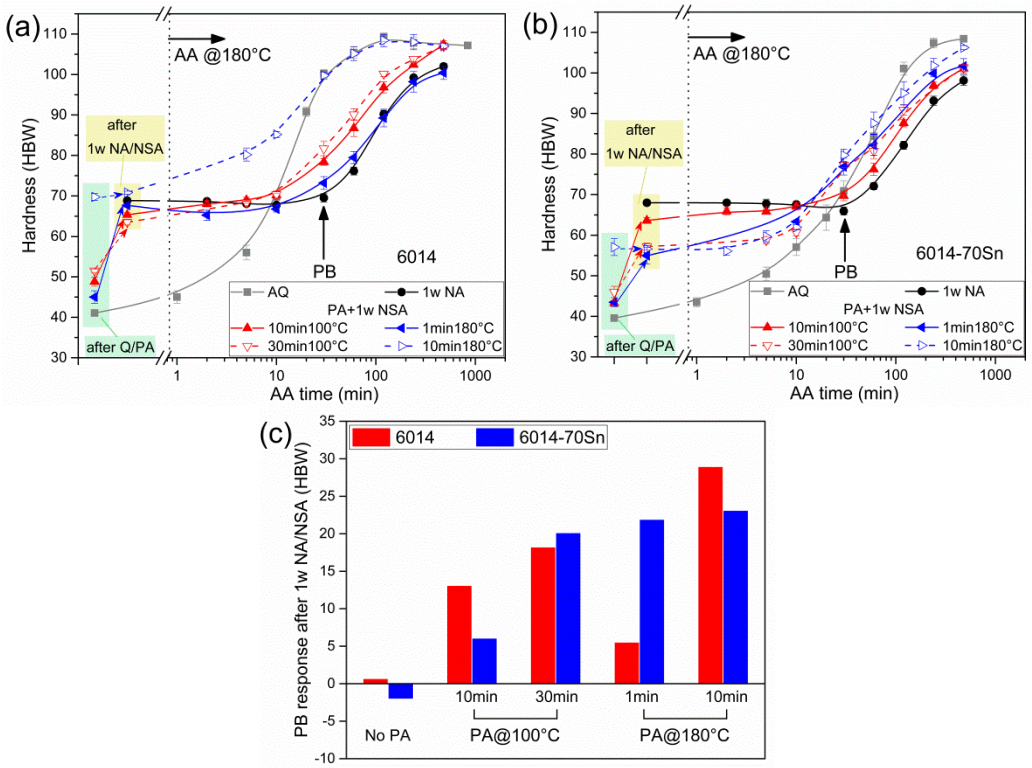

Fig. 5. Hardness evolution in 1 week of NA/NSA and in the subsequent AA in alloys (a) 6014 and (b) 6014-70Sn. (c) PB response after 1 week of NA/NSA obtained by subtracting the hardness after NA/NSA from PB hardness.

Fig. 5a, b compares the hardness evolution in 1 week of NA/NSA and in the subsequent AA at 180 °C in alloys 6014(Sn). The hardness directly after solutionising and quenching and after ensuing PA is taken from Fig. 2 and marked with green boxes. After quenching and 1 week of NA, a hardness value ~69 HBW is reached for both alloys. When PA is carried out, the hardness after 1

week of NSA is smaller and the reduction is much more pronounced in alloy 6014-70Sn than in alloy 6014 (yellow boxes). During AA, hardness in as-quenched alloys 6014(Sn) starts from ~40 HBW and increases continuously (grey curves). After 1 week of prior NA, a stagnation of hardness or even a slight drop is observed in the early stage of AA in both alloys (black curves). This NA also delays the AA kinetics and reduces the AA hardening response.

Compared to the alloys only naturally aged for 1 week, alloys after PA and NSA do not show any initial decrease during AA except for alloy 6014 after 1 min PA at 180 °C. The hardness increase with prolonged AA time is accelerated and the achievable hardness is improved by prior PA. Paint baking (PB = 30 min AA at 180 °C) response is improved by PA for both alloys (Fig. 5c). It is noteworthy that for alloy 6014-70Sn, 1 min PA at 180 °C even generates a hardness response superior to 30 min PA at 100 °C.

3.4. Influence of NPA on the effect of PA in alloy 6014-70Sn

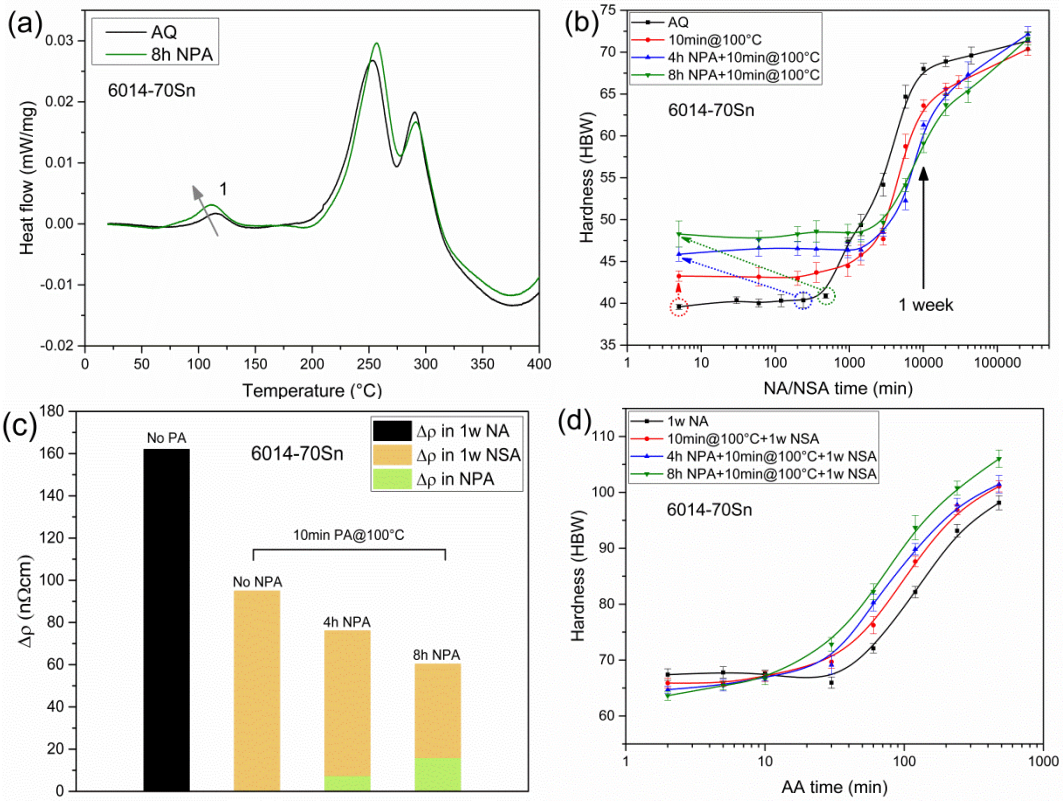

Fig. 6. (a) DSC traces for alloy 6014-70Sn directly after solutionising and quenching and after 8 h NPA. Influence of PA (10 min at 100 °C) and additional NPA (4 h and 8 h) before PA on (b) the hardness evolution during NA/NSA, (c) Δρ in 1 week of NA/NSA and (d) AA after 1 week of NA/NSA. The hardness data for the black and red curves in (b) and (d) are taken from Fig. 2a and Fig. 5b, respectively. The resistivity data for the cases of "No PA" and "10 min PA without NPA" in (c) are taken from Fig. 3a.

The DSC trace obtained for a sample after 8 h natural pre-ageing (NPA) exhibits a larger peak 1 with a lower peak temperature than the as-quenched one (Fig. 6a). NPA up to 8 h hardly changes

hardness but promotes the hardness increase during the subsequent 10 min PA at 100 °C (see dotted arrows in Fig. 6b). Such NPA delays the ageing kinetics during NSA after PA and notably reduces the hardness value reached after 1 week of NSA. Even taking the resistivity increase during NPA into account, the effect of PA in suppressing the total resistivity increase in 1 week of NSA can still be further enhanced by NPA (Fig. 6c). In addition, NPA promotes both the kinetics and the hardening response during AA after 1 week of NSA (Fig. 6d).

4. Discussion

4.1. State during NA/NSA

During NA after solutionising and quenching, solute atoms diffuse and form NA clusters with the assistance of quenched-in vacancies [24,25]. On the one hand, as these NA clusters can act as obstacles that moving dislocations have to overcome [26,27], the alloys are hardened, see Fig. 2a, c. On the other hand, the increasing electron scattering arising from NA clusters [28] leads to the increase in electrical resistivity (Fig. 3a). The observed retarding effect of Sn on both hardness and resistivity is consistent with earlier works [5,6,29–31] and can be ascribed to the strong interaction between Sn atoms and vacancies (0.281 eV [32]). After quenching, in comparison with alloy 6014, vacancies tend to bind with Sn atoms instead of Mg/Si atoms in alloy 6014-70Sn. Vacancy-assisted solute diffusion is thus retarded, resulting in the slower NA kinetics. In alloy 6014, the observed gradual decrease in dρ/dt with longer NA (Fig. 3b), which was also reported in Refs. [33,34], might be a consequence of the continuous drop in vacancy and solute concentration. In contrast, smaller dρ/dt with an initial roughly constant stage is found in alloy 6014-70Sn, caused mainly by fewer less vacancies available for diffusion and much slower loss of vacancies in the presence of Sn atoms because the early stage of NA has been shown to be dominated by vacancy loss [33].

The increase of hardness during PA in both alloys with and without Sn (insets in Fig. 2a, c) is thought to be caused by the formation of PA clusters, and the relatively lower hardness in alloy 6014-70Sn than in alloy 6014 after the same PA treatment indicates that Sn still delays the ageing kinetics even at 100 °C and 180 °C [23]. PA has been proposed to be able to reduce and even suppress subsequent clustering at RT [7,35], in agreement with the observed slower kinetics of hardness and resistivity evolution during NSA. Beside the consumption of solutes caused by the formation of PA clusters, the lowered vacancy concentration after PA [23] may also account for the reduced kinetics. When considering the effect of Sn addition, much slower NSA kinetics is still found in alloy 6014-70Sn than in alloy 6014 after same PA treatment (Fig. 2a, c and Fig. 3a). Our previous study [23] has revealed that Sn-vacancy complexes are stable up to 1 week at 100 °C while the detachment of vacancies from Sn occurs in a few minutes at 180 °C. Therefore, it appears that vacancies, which may be released from Sn during PA (especially at 180 °C), are recaptured by Sn

atoms during subsequent quenching and NSA. The rate of resistivity change in alloy 6014 during NSA is similar as during NA, i.e. gradually decreases with ageing time, while dρ/dt in alloy 6014-70Sn exhibits a distinct increase and even crosses that of alloy 6014. This increase is not explainable in terms of the not-increasing solute supersaturation and vacancy concentration but possibly related to a composition change of the matrix as claimed to cause anomalous resistivity increase during NSA after reversion ageing, however without experimental proof [33].

In spite of the slower ageing kinetics during NSA in alloy 6014-70Sn than in alloy 6014, the total increment of hardness (Fig. 2b) and resistivity (Fig. 3a) after the same PA treatment at 100 °C is eventually larger in alloy 6014-70Sn, i.e. the curves cross. The larger resistivity increment in alloy 6014-70Sn is linked to the higher derivative dρ/dt in late stages of NSA than alloy 6014 as discussed in the previous paragraph. As the formation of PA clusters at 100 °C is still retarded by Sn addition, a lower consumption of solutes during PA in alloy 6014-70Sn can be deduced, which is reflected by the smaller hardness increase during PA. Moreover, it has been demonstrated that Sn alters the ageing course only through controlling the vacancy migration [6], therefore, the more remaining solutes seem to be the reasonable explanation for the larger NSA potential in alloy 6014-70Sn.

4.2. State after 1 week of NA/NSA

Although Sn addition slows down the formation of NA clusters, after 1 week of NA, a similar increment of hardness and resistivity is still reached in alloys 6014 with and without Sn (first points in Fig. 7a, b). The disappearance of the clustering peak ‘1’ in the DSC traces after 1 week of NA (Fig. 4a, b), which was also reported for a naturally aged Al-0.59 wt.% Mg-0.82 wt.% Si alloy by Chang et al. [36], also reveals the formation of NA clusters. The dissolution of such clusters during the linear heating of DSC measurements results in the notable trough ‘2’.

In the case of samples after PA, the increment of hardness and resistivity (Fig. 7a, b) and the area of the dissolution trough ‘2’ after 1 week of NSA (Fig. 7c) are all reduced, implying the suppression of NA cluster formation as described in Section 4.1. In addition, the influence of PA on 1 week of NSA shows a dependence on the PA temperature and the addition of Sn – PA at 100 °C is more effective in alloy 6014 than in alloy 6014-70Sn while alloy 6014-70Sn is more significantly influenced by PA at 180 °C. At 100 °C, the strong Sn-vacancy binding still exists, which slows down PA kinetics greatly and retains higher solute and vacancy concentrations for the following NSA in alloy 6014-70Sn than in alloy 6014. However, when increasing PA temperature to 180 °C, vacancies in alloy 6014-70Sn are released in a short time with weakened binding between Sn atoms and vacancies and newly formed thermal vacancies will no longer be strongly bound to Sn atoms. This accelerates the formation of PA clusters and leads to a faster vacancy loss compared to PA at 100 °C. Furthermore, the difference in the PA cluster formation rate between alloys with and

without Sn is also reduced at 180 °C. During following NSA, Sn atoms become effective again in trapping vacancies. All these factors result in the superior capability of the combination of Sn addition and PA at 180 °C to prevent NSA for 1 week. Fig. 7d demonstrates that the decrease of hardness increment in 1 week of NA/NSA scales with PA hardness, reflecting the more suppressed NSA by larger solute consumption during PA. Moreover, benefiting from the influence of Sn on vacancies during NSA, a lower PA hardness in alloy 6014-70Sn than in alloy 6014 is required to inhibit NSA in 1 week.

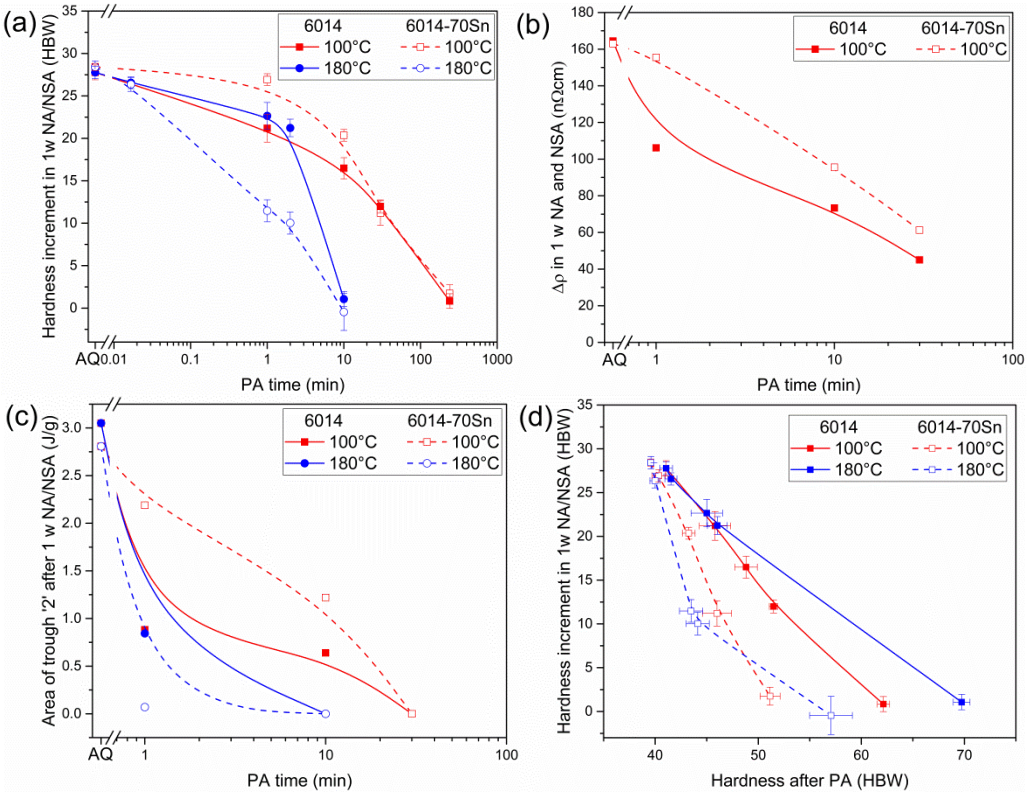

Fig. 7. (a) Hardness and (b) electrical resistivity increment during 1 week of NA/NSA as function of PA time with data taken from Fig. 2b, d and Fig. 3a. (c) Area of DSC dissolution trough '2' for alloys after various PA times and 1 week of NA/NSA as calculated from Fig. 4a, b. (d) Hardness increment during 1 week of NA/NSA as a function of PA hardness.

4.3. State during AA

Directly after solutionising and quenching, the high solute supersaturation and, for short period, probably also the high initial vacancy concentration result in the fast formation of β'' (main strengthening precipitate [37,38]) and thus the hardness increases during AA (Fig. 5). 1 week of NA, however, influences AA kinetics adversely, reduces the hardening response and postpones the formation of β'' (peak '3' in Fig. 4) to higher temperatures. The lowered vacancy concentration resulting from the annihilation of vacancies into sinks [39] and the "vacancy-prison" effect of the formed NA clusters [40] is among the possible explanations. The dissolution of NA clusters and the associated release of the prisoned vacancies, which have been previously reported to occur at a

relatively high temperature, e.g. 250 °C [40], is limited at 180 °C (see the slight "softening" in the early AA stage in Fig. 5). Another reason for the negative effect of NA might lie in the fact that NA clusters cannot transform into β'' during AA [41] but rather reduce the solute supersaturation. In addition, the potential of Sn in promoting AA of naturally aged alloys as previously reported in Refs. [3,4] is not found in our case. This means that although Sn addition slows down the NA ageing kinetics by trapping vacancies, the NA clusters formed, which still cause a negative effect on the following AA, are not changed in type.

It has been shown that PA mitigates the negative effect of NA on AA in both alloys (Fig. 5a, b). The PB response after 1 week of NSA (Fig. 5c) is found to be consistent with the extent of the suppression in NSA response for 1 week (reduction in the increment of hardness and resistivity and in the area of the DSC dissolution trough, Fig. 7). In other words, a larger PB response is obtained with smaller NSA response and vice versa. Furthermore, it has been reported that for Al-Mg-Si alloys, clusters (mainly Si-rich) formed during NSA after PA can still lead to a sluggish PB response [10,42]. Therefore, the positive effect of PA might be partly associated to the suppression of NSA caused by the reduced solute and vacancy concentrations after PA. Besides, the enhanced AA can also originate from the behavior of PA clusters during AA. Compared to NA clusters formed at RT, PA clusters with a larger size [11,15,43] and an average Mg/Si ratio closer to that of β'' [11,13,44] can act as nuclei for β'' during following AA (thus PA clusters are sometimes also mentioned as 'good clusters' [45]). The lowered peak temperatures and reduced peak size of β'' observed after PA (Fig. 4) is thought to be a result of the existence of nuclei for β''.

Owing to the PA kinetics delayed by Sn, alloy 6014 may be preferred rather than alloy 6014-70Sn from the single perspective of the formation of PA clusters. However, its relatively higher hardness after 1 week of NSA than in the Sn-added alloy (yellow boxes in Fig. 5a, b), either resulting from the higher PA hardness or the NSA response, may cause problems in the engineering practice, where a good stampability after RT storage is desired [46,47]. The lower hardness obtained with the combination of Sn addition and PA would just meet this requirement without compromising the AA response. It should also be noted that to achieve the optimum performance of PA in Sn-added alloy, a higher temperature (e.g. 180 °C in our study) is necessary.

4.4. Influence of NPA on the effect of PA in alloy 6014-70Sn

Surprisingly, the application of NPA before PA can improve the performance of PA at 100 °C in alloy 6014-70Sn (Fig. 6). This is contrary to the findings in Sn-free Al-Mg-Si alloy reported by Torsæter et al. [44], who found that the formation of PA clusters is adversely influenced by 1 week of NPA, which was explained by the depletion of solute in the vicinity of formed NA clusters. It has been speculated that the Si-vacancy complexes or small Si clusters formed during quenching are able to promote the formation of PA clusters [7]. We suspect that this discrepancy might be

associated to the size of NA clusters, pointing at the NA clustering process being modified by Sn addition. Compared to the Sn-free alloy, the distance that solutes in the presence of Sn can diffuse in unit time during NPA is largely reduced owing to the decreased number of available vacancies (as described in Section 4.1). As a consequence, smaller but more densely distributed clusters are formed in alloy 6014-70Sn than in alloy 6014. This is supported by previous resistivity measurements [6] and a comparable phenomenon was also reported for Al-Mg-Si alloys containing Cu, which also has a stronger binding with vacancy than Mg/Si solutes [48]. After 8 h NPA, clusters are formed, which are still not big enough to contribute to hardness (black curve in Fig. 6b) but have increased electrical resistivity (Fig. 3a and Fig. 6c), because it has been reported that hardness is more sensitive to the size of clusters [5] while resistivity depends more on their number density [5,49]. These clusters can either further grow into larger NA clusters at RT (the appearance of hardening after incubation of 8 h in Fig. 6b) or transform into PA clusters at 100 °C (promoted DSC clustering peak 1 in Fig. 6a and elevated PA hardness in Fig. 6b). The accelerated formation of PA clusters generates the suppressed NSA (Fig. 6b, c) and promoted AA (Fig. 6d), in agreement with the discussion in Sections 4.1 and 4.3.

5. Conclusions

In this study, we investigated the combined effect of Sn addition and PA on the ageing behavior of Al-Mg-Si alloys, aiming to find a favorable combination to suppress NSA and enhance subsequent AA.

1. PA can suppress the formation of NA clusters and improve the AA kinetics and response after 1 week of NSA in alloys with and without Sn.
2. The strong interaction between Sn and vacancies delays the PA kinetics at 100 °C greatly. Therefore, a higher temperature (e.g. 180 °C) is required for a better PA performance in Sn-added alloy by weakening the Sn-vacancy binding.
3. The undesired high hardness after PA and subsequent NSA in Sn-free alloy can be lowered by adding Sn.
4. The effect of PA at 100 °C in 6014-70Sn can be promoted by prior NPA. The reason might be the Sn-induced smaller clusters at RT, which can transform to PA clusters at 100 °C.

Acknowledgements

The Deutsche Forschungsgemeinschaft (DFG) partially funded this project (Ba1170/22). Xingpu Zhang thanks the China Scholarship Council (CSC) for a research fellowship (No. 201506170013). We thank Dr. Zeqin Liang and David Leyvraz of Novelis Research and Technology Center Sierre for providing the alloys.

References

[1] D.W. Pashley, J.W. Rhodes, A. Sendorek, Delayed ageing in aluminium-magnesium-silicon alloys: effect on structure and mechnical properties, J. Inst. Met. Lond. 94 (1966) 41–49.

[2] P. Brenner, H. Kostron, Über die Vergütung der Aluminium-Magnesium-Silizium Legierungen (Pantal), Zeitsschrift Für Met. 31 (4) (1939) 89–97.

[3] S. Pogatscher, H. Antrekowitsch, M. Werinos, F. Moszner, S.S.A. Gerstl, M.F. Francis, W.A. Curtin, J.F. Löffler, P.J. Uggowitzer, Diffusion on demand to control precipitation aging: Application to Al-Mg-Si alloys, Phys. Rev. Lett. 112 (2014).

[4] M. Werinos, H. Antrekowitsch, T. Ebner, R. Prillhofer, W.A. Curtin, P.J. Uggowitzer, S. Pogatscher, Design strategy for controlled natural aging in Al-Mg-Si alloys, Acta Mater. 118 (2016) 296–305.

[5] M. Werinos, H. Antrekowitsch, T. Ebner, R. Prillhofer, P.J. Uggowitzer, S. Pogatscher, Hardening of Al-Mg-Si alloys: Effect of trace elements and prolonged natural aging, Mater. Des. 107 (2016) 257–268.

[6] M. Liu, X. Zhang, B. Körner, M. Elsayed, Z. Liang, D. Leyvraz, J. Banhart, Effect of Sn and In on the natural ageing kinetics of Al-Mg-Si alloys, Materialia. 6 (2019) 100261.

[7] K. Yamada, T. Sato, A. Kamio, Effects of quenching conditions on two-step aging behavior of Al-Mg-Si alloys, Mater. Sci. Forum. 331–337 (2000) 669–674.

[8] L. Ding, Y. Weng, S. Wu, R.E. Sanders, Z. Jia, Q. Liu, Influence of interrupted quenching and pre-aging on the bake hardening of Al-Mg-Si Alloy, Mater. Sci. Eng. A. 651 (2016) 991–998.

[9] L. Cao, P.A. Rometsch, M.J. Couper, Effect of pre-ageing and natural ageing on the paint bake response of alloy AA6181A, Mater. Sci. Eng. A. 571 (2013) 77–82.

[10] Y. Zi, L. Zeqin, D. Leyvraz, J. Banhart, Effect of pre-ageing on natural secondary ageing and paint bake hardening in Al-Mg-Si alloys, Materialia. 7 (2019) 100413.

[11] M.W. Zandbergen, Q. Xu, A. Cerezo, G.D.W. Smith, Study of precipitation in Al-Mg-Si alloys by Atom Probe Tomography I. Microstructural changes as a function of ageing temperature, Acta Mater. 101 (2015) 136–148.

[12] M. Saga, Y. Sasaki, M. Kikuchi, Z. Yan, M. Matsuo, Effect of pre-aging temperature on the behavior in the early stage of aging at high temperature for Al-Mg-Si alloy, Mater. Sci. Forum. 217–222 (1996) 821–826.

[13] A. Serizawa, S. Hirosawa, T. Sato, Three-Dimensional Atom Probe Characterization of Nanoclusters Responsible for Multistep Aging Behavior of an Al-Mg-Si Alloy, Metall. Mater. Trans. A. 39 (2008) 243–251.

[14] G.A. Edwards, K. Stiller, G.L. Dunlop, M.J. Couper, The precipitation sequence in Al-Mg-Si alloys, Acta Mater. 46 (1998) 3893–3904.

[15] M. Murayama, K. Hono, Pre-precipitate clusters and precipitation processes in Al-Mg-Si alloys, Acta Mater. 47 (1999) 1537–1548.

[16] C.D. Marioara, S.J. Andersen, J. Jansen, H.W. Zandbergen, The influence of temperature and storage time at RT on nucleation of the beta’’ phase in a 6082 Al-Mg-Si alloy, Acta Mater. 51 (2003) 789–796.

[17] Y. Birol, Pre-aging to improve bake hardening in a twin-roll cast Al-Mg-Si alloy, Mater. Sci. Eng. A. 391 (2005) 175–180.

[18] M.W. Zandbergen, A. Cerezo, G.D.W. Smith, Study of precipitation in Al-Mg-Si alloys by atom probe tomography II. Influence of Cu additions, Acta Mater. 101 (2015) 149–158.

[19] W.F. Miao, D.E. Laughlin, Effects of Cu content and preaging on precipitation characteristics in aluminum alloy 6022, Metall. Mater. Trans. A. 31 (2000) 361–371.

[20] Y. Weng, Z. Jia, L. Ding, M. Liu, X. Wu, Q. Liu, Combined effect of pre-aging and Ag/Cu addition on the natural aging and bake hardening in Al-Mg-Si alloys, Prog. Nat. Sci. Mater. Int. 28 (2018) 363–370.

[21] F. Schmid, P.J. Uggowitzer, R. Schäublin, M. Werinos, T. Ebner, S. Pogatscher, Effect of Thermal Treatments on Sn-Alloyed Al-Mg-Si Alloys, Materials. 12 (2019) 1801.

[22] J. Banhart, C.S.T. Chang, Z.Q. Liang, N. Wanderka, M.D.H. Lay, A.J. Hill, Natural aging in Al-Mg-Si alloys - A process of unexpected complexity, Adv. Eng. Mater. 12 (2010) 559–571.

[23] X. Zhang, M. Liu, H. Sun, J. Banhart, Influence of Sn on the age hardening behavior of Al-Mg-Si alloys at different temperatures, Materialia. 8 (2019) 100441.

[24] L.A. Girifalco, H. Herman, A model for the growth of Guinier-Preston zones-the vacancy pump, Acta Metall. 13 (1965) 583–590.

[25] H.S. Zurob, H. Seyedrezai, A model for the growth of solute clusters based on vacancy trapping, Scr. Mater. 61 (2009) 141–144.

[26] M.J. Starink, L.F. Cao, P.A. Rometsch, A model for the thermodynamics of and strengthening due to co-clusters in Al-Mg-Si-based alloys, Acta Mater. 60 (2012) 4194–4207.

[27] S. Esmaeili, D.J.J. Lloyd, W.J.J. Poole, Modeling of precipitation hardening for the naturally aged Al-Mg-Si-Cu alloy AA6111, Acta Mater. 51 (2003) 3467–3481.

[28] C. Panseri, T. Federighi, A resistometric study of preprecipitation in an aluminium-1.4 % Mg2Si alloy, J. Inst. Met. London. 94 (1966) 99–197.

[29] S. Muromachi, T. Mae, On the two-step aging behavior of Al-1.3 wt%Mg2Si alloy, J. Jap. Inst. Met. 38 (1974) 130–138.

[30] H. Shishido, Y. Takaki, M. Kozuka, K. Matsumoto, Y. Aruga, Effects of Sn addition on clustering and age-hardening behavior in a pre-aged Al-Mg-Si alloy, Mater. Sci. Forum. 877 (2017) 455–460.

[31] T. Cheng, Z. Jia, Y. Weng, L. Hao, Q. Liu, Effects of Sn/In additions on natural and artificial ageing of Al-Mg-Si alloys, Mater. Sci. Technol. 34 (2018) 2136–2144.

[32] P. Lang, Y. V. Shan, E. Kozeschnik, The life-time of structural vacancies in the presence of solute trapping, Mater. Sci. Forum. 794–796 (2014) 963–970.

[33] M. Madanat, M. Liu, J. Banhart, Reversion of natural ageing in Al-Mg-Si alloys, Acta Mater. 159 (2018) 163–172.

[34] H. Seyedrezai, D. Grebennikov, P. Mascher, H.S. Zurob, Study of the early stages of clustering in Al-Mg-Si alloys using the electrical resistivity measurements, Mater. Sci. Eng. A. 525 (2009) 186–191.

[35] Y. Yan, Investigation of the negative and positive effects of natural aging on artificial aging response in Al-Mg-Si alloys, Technische Universität Berlin, Berlin, 2014.

[36] C.S.T. Chang, J. Banhart, Low-temperature differential scanning calorimetry of an Al-Mg-Si alloy, Metall. Mater. Trans. A Phys. Metall. Mater. Sci. 42 (2011) 1960–1964.

[37] H.W. Zandbergen, S.J. Andersen, J. Jansen, Structure determination of Mg5Si6:particles in Al by dynamic electron diffraction studies, Science. 277 (1997) 1221–1225.

[38] W.F. Miao, D.E. Laughlin, Precipitation hardening in aluminum alloy 6022, Scr. Mater. 40 (1999) 873–878.

[39] A. Falahati, P. Lang, E. Kozeschnik, Precipitation in Al-alloy 6016 - the role of excess vacancies, Mater. Sci. Forum. 706–709 (2012) 317–322.

[40] S. Pogatscher, H. Antrekowitsch, H. Leitner, T. Ebner, P.J. Uggowitzer, Mechanisms controlling the artificial aging of Al-Mg-Si Alloys, Acta Mater. 59 (2011) 3352–3363.

[41] Y. Aruga, M. Kozuka, Y. Takaki, T. Sato, Formation and reversion of clusters during natural aging and subsequent artificial aging in an Al-Mg-Si alloy, Mater. Sci. Eng. A. 631 (2015) 86–96.

[42] Y. Aruga, M. Kozuka, Y. Takaki, T. Sato, Effects of natural aging after pre-aging on clustering and bake-hardening behavior in an Al-Mg-Si alloy, Scr. Mater. 116 (2016) 82–86.

[43] Y. Aruga, M. Kozuka, Y. Takaki, T. Sato, Evaluation of Solute Clusters Associated with Bake-Hardening Response in Isothermal Aged Al-Mg-Si Alloys Using a Three-Dimensional Atom Probe, Metall. Mater. Trans. A Phys. Metall. Mater. Sci. 45 (2014) 5906–5913.

[44] M. Torsæter, H.S. Hasting, W. Lefebvre, C.D. Marioara, J.C. Walmsley, S.J. Andersen, R. Holmestad, The influence of composition and natural aging on clustering during preaging in Al-Mg-Si alloys, J. Appl. Phys. 108 (2010).

[45] S. Wenner, K. Nishimura, K. Matsuda, T. Matsuzaki, D. Tomono, F.L. Pratt, C.D. Marioara, R. Holmestad, Muon kinetics in heat treated Al (-Mg)(-Si) alloys, Acta Mater. 61 (2013) 6082–6092.

[46] O. Engler, J. Hirsch, Texture control by thermomechanical processing of AA6xxx Al-Mg-Si sheet alloys for automotive applications - a review, Mater. Sci. Eng. A. 336 (2002) 249–262.

[47] S.M. Hirth, G.J. Marshall, S.A. Court, D.J. Lloyd, Effects of Si on the aging behaviour and formability of aluminium alloys based on AA6016, Mater. Sci. Eng. A. 319–321 (2001) 452–456.

[48] M. Liu, J. Banhart, Effect of Cu and Ge on solute clustering in Al-Mg-Si alloys, Mater. Sci. Eng. A. 658 (2016) 238–245.

[49] S. Esmaeili, D. Vaumousse, M.W. Zandbergen, W.J. Poole, A. Cerezo, D.J. Lloyd, A study on the early-stage decomposition in the Al-Mg-Si-Cu alloy AA6111 by electrical resistivity and three-dimensional atom probe, Philos. Mag. 87 (2007) 3797–3816.

6. Conclusions

In the present work, we investigated the ageing behaviors of Sn-added Al-Mg-Si alloys at various temperatures (from 20 °C to 250 °C) and the combination of Sn addition and pre-ageing. Five techniques including positron annihilation lifetime spectroscopy (PALS), hardness, differential scanning calorimetry (DSC), electrical resistivity and transmission electron microscopy (TEM) measurements were employed. The main findings are summarized as follows:

Natural ageing (NA) at room temperature can be suppressed by reducing the vacancy concentration available for solute diffusion via adding Sn/In, which has a strong binding with vacancies. Beside single Sn atoms, the formed Sn-containing clusters can also immobilize vacancies and further reduce the clustering rate. Sn addition simply delays the clustering in the early ageing stages (Stage I and Stage II), while Stage III becomes less pronounced when Sn is present. Cluster coarsening occurring during Stage III leads to an abnormal reincrease in the intensity of the vacancy component of positron lifetimes. Sn addition leads to the formation of smaller but more densely distributed clusters, resulting in the larger electrical resistivity increase in the Sn-added alloy than in the Sn-free alloy.

Sn atoms can still bind vacancies strongly enough at 100 °C and 140 °C to delay ageing kinetics. The interaction between vacancies and pre-ageing (PA) clusters results in a similar positron lifetime evolution as at RT. When ageing temperature is increased to 180 °C, the influence of Sn addition depends on the composition of the alloys. For the lean alloy, Sn atoms can prevent the fast vacancy loss during heating and release vacancies subsequently, thus accelerating ageing kinetics. In addition, Sn atoms act as nucleation sites for precipitation, increasing the precipitate number density largely. For the concentrated alloy, the high solute concentration facilitates the formation of clusters, which retain vacancies during heating even without the assistance of Sn atoms. When Sn is added, the stronger binding between Sn (Sn-containing clusters) and vacancies than between Sn-free clusters and vacancies rather delays the subsequent ageing kinetics. At even higher temperatures (210 °C and 250 °C), Sn ensures a higher vacancy concentration in the early stage of ageing and helps in nucleating of precipitates, resulting in the promoted ageing kinetics and hardening response. The higher activation energy (by 0.22 eV–0.29 eV) found in Sn-added alloys than in Sn-free alloys reveals the additional separation of Sn-vacancy complexes during ageing process.

NA clusters formed in the presence of Sn still have a negative effect on the subsequent artificial ageing (AA). PA can further enhance the retarding effect of Sn on NA clustering and improve the AA kinetics and response. The delayed PA kinetics at 100 °C by Sn addition results in a higher solute concentration in the matrix and thus leads to a larger natural secondary ageing (NSA) response in Sn-added alloys. A higher PA temperature (e.g. 180 °C), at which the binding between

Sn and vacancies is weaker, largely improves the effectiveness of PA. By combining Sn addition and PA, an advantage of lowered hardness (better formability) after PA and 1 week of NSA is obtained. During natural pre-ageing (NPA) prior to PA in Sn-added alloy, smaller clusters, which can subsequently transform to PA clusters at 100 °C, are formed, accounting for the positive effect of NPA on the effect of PA.

7. Acknowledgements

First of all, I would like to express my special thanks to my supervisor Prof. Dr. John Banhart, a respectable and responsible German scholar, for providing me the precious opportunity to pursue my PhD at Technische Universität Berlin and Helmholtz Zentrum Berlin. His enthusiasm and rigorous attitude toward scientific work impressed me deeply and will continue to have influence on me in my future career. This dissertation would have been impossible without his valuable guidance and support.

I would like to thank Prof. Dr. Reinhard Krause-Rehberg (University of Halle) for being the examiner for this dissertation and for his support on producing positron isotopes and on positron annihilation lifetime spectroscopy measurements.

Sincere thanks to Dr. Meng Liu, humorous and wordy, for his help in my work and life. He has shared so much experience on the data analysis, data presentation and paper writing throughout every stage of my PhD work.

I would like to thank Dr. Zeqin Liang and David Leyvraz of Novelis Research and Technology Center Sierre and Prof. Dr. Stefan Pogatscher from Montanuniversität Leoben for providing the high-quality alloys. I am deeply indebted to Dr. Mohamed Elsayed from University of Halle for the production of positron isotopes, positron annihilation lifetime spectroscopy measurements and fruitful discussion on the results. The assist of Dr. Haiming Sun (University of Yanshan) on the TEM measurements has contributed a lot to this work.

I would also like to thank Claudia Leistner and Christiane Förster for their help in the sample preparation and in the use of experimental equipment and Ms. Ciceron for all the help since the first day of my Ph.D. work.

Dr. Mazen Madanat, Dr. Anna Manzoni, Dr. Florian Vogel, Dr. Andria Fantin, Zi Yang, Qianning Guo, Kang Dong, Qin Tan, Li Zhang, Yajie Wang and Fanxing Xi for their help in my study and daily life.

Many thanks to China Scholarship Council for the financial support.

Last but not least, I would like to give my gratitude to my family. 爸爸妈妈，感谢你们一路以来不计回报的支持，我爱你们，愿你们健康快乐。姐姐要幸福，宣宁健康成长。My beloved Fei, you complete me.

8. List of publications

Paper I (Section 5.1)

Effect of Sn and In on the natural ageing kinetics of Al-Mg-Si alloys, Materialia 6 (2019) 100261. (Postprint)

DOI: http://doi.org/10.1016/j.mtla.2019.100261.

URL: https://www.sciencedirect.com/science/article/pii/S2589152919300572

Paper II (Section 5.2)

Influence of Sn on the age hardening behavior of Al-Mg-Si alloys at different temperatures, Materialia 8 (2019) 100441. (Postprint)

DOI: https://doi.org/10.1016/j.mtla.2019.100441.

URL: https://www.sciencedirect.com/science/article/pii/S2589152919302376

Paper III (Section 5.3)

Combined effect of Sn addition and pre-ageing on natural secondary and artificial ageing of Al-Mg-Si alloys. Submitted to “Materials Science and Engineering: A”. (Preprint)